MÖSSBAUER EFFECT STUDY OF POINT DEFECTS IN PURE IRON

Yutaka Yoshida

OSAKA UNIVERSITY
GRADUATE SCHOOL OF ENGINEERING SCIENCE
DEPARTMENT OF MATERIAL PHYSICS
TOYONAKA OSAKA

MÖSSBAUER EFFECT STUDY OF POINT DEFECTS IN PURE IRON

Yutaka Yoshida

Department of Material Physics
Faculty of Engineering Science
Osaka University

February 1983

SYNOPSIS

The study of the point defects in the neutron, electron and self-ion irradiated pure iron is performed by combining the "defect trapping method" and the "new thermal scan method" in the Mössbauer spectroscopy. In the pure iron irradiated by neutrons at low temperature, clear annealing stages below 110 K, around 160 K , and around 220 K are found in the measurement of the count rate at zero velocity, total resonance area, average hyperfine field and full width at half maximum. These temperature of the annealing stages is in good agreement with the previous results by other investigators using other techniques, and are attibuted to the recovery of interstitials, their small clusters, and vacancies, respectively. Comparison of the annealing stages and the Mössbauer parameter changes leads to the conclusion that the existence of interstitial atoms increases the hyperfine field and that of vacancies decreases the Debye-Waller factor of iron atoms. In the electron irradiated and neutron irradiated specimens, the changes in the hyperfine field and total resonance area at 77 K are quite different probably due to the difference in the defect distribution in the specimens. At 4.2 K , these differences are scarcely observed even when the spectra are subtracted from each other to see the smallest differences. This means that introduction of vacancies and interstitials in iron lattice give rise to the appreciable changes in the Debye temperature and Curie temperature depending upon their distributions.

In the self-ion irradiated iron, the subtraction analysis can successfully separate the defect perturbations consisting of two components probably arising from the vacancy clusters associated with a low hyperfine field and existing in the shallower part of the specimen and from the interstitial clusters with a large hyperfine field existing in the deeper part.

Contents

1. INTRODUCTION

1.1 General Introduction

Mössbauer effect study on point defects in pure iron irradiated by neutrons, electrons, and self-ions will be described in this thesis. Iron is one of the largest industrial productions and most widely used among all other metals in the world. However, many fundamental problems concerning the properties of iron still remain unsolved, although much effort has been made by many investigators in the field of materials science. For instance, the nature of point defects in pure iron is still a large open question. As will be mentioned later, there have been controversies in the experiments and discussions whether a single vacancy becomes mobile in pure iron around "200 K" or "200 °C". This is also closely related with the theoretical arguments on the "one interstitial model", or "two interstitial model". Since the problem is commonly concerned with all other metals, the "iron point defects problem" is one of the most important and fascinating subjects in the field of point defects study in metals.

Recently, a number of new techniques, like the positron-electron annihilation, muon spin rotation, perturbed angular correlation, nuclear magnetic resonance, and Mössbauer spectroscopy, have been rapidly developed and applied to the study of lattice defects, and some problems, for instance, such as of the migration behavior of vcancy have been gradually clarified. Nevertheless, atomic and electronic perturbations around vacancies, interstitials, their clusters, and complexes are still not clear in most metal lattices, especially in the bcc iron lattice. The ^{57}Fe Mössbauer spectroscopy seemed to be a most powerful tool to solve the above problems.

So that, the Mössbauer effect study combined with the technique of irradiation by high energy particles and electron microscopy was intended in the present investigation.

There are various interesting aspects in the study of point defects in the irradiated iron. For example, irradiation produces a large amount of non-equilibrium vacancies, interstitials,and their clusters, which move around in the lattice and react with each other and are converted to the secondary defects, such as interstitial type dislocation loops, vacancy type loops, stacking fault tetrahedra, and voids. Since the secondary defects are observable by electron microscope, their growth and shrinkage processes can be measured quantitatively in-situ during high energy electron irradiation in the high voltage electron microscope and be analysed by using a set of reaction rate equations as was successfully shown by M. Kiritani, et. al [1-3]. However, the individual motions and reactions of point defects are invisible under the microscope, and, therefore, direct information about point defects behavior and their interations is lacking as far as the observation is confined to the micorscopic techniques. On the other hand, conventional methods, like the electrical resistivity, magnetic after effect, and X-ray diffuse scattering measurement, are sometimes useful to detect the above invisible reactions. However, it is still very difficult by these techniques to identify various reactions and to find the electronic and atomic configurations associated with the point defects and their complexes. In this respect, the Mössbauer effect study seems to be fruitful, since the Mössbauer parameters affected by the electronic, magnetic, and phonon perturbations around defects are expected to show the electronic structures and dynamical motions of isolated and interacting point de-

fects.

There is an experimental difficulty in the Mössbauer measurement, concerning the sensitivity to detect the perturbations by irradiation. As well known, the concentration of the defects introduced by irradiation is expected to be less than 0.1 at.% , which is usually too low to detect an appereciable change by them in the Mössbauer spectrum, unless a special technique in the measurement is introduced. Another difficulty is a relatively long time of the order of a few days needed to take one spectrum with an enough accuracy. When the measurement is combined with the conventional isochronal annealing experiment to see the recovery processes of point defects, in which the annealing temperature is changed stepwise, for instance, with twenty steps, the total measurement time in each run will be too long to be completed, for instance, within several months.

In order to overcome the above difficulties, a "defect trapping method", a "^{57}Fe self-ion irradiation method", and a "thermal scan method" were developed and used in this investigation. Combination of these new techniques extensively improved the sensitivity to detect the defects of the concentration less than 0.1 % and their interactions in a relatively short time of about a month in one annealing cycle, as will be precisely discribed in later sections.

In the following sections of the chapter I are mentioned, in the first place, the former studies on the point defects in iron, the principles and conventional techniques of the Mössbauer effect, those of the radiation damage experiment, and the purpose and the employed methods in this investigation. In the second, the experi-

mental procedures of the neutron, electron, and self-ion irradiations will be described in the chapter II, which will be then followed by the experimental results in the chapter III. Finally, in the chapter IV, the differences between the results of the three kinds of irraditaion and annealing experiments, the electronic and magnetic perturbations around vacancies, interstitials, and their aggregates will be precisely discussed. The conclusion, summary, and acknowledgement will be given in the last.

1.2 Problems and Previous Studies of "Point Defects of Iron"

There have been many studies on the point defects in pure iron which were reviewed in the literatures [4-7]. Among other point defects in iron problems, it is especially worthy of note that controversial results and interpretations on the onset temperature of vacancy migration have been reported. Occurrence of vacancy migra tion at 200 K to 250 K with activation energies around 0.5 eV was suggested by Cuddy and Raley [8], Cuddy [9], Kugler, Schwirtlich, Takaki, Ziebart and Schultz [10], while the migration temperatures from 460 K to 630 K with activation energies between 1.0 eV and 1.4 eV were given by Glaeser and Wever [11], Ikeda, Goto, Abiko and Kimura [12], Weller, Diehl and Triftshäuser [13], Yoshida, Kiritani and Fujita [14], Diehl, Merbold and Weller [15], Kiritani, Takata, Moriyama, Fujita [16]. In the earliest irradiation experiment on iron by Fujita and Damask [17], a recovery stage at around 200 K and one at 570 K were already found. The investigators concluded that the former is likely associated with the migration of interstitials released from impurities or that of divacancies and the latter could be the migration of vacancies released from carbons, although a clear cut conclusion on the latter was largely reserved. Today, self-interstitial migration is generally accepted to occur at around 120 K [18].

These results have been critically discussed in close relation with the disputes on the "one interstitial model", or "two interstitial model", as well as for most other metals. Five typical recovery stages have been found in many pure metals after high energy paricles at low temperatures, and given the rotations, I, II, III, IV and V, common to the various metals [19]. According

to the one interstitial model [19], the single self-interstitial will start to migrate, mostly annihilate with the radiation produced vacancies, and partly form small clusters at the stage I. The growth of interstitial clusters will occur, leading to observable small interstitial loops, at the stage II. At the stage III, vacancies will migrate and annihilate at interstitial clusters, and at the same time vacancy agglomeration will occur to form the vacancy clusters, which will then grow in size at the stage IV, and finally the vacancy clusters will dissociate thermally at the stage V. In the two interstitial model [20], the crucial difference from the above model is found in the stage III; the migration of the second type of interstitials, which are formed by convers ion from metastable stage I interstitials, will occur at the stage III.

In the case of the recovery in irradiated iron, the stage I, II, III, IV and V occur at around 120 K , 160 K , 220 K , 350 K , and 550 K , respectively, so that the onset of vacancy migration was assigned to the stage III in the one interstitial model and to the stage V in the two interstitial model, respectively. Since carbon impurities have been observed to interact strongly with both interstitials [21] and vacancy-type defects [11,22,23] in α-iron, it has been strongly recommended and tried to take out carbon from the specimens as much as possible. But the high purity iron specimen containing, for instance, less than 10 p.p.m. carbon is not easy to obtain. Therefore, the annealing behavior of irradiated iron in earlier works must have been strongly affected by impurities, especially by carbon, giving rise to a large confusion in the interpretations of the recovery processes processes in the earlier works and even in the above controversies.

Recently, new techniques, such as positron-life measurements [24-27] , muon spin rotation [28], and high voltage electron microscopy [3] , showed one after another that in electron irradiated iron with extremely low carbon impurity concentration, vacancies could become mobile at around 220 K . For later comparison with our Mössbauer result, they will be referred briefly below. Accordingly to Hautojärvi, et. al [24-27], positron life-time in electron irradiated iron increased remarkably after annealing at the stage III, which was caused by the appearance of a long life-time $\tau_2 \cong 300$ psec due to vacancy clustering. Taking into account of the results from carbon-doped specimen, they concluded that during the stage III recovery, stable vacancy-carbon pairs were formed when migrating vacancies were captured by immobile carbon atoms, and these pairs dissociated at about 480 K causing a second release of free vacancies. Furthermore, after neutron irradiation, a component with $\tau_2 \cong 200$ psec, which was larger than the value of monovacancies, 175 psec, was observed, and they concluded that a fraction of vacancies created by neutron irradiation was in a form of small clusters, and a shift of the vacancy-migration temperature from 220 K to around 170 K was due to correlated vacancy migration within collision cascades.

Möslang et. al [28] successfully observed a signal from monovacancies in electron irradiated iron by the μSR technique. After irradiation, a new frequency of 30 MHz different from the value of unirradiated iron, 50 MHz, was found. Symmetry consideration showed that the new signal was most likely originated from muon trapped at monovacancies. After annealing above the stage III, this line disappeared completely, which strongly suggested vacancy migration at 220 K .

Kiritani [3] showed by the observation of the behavior of interstitial type dislocation loops formed at 150 K that the number density of interstitial loops started to decrease at 220 K , and he concluded that a large part of interstitial loops surrounded by a high density of dispersed vacancies disappeared at around 220 K and the vacancy migration temperature could be assigned to the stage III recovery.

The above three observation on vacancy migration almost convinced us that the vacancy migration occurs at around 220 K in agreement with the one interstitial model. In the course of the study of carbon interstitials and their precipitation behavior in pure iron by the Mössbauer effect measurement [29], it was hopefully suggested that the behavior of self point defects could be observed in irradiated iron by using the same technique and a clear cut conclusion could be drawn to compare with those from the above observations. In addition, it was wxpected that the electronic, magnetic and lattice perturbations associated with the point defects, which were not always elucidated by the above techniques, could be found by the Mössbauer spectroscopy and essential questions on the nature of point defects in iron could be solved. In this respect, it may be worthy of note that the monovacancies migration temperature, 220 K , if it is true, is fat below those of other bcc metals and this peculiar nature might be connected with the above structures observable by tne Mössbauer effect.

1.3 Hyperfine Interaction Study of Point Defects in Metals

Mössbauer Effect, which is the recoilless resonance absorption of gamma rays in solids, was discovered by R. L. Mössbauer in 1958 [30]. Since that time, the Mössbauer spectroscapy has been rapidly developed to be widely in use as one of the most powerful fruitful techniques for the researches in various sciences, especially in materials science. A large number of literatures on the technologies and applications of it have been publixhed until today [31-34].

In this section, first, general information obtainable from Mössbauer measurement will be described briefly, and in the second, previous studies on point defects in metals using Hyperfine interactions, paticurally concerning pure α-Fe studied by Mössbauer effect and perturbed angular correlation, will be given.

1.3.1 General information from Mössbauer measurement

1.3.1(a) Hyperfine interactions of ^{57}Fe

In Mössbauer spectroscopy, it is sufficient to consider three kinds of hyperfine interations between nucleus and electrons, which are electric monopole interaction, electric quadrupole interaction, and magnetic dipole interaction. The first one affects the position of resonance lines and gives rise to an isomer shift (δ) in the Mössbauer spectrum. The two latters remove the degeneracy of nuclear levels and cause the electric quadrupole splitting ΔE_q, and the magnetic Zeeman splitting ΔE_m, respectively.

The electric monopole interaction energy, i.e. Coulomb interaction energy between nucleus and s-electrons penetrating into nucleus, is given by

$$E_I = 2\pi/3|\psi(0)|^2 Ze\langle r_n^2 \rangle \qquad (1.1)$$

where $|\psi(0)|^2$ is the electron density at the nucleus, Ze nuclear charge, and $\langle r_n^2 \rangle$ the expectation value of the square of nuclear radius. In the Mössbauer spectrum, the isomer shift appears as

$$\delta = C[|\psi(0)|_A^2 - |\psi(0)|_S^2] \qquad (1.2)$$

due to the difference in the charge densities between source (S) and absorber (A). Since s-like valence and conduction electrons contribute to the electron density $|\psi(0)|^2$, both the changes in the number of conduction electrons and that of core electrons, which are screening the outer s-electrons, affect the isomer shift; for instance, an increase of valence electron density of d-character will decrease the attractive interaction between conduction electrons and nuclear charge, leading to a decrease of $|\psi(0)|^2$. As a reference standard position of isomer shift, the center position of the six-line Mössbauer spectrum of pure iron at room temperature was used in this investigation.

For irradiated iron, in addition to the above electric monopole interaction, the nuclear state of iron is expected to be perturbed simultaneously by magnetic dipole, E_m, and electric quadrupole intensity, E_q. In the general case of $E_m \cong E_q$, a numerical calculation is necessary to obtain the eigen values and eigen states of the Hamiltonian,

$$H = \frac{eQV_{zz}}{4I(2I-1)}\left[3I_z^2 - I(I+1) + \eta(I_x^2 - I_y^2)\right] - \mu(I_xH_x + I_yH_y + I_zH_z) \qquad (1.3)$$

where the electric quadrupole field is discribed by $V_{zz} = eq$ and the asymmetry parameter by $\eta = (V_{xx} - V_{yy})/V_{zz}$ with the conditions, $|V_{zz}| \geq |V_{yy}| \geq |V_{xx}|$ and $V_{xx} + V_{yy} + V_{zz} = 0$. The magnetic field is

given by $H = (H_x, H_y, H_z)$, and for the excited state (I=3/2) and ground state (I=1/2), the magnetic moments of each state are shown by μ_I. Assuming $E_q \ll E_m$ and the electric field gradient (EFG) tensor to be axially aymmetric, the energy eigen values can be ecpressed by a first-order perturbation,

$$E_{m,q}(I,m_I) = -g_N\beta_N m_I H + (-1)^{|m_I| + \frac{1}{2}} \cdot \frac{eQV_{zz}}{8} (3\cos^2\theta - 1)$$

$$(-I \leqq m_I \leqq I) \qquad (1.4)$$

where θ is an angle between z-axis of EFG and magnetic field acis. In the Fig. 1.1, the nuclear levels of ^{57}Fe shifted and split by the above three interactions and the corresponding Mössbauer spectra are given schematically [35]. The magnetic field H is originated from a core polarization by the Fermi contact interaction,

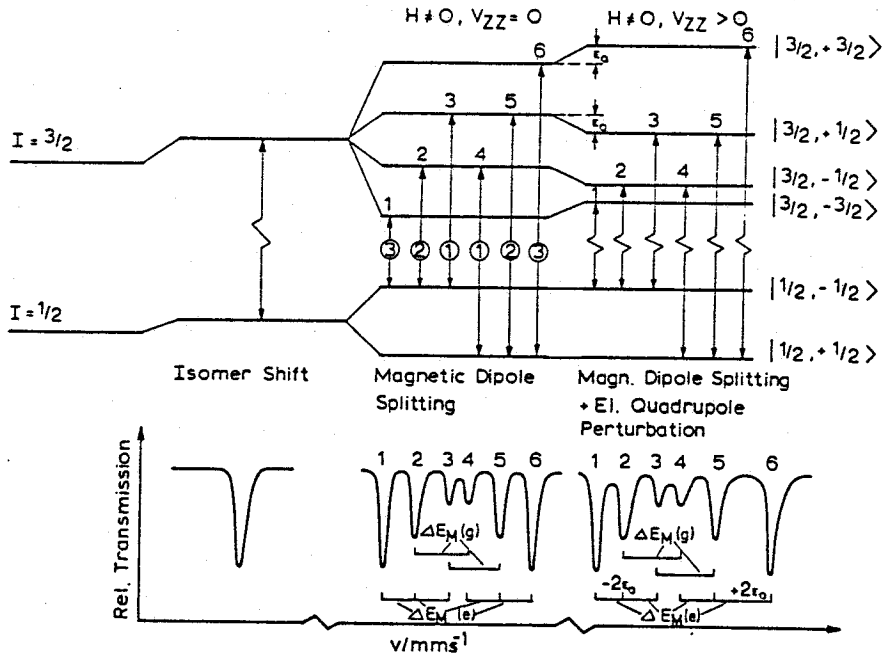

Fig. 1.1 Magnetic dipole splitting in ^{57}Fe without ($H = 0$, $V_{zz} = 0$) and with electric quadrupole perturbation ($H = 0, V_{zz} > 0$) and resultant Mössbauer spectra.

a nonzero orbital magnetic moment, a dipolar interaction of the nucleus with the atomic spin moments on neighbor atoms, and an external magnetic field. The dominant term, that is the core polarization, is influenced by both the spin density of unpaired outer electrons and the poralization of conduction electrons, which are supposed to be perturbed by vacancies, and interstitials to any extent. Furthermore, the EFG arises from a nonspherical distribution of charges around the prove nucleus, so that the charge perturbations by defects are thought to reflect on the electric quadrupole splitting too.

1.3.1(b) Intensity and line shape of resonance line

The peak absorption intensities in the Mössbauer spectrum of iron are proportional to the transition probabilities between energy levels of ^{57}Fe as shown in Fig. 1.1 . Their relative probabilities are

$$\begin{aligned} P(\pm\tfrac{1}{2},\pm\tfrac{1}{2}) &= \sin^2\theta && \text{for } \Delta m = 0 \\ P(\pm\tfrac{1}{2},\mp\tfrac{1}{2}) &= 1/4(1+\cos^2\theta) && \text{for } \Delta m = \mp 1 \\ P(\pm\tfrac{1}{2},\pm\tfrac{1}{2}) &= 3/4(1+\cos^2\theta) && \text{for } \Delta m = \pm 1 \end{aligned} \qquad (1.5)$$

where θ is an angle between the magnetic field and gamma-ray direction. For instance, the intensity ratios between the first, second, and third lines, as indicated in Fig. 1.1, are 3:2:1, 3:4:1, and 3:0:1 in the specimen with the random spin orientations, with the spins parallel to the specimen surface, and with those and perpendicular to it, respectively.

The line width and the energy profile of Mössbauer gamma-rays on the occasion of emission and/or absorption are controled by the transition probabilities so that it is described by a Lorentzian function,

$$I(E) \sim \frac{\Gamma/2\pi}{(E-E_0)^2+(\Gamma/2)^2} \tag{1.6}$$

where Γ is the line width. Only in a thin foil specimen, a Mössbauer transmission spectrum observed at a Doppler energy, ε, by gamma-ray countings, $N(\varepsilon)$, can be represented by a Lorentzian form,

$$\frac{N(\infty)-N(\varepsilon)}{N(\infty)} = \frac{\rho\beta d f_s \cdot f_a \sigma_0}{2} \cdot \frac{\Gamma^2}{E_0{}^2\varepsilon^2+\Gamma^2} \tag{1.7}$$

where ρ is the density of absorber, β the natural abundance of the Mössbauer isotope, d the thickness of the absorber, σ_0 is the maximum resonant cross section, and f_s and f_a the recoilless fractions of the source and absorber.

The total resonance area, A, can be obtained by integrating the above expression over the whole doppler energy range, as in the following,

$$A = \frac{\pi}{2} \cdot N(0) \cdot \Gamma_{exp} \tag{1.8}$$

which is roughly proportional to the recoilless fraction, f, neglecting the second order term of f. In an irradiated specimen, the resultant spectrum is expected to consist of various components depending on different hyperfine interactions and f-values at different surroundings.

The recoilless fraction, or Debye-Waller factor, is shown by

$$f(T) = \exp(-k_B{}^2 \cdot \langle x^2 \rangle_T) \tag{1.9}$$

with the mean square displacement of atom, $\langle x^2 \rangle_T$, which is generally described by the phonon spectrum $g(\omega)$,

$$\langle x^2 \rangle_T = \hbar/2m \cdot \int_0^\infty \frac{1}{\omega} \coth(\hbar\omega/2k_BT)\, g(\omega)\, d\omega \tag{1.10}$$

Furthermore, in Debye's approximation, it is given by

$$f(T) = \exp\left[-\frac{E_R^2}{2k_B\theta_D} \cdot \left\{1 + 4\left(\frac{T}{\theta_D}\right)^2 \int_0^{\theta_D/2} \frac{x\,dx}{e^x - 1}\right\}\right] \qquad (1.11)$$

Accordingly, the Debye-Waller factor is supposed to reflect directly the local dynamical properties around radiation introduced defects. For example, in vacancy associated sites, the mean square displacement $\langle x^2 \rangle_T$ is expected to become larger than that in normal sites, so that the f-value probably seems to decrease.

Furthermore, the mean square velocity $\langle v^2 \rangle_T$ can be obtained by the second order Doppler shift,

$$\frac{\delta E}{E} = -\langle v^2 \rangle_T / 2c^2 \qquad (1.12)$$

which is usually a small addition to the isomer shift, and can be measured by the temperature dependence of the center shift of the spectrum. In this investigation, it can not be determined because the defect distribution will change with as increase of temperature. So that, the term of the "isomer shift", obtained from the center shift in this investigation, will include the small second order Doppler shift.

Finally, the influences of the jumping motion of atoms to the Mössbauer line shape will be mentioned below. The sudden jump motion of the ^{57}Fe atom emmitting gamma-ray would induce to break the coherency of the gamma-ray, so that an effective life time of the ^{57}Fe might be observed to be shorter than the real life time of ^{57}Fe, $\sim 10^{-7}$ sec. Taking into account of the Heisenberg uncertainly relation,

$$\Delta E_{exp} \cdot \Delta t_{exp} \approx \hbar \qquad (1.13)$$

the shorter effective life time, Δt_{exp}, will lead to a larger energy uncertainty, ΔE_{exp}. Accordingly, the observe width of the

Mössbauer spectrum is expected to become broader than that without the jump motions.

1.3.2 Previous hyperfine interaction studies on point defects in metals

Vaious new techniques using the hyperfine interactions have been applied to the study of point defects in metals. The Mössbauer effect [36-40], the nuclear magnetic resonance [41], and the perturbed angular correlation [42] have made a great contribution to clarify the nature of point defects from microscopic view points.

The previous Mössbauer studies on point defects in pure iron are summarized in Table 1.1 . As in the gable, various methods to detect perturbations in the defect-introduced pure iron were performed. The on-line Mössbauer investigations using the $^{56}Fe(d,p)^{57}Fe$ reaction [43,44], the $^{56}Fe(n,\gamma)^{57}Fe$ reaction [45] and the Coulomb excitation and recoil implantation of ^{57}Fe [46,47] are supposed to be useful for the observation of defect perturbations, because the defect production process are accompanied with the prove excitation process, so that the prove nuclei are expected to be associated with the defects produced by the implantation. Nevertheless, no appreciable changes were observed in the Mössbauer spectrum in the above three trials.

On the other hand, the defect perturbed components with different hyperfine fields and different Debye Temperatures in the ion implantation experiments by using an isotope separator and the impurity Mössbauer parents, for instance, ^{129m}Te [48,38], ^{151}Gd [49], ^{133}Xe [51-53], ^{131}I and ^{125}I [54]. Reinstema et.al [52,53] concluded that after implantation of ^{133}Xe ions into polycrystalline iron at 7 K , the four different components existed in the spectrum

Way of irrad. (implantation)	Mössbauer parent → Mössbauer nucleus	Transfered energy (eV)	Temp. of irrad. (K)	Results	Annealing results	Ref.
IIS	$^{129m}Te \rightarrow {}^{129}I$	50×10^3	RT	h.f.sites + l.f.sites		[48]
5.5 MeV deuterons	$^{56}Fe + d \rightarrow {}^{57}Fe + p$	$10^5 - 10^6$	77/RT	no effects		[43,44]
CE+RI 25 MeV O^{16} (recoil into backing)	^{73}Ge CE	$\simeq 10^7$	$\simeq$ 80	reduction of DWF		[45]
CE+RI 25 MeV O^{16} (recoil thru vacuum)	^{57}Fe CE	$\lesssim 17 \times 10^6$	5/RT	no effects		[46,47]
IIS	$^{133}Xe \rightarrow {}^{133}Cs$ $^{161}Tb \rightarrow {}^{161}Dy$	5×10^3 - 150×10^3	RT	high, intermediate and low field sites	725K → loss of high field sites	[51]
thermal neutrons	$^{56}Fe + n \rightarrow {}^{57}Fe + \gamma$	$\lesssim$ 550	80/RT/570/770	no effects (Fe_3Al:disorder)		[55]
IIS	$^{129m}Te \rightarrow {}^{129}I$	150×10^3	RT	at least 2 sites	670K → loss of high field sites	
IIS	$^{151}Gd \rightarrow {}^{151}Eu$	50×10^3	RT	2 sites	350K → loss of high field sites	[49]
IIS	$^{133}Xe \rightarrow {}^{133}Cs$	140×10^3	90/RT/380/480	4 sites with different field	90-480K → loss of high field sites	[52]
IIS	$^{131}I \rightarrow {}^{131}Xe$ $^{125}I \rightarrow {}^{125}Te$	- 100×10^3	RT	3 sites with different field		[54]
IIS	$^{129m}Xe \rightarrow {}^{129}Xe$	75×10^3	RT	2 sites		[56]
IIS	$^{133}Xe \rightarrow {}^{133}Cs$	130×10^3	5	4 sites with different field	60-575K → loss of high field sites	[53]
^{57}Fe implantation	$^{57}Co \rightarrow {}^{57}Fe$:CEMS	70×10^3	RT	amorphigation (dose $3 \times 10^{16}/cm^2$)	200°C → 700°C gradual recovery	[57]

Table 1.1 Previous Mössbauer studies on point defects in pure iron

corresponding to Xenon atoms associated with different number of vacancies; three visible spectral components with high, intermediate and low hyperfine fields and different recoilless fractions, and a fourth, invisible component with a recoilless fraction very close to zero, and from the annealing experiments they concluded that the migration energy of vacancies in iron were 1.27 ± 0.09 eV. It is thinkable that in the above case of XeFe, the large mismatch of the Xenon atoms in the iron lattice cause the trapping of vacancies by the Xenon atoms, and the reason why the low temperature recovery stages were not observed is that the binding energy between the vacancies and Xenon atoms might be too large to detect the migration behavior of vacancies in pure iron like the trapping of vacancies by carbon found by Fujita and Damask [17].

The ^{57}Fe self-ion irradiation experiments were reported in various metals by conversion electron Mössbauer spectroscopy [57,58]. According to Sawicka and Sawicki the ^{57}Fe implanted in iron with a total dose of 10^{16}ions/cm^2 at room temperature showed some indication of γ-phase iron existing, and with that of 3×10^{16} ions/cm^2, a complex spectrum was observed, which suggested implantation-induced amorphzation.

Finally, relating to our investigation using the ^{57}Co doped Fe source experiment, a possibility of a thermal spike produced by the decay of $^{57}Co(EC,\gamma)^{57}Fe$ must be mentioned: In a delayed coincidence experiments, where the Mössbauer spectrum was accumulated by changing the measuring thime of the order of the life time of the excited Mössbauer level after the nuclear decay, Lynch et.al [59] found that the recoilless fraction of the source increased with the time. They suggested that the nuclear transformation induced a thermal spike and a creation of long-lived excited phonon

states, which eventually decayed during the life time of the Mössbauer level of ^{57}Fe.

1.4 Damage Production by High Energetic Particle Irradiation

In this investigation, the fast neutrons, electrons and self-ions were used for the production of defects in the iron foils. There are many review articles about the production of defects by high energy particles [60-63], so that in this section, a short survey will be given in order to evaluate the defect distribution and the defect concentration after the irraditaions by the three kinds of the particles.

The fast neutrons with a kinetic energy E can interact with atoms in the lattice mainly by elastic collisions, leading to the displacement of the atoms with the maximum transfered energy,

$$E_{max} = \frac{4m_1 \cdot m_2}{(m_1 + m_2)^2} E \qquad (1.14)$$

where m_1 is the mass of neutron and m_2 that of the knock-on atom. According to the Kinchin-Pease model [64], the average number of Frenkel pairs, $\bar{\nu}$, produced by an primary knock-on atom of the average enrgy $\overline{E_p}$ is given by

$$\bar{\nu}(\overline{E_p}) = \frac{\kappa \cdot \overline{E_p}}{2E_d} \qquad (1.15)$$

where E_d is the threshold energy for the displacement of atoms in the lattice and κ is the so-called displacement efficiency factor. In iron, E_d is about 25 eV. Although in the original Kinchin-Pease model, $\kappa = 1$, both analytical calculation [65] and computer simulation [66] suggested $\kappa = 0.8$. Then, the $\bar{\nu}$ is evaluated as about 180 for the reactor fast neutrons when the average energy of the primary knock-on atom is about 12 keV. When the irradiation is done with a neutron flux, ϕ n/cm^2/sec, for t sec, the magnitude of the displacements per atom (dpa) are given by

$$C_d = \phi t \sigma_p \cdot \frac{\overline{E_p}}{2E_d} \qquad (1.16)$$

where σ_p is the total cross section for the primary knock-on collision. Before the knock-on atoms are finally stopped, the moving atoms losed those kinetic energies by subsequent collision processes so that a cascade damage will be produced in the lattice. The cascade damage structure may roughly consist of two parts; the depleted zone (vacancy rich region) and the iterstitial rich region in consequence of the replacement sequence collisions [67].

In the case of high energy electrons of 28 MeV generated by the LINAC, the maximum (T_m) and mean transfer energies ($\overline{T}$) from electrons to atoms are reperesented by

$$\begin{aligned} A \cdot T_m &= 560.8 \cdot x(x+2) \quad (eV) \\ \overline{T} &= E_d[\log(T_m/E_d) - 1 + \pi\alpha] \end{aligned} \qquad (1.16)$$

where A is the mass of the target atom, $x = E/m_1c^2$ and $\alpha = Z_2/137$ (Z_2 is the atomic number) [68]. In the case of Fe, the T_m and $\overline{T}$ are calculated as 30 keB and $6 \cdot E_d$, so that the average number of the displaced atoms is estimated as $\overline{\nu} \cong 3$, which means that about three Frenkel pairs are producted per one collision in LINAC electron irradiation. According to the results of the electrical resistivity measurement of iron during the isochronal annealings by Kitajima et.al [68], the amounts of resistivity recovery at the stage I was smaller than that of 3 MeV electron irradiated iron, as is shown in Fig. 1.2 , whichsuggested that the small defect clusters already existed as the irradiated specimen.

In the self-ion irradiation, the ion stopping range and the distribution of energy deposition was calculated by the computer program, so called E-DEP-I [69]. The ranges and range distributions

of implants were calculated from the specific energy losses dE/dR for the two processes of slowing down of a particle penetrating a target, that is the elastic collisions with nuclei and the excitations of target atom electrons. The range profile is described by a Gaussian function with the parameters of the projected range, R_p and the range struggling, ΔR_p: The concentration of implants was defined as a ratio between the number of implanted ions to the number of host atoms in the implanted depth $4 \cdot \Delta R_p$, $\bar{x} = N_{proj}/(N_{proj} + N_{host})$.

After the collision process, a large part of the displacement atoms will return back on the normal lattice site by the correlated mutual annihilation between the vacancies and interstitials during irradiation and subsequently, a small part of those will remain as the vacancies, interstitials, and their aggregates in the lattice.

1.5 Puposes and Methods in This Investigation

It is the purpose of the present research to clarify the nature of point defects in pure iron by the Mössbauer spectroscopy. Nevertheless, as was mentioned before, no appreciable effects of vacancies, interstitials and their aggregates have been observed in the previous Mössbauer studies, except for the implantation experiments using the impurity Mössbauer parent atoms with a large atom size. In the implantation methods, the observed defect perturbations and include not only the effects of defects, but also those of the impurity Mössbauer probe atoms, so that the electronic, magnetic and lattice perturbations around vacancies, interstitials, and their aggregates in "pure iron" can never be observed in these methods. Accordingly, a challenging research to detect the effects of defects in "pure iron" was desired and expected to clarify the narure of point defects in "pure iron".

The difficulties of the present research is supposed to lie in the facts that the defect concentration producted by irradiations usually too low to detect the perturbations in the normal absorber experiments and that, even if the perturbations can be found in the Mössbauer spectrum, the long period is necessary to investigate the detailed annaling behavior of the point defects, as were mentioned before. In order to overcome the above difficulties in the present research, the followint three new techniques were applied to the Mössbauer study on point defects in pure iron; the source experiment using the ^{57}Co-doped-Fe source, the new thermal scan method, and the $^{57}Fe^{+}$ self-ion irradiation experiment. These three methods will be explained below in this order.

1.5.1 Source experiments

In order to improve the sensitivity to detect the effects of defects, it is desirable that the probe atoms will preferentially interact and associate with defects and form the complexes, leading to a high probability to find the defect perturbation. Therefore, the probe isotope necessitated for that purpose must play a role of an impurity in the pure iron matrix to find with the defects during the irradiation and annealings and, in addition, must behave just like the host iron when emitting Mössbauer gamma-rays. Only one which can satisry the above demands is supposed to be the ^{57}Co Mössbauer parent, which decays to the 14.4 keV excited Mössbauer level of ^{57}Fe as is shown in Fig. 1.2 .

The ^{57}Co atoms were expected to have certain binding character with vacancies, intersititials or their clusters in bcc Fe matrix and form the complexes. Then, the defect lines in the Mössbauer spectrum would be observed by means of the changes in hyperfine interactions by defects. It must be noted that the ^{57}Co atoms

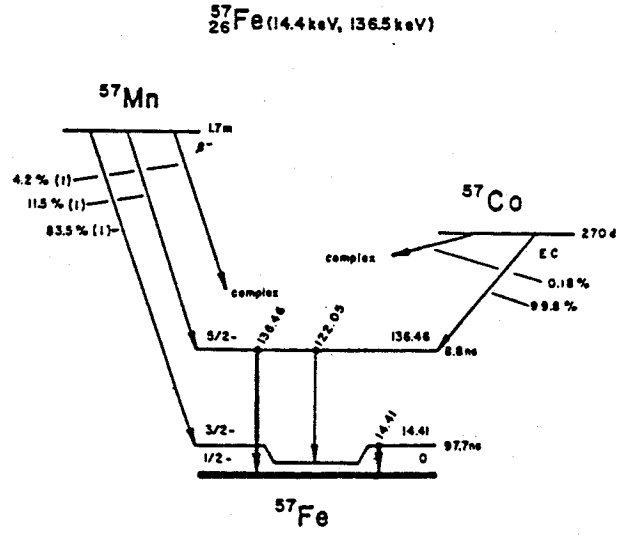

Fig. 1.2 Decay scheme of ^{57}Fe indicating the population of the two levels and transitions (14.41 and 136.46 keV) of this isotope

trapping the point defects will be transmuted to ^{57}Fe before emitting the Mössbauer gamma-rays, as mentioned in the above, and accordingly it will enable us to preferentially investigate the point defects in pure iron eliminating the impurity effect in the Mössbauer signals. In this respect, the magnitude of the binding energis between ^{57}Co atoms and point defects are very important. The impurity trapping method has been used successfully by Vogl, et al. for the Al-^{57}Co system, Ag-^{57}Co system [70,71], and the Mo-^{57}Co system [72], in which defect lines arising from the complexes formed by interstitials and ^{57}Fe impurity atoms were detected. In these examples, the ratio of atomic radii betweem the host and the probe atoms is considerably large, for instance 1.15 for the Al-^{57}Co system, but in the Fe-^{57}Co system in the present investigation, it is only 1.03, so that the binding energies seem to be too small. Nevertheless, since the interactions between the Co atoms and defects realized in the irradiated specimen have never been directly estimated experimentally, it is expected that the employment of the impurity trapping method in the present experiment will give only the defect lines in the Mössbauer spectrum but also the interaction parameters between the ^{57}Co impurity atoms and the defects in the pure iron.

1.5.2 Thermal scan method

In addition to the above "defect trapping method", the "thermal scan method" was used for the detailed analysis of the annealing processes. In the thermal scan method in this experiment, the cout ratio at zero velocity was accurately measured by using an absorber of pure iron as a function of the isochronal annealing temperature, or the specimen temperature during continuous heating. The count rate at zero velocity strongly depends on the whole shape

of Mössbauer spectrum, being influenced by not only the defect lines but also the changes in the matrix lattice, such as Debye-Waller factor, hyperfine field,etc. Therefore, production, movements and reactions of the defects can be detected and examined by utilizing all changes arising not only from the probe atom-defect complexes but from their environments. In addition, this method can reduce the measurement-time remarkable, and completely eliminate the mechanical errors in the transducer system and the unavoidable broadening in the spectrum measurement. Accordingly, the existence and movements of point defects were expected to be examined by very small changes in the Mössbauer spectrum which were unrecognizable in the usual spectrum measurements.

The thermal scan method has already been applied to the study of the clustering and process of carbon in iron [30], some results of which are shown in Fig. 1.3 . As is seen in the upper most

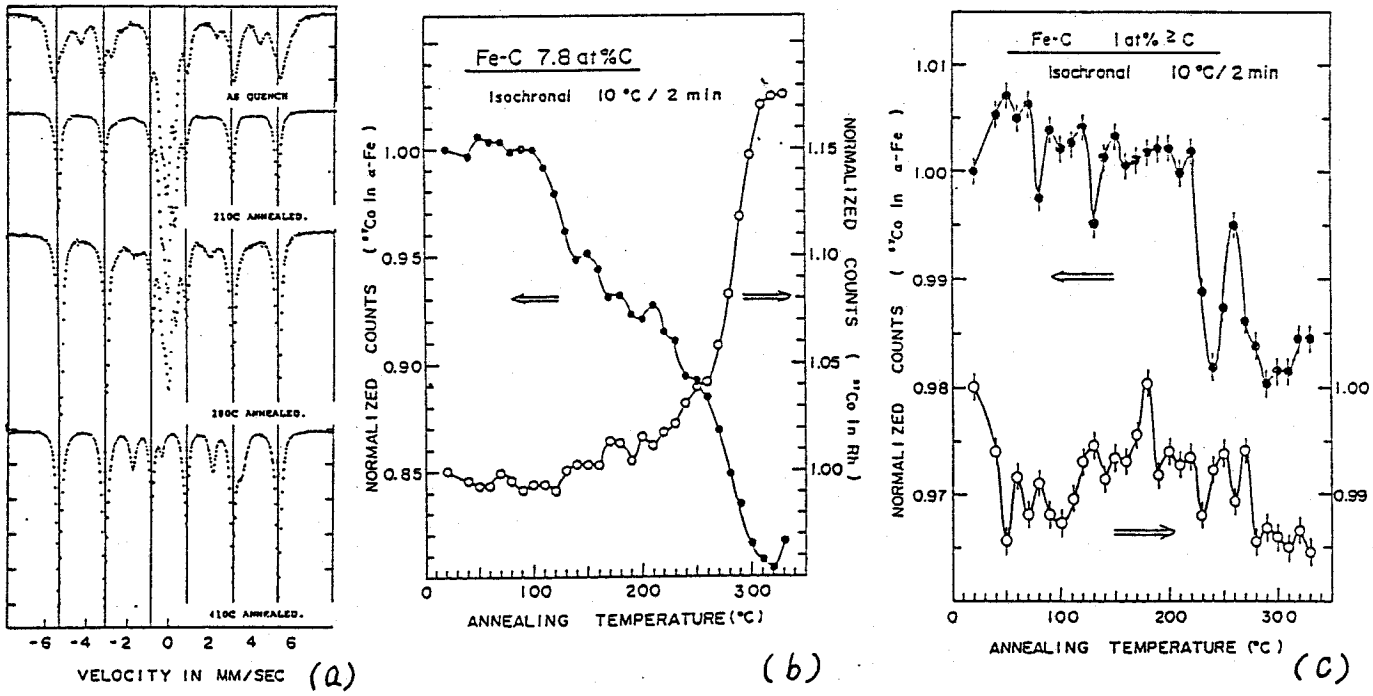

Fig. 1.3 Thermal scan measurements on Fe-C alloys

part of the figure (a), an Fe-7.8at.%C alloy specimen quenched from 1100°C into ices water showed the Mössbauer spectrum consisting of two components; a paramagnetic component arising from the residual Austenite phase, and a ferromagnetic component from the Martensite phase. Both phases contained the super-saturated interstitial carbon atoms, and, therefore, the two components changed during the isochronal annealing due to the clustering and precipitation processes of carbon, as is clearly seen in the other figures in (a). These processes were also clearly observed as the steps in the curves of thermal scan measurement, as shown in the fugure (b), in which an Fe-7.8at.%C absorber specimen, and both the ^{57}Co-in-Fe six line source (open circle) and the ^{57}Co-in-Rh single line source (closed circle) were used alternately for the zero valocity counting. The small changes below 100°C correspond to the clustering process of carbon in the Martensite phase, and the remarkable changes between 100°C and 250°C are due to the precipitation processes of carbon in that phase, and finally those between 250°C and 320°C are the decomposing process of the residual Austenite phase. Even with the low concentration of carbon, as low as 0.5 % , appreciable changes were detected in Fig. 1.3(c).

These thermal scan measurements on the Fe-C system convinced us that the zero velocity counts will be sensitive enough to detect very small changes arising from the defects and defect movements in pure iron spectrum.

1.5.3 Self-ion irradiation

Another possibility to improve the sensitibity to detect the effects of defects was considered by applying the $^{57}Fe^{+}$ self-ion irradiation technique. As shown schematically in Fig. 1.4 , the

projected Mössbauer probe nuclei of ^{57}Fe are expected to produce the defects in the iron lattice, and associate with the defect rich regions consisting of the depleted zone and the interstitial rich zone. So that, the prove nuclei can find the defects with a probability higher than that of the $^{56}Fe^{+}$ irradiation. In the self-ion irradiation, the number of the displacements per atom is very large and the distribution of defects was localized near the specimen surface. Accordingly, the conversion Mössbauer spectroscopy is a powerful tool to detect the effects of defects near the surface. In addition, the specimen after the self-ion irradiation is not radioactive, so that the specimen handlings is much easier than that in the neutron and electron irradiation. The non-activity in the self-ion irradiation will make it possible to observe the irradiated specimen by the electron microscope.

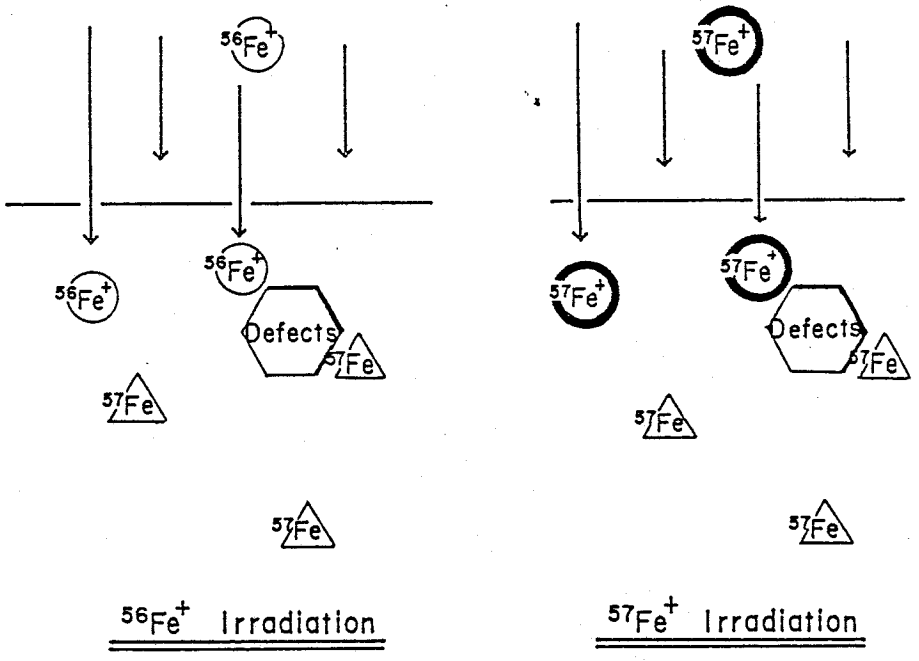

Fig. 1.4 Comparison between $^{56}Fe^{+}$ irradiation

2. EXPERIMENTAL PROCEDURE

2.1 Specemen preparation

In this study, two kinds of iron foils, of which the values of the residual resistivity ratio RRR_H were about 500 and more than 5000, respectivity, were used. Figure 2.1 shows the block diagram of the process of specimen preparation. The ultra-high purity iron with $RRR_H = 5000$ was supplied by Prof. Igaki in Tohoku University. The high purity iron foils $RRR_H = 500$ were prepared

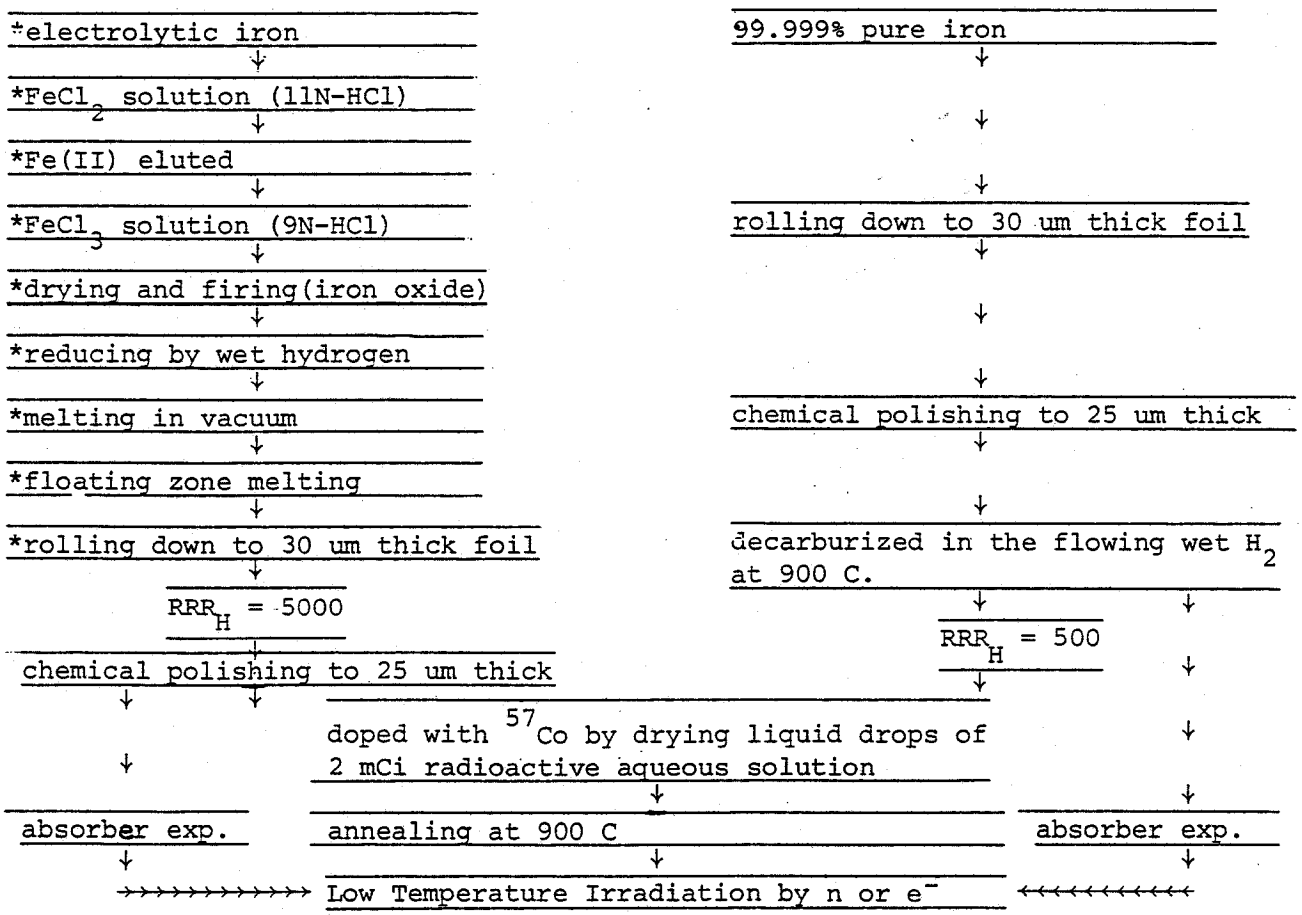

Fig. 2.1 Block Diagram for Specimen Preparation

The specimen preparations with * mark were done at Igaki Laboratory.

in our laboratory. For the Mössbauer source experiment, doping of ^{57}Co into the specimens withour injuring their purity otherwise was required. In the following paragraphs, the purification and ^{57}Co doping technique are presented.

2.1.1. Purification of iron

Because of the high sensitivity of point defects to interstitial impurity, like carbon, the purification of iron is very important in order to investigate the nature of point defects in pure iron. The influences of carbon impurities to the nature of point defects were already discussed in the section 1.2.

99.999 % pure iron was rolled down to 30 μm thick foils, and polished chemically to 25 μm thick foils in order to remove the contaminations during rolling treatment. The purification of iron foils were performed by using a electric furnace as shown in Fig. 2.2 . The foils were held in an open quartz tube in the furnace

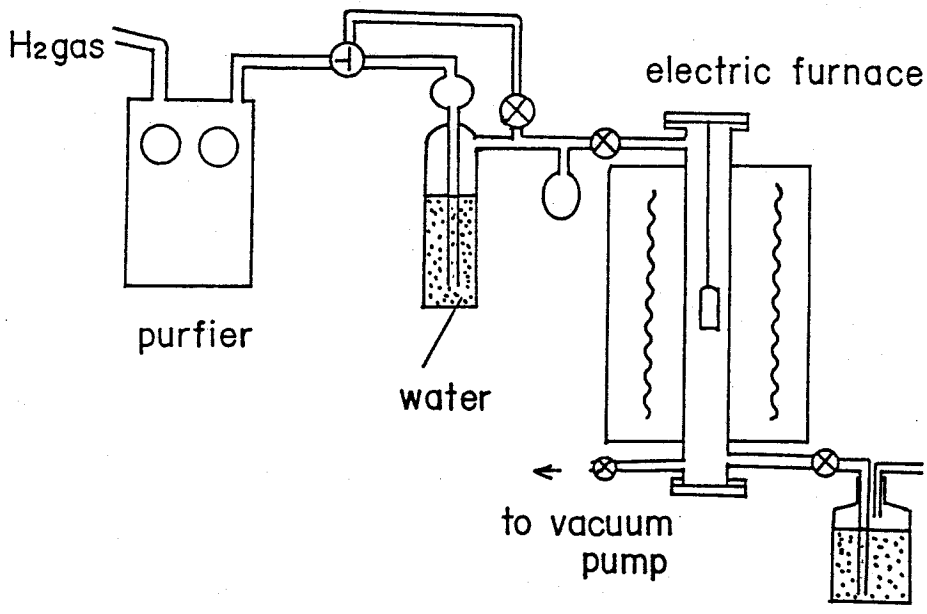

Fig. 2.2 A sketch of the electric furnace for specimen purification

by using an iron wire, and decarburized in the flowing wet H_2 gas was purified by using the Palladium filter method, and passed through water in order to avoid the contamination of the specimen by Si of quartz tube [73,74]. After the above purification, the RRR_H became from about 100 to 500, which was checked by a simmilar ribon specimen for measuring the resistivity hanged together with the main specimen. For the absorber experiments, no other treatments were done on the foil specimens after this purification.

2.1.2. Doping technique of ^{57}Co for source experiment

2 or 3 drops of 2 mCi $^{57}CoCl_2$ aqueous solution were put on the foil surface and dried by a small lump in a closed vessel as shown in Fig. 2.3 . The foil was annealed in the flowing H_2 gas at 900 °C for 6 hours in order to let the isotope diffuse in it, and the remnant Co isotope on the specimen surface was washed off Acetone. After doping ^{57}Co into Fe foil, the Mössbauer spectrum at 77K showed a perfect six line profile as in Fig. 2.4 , indi-

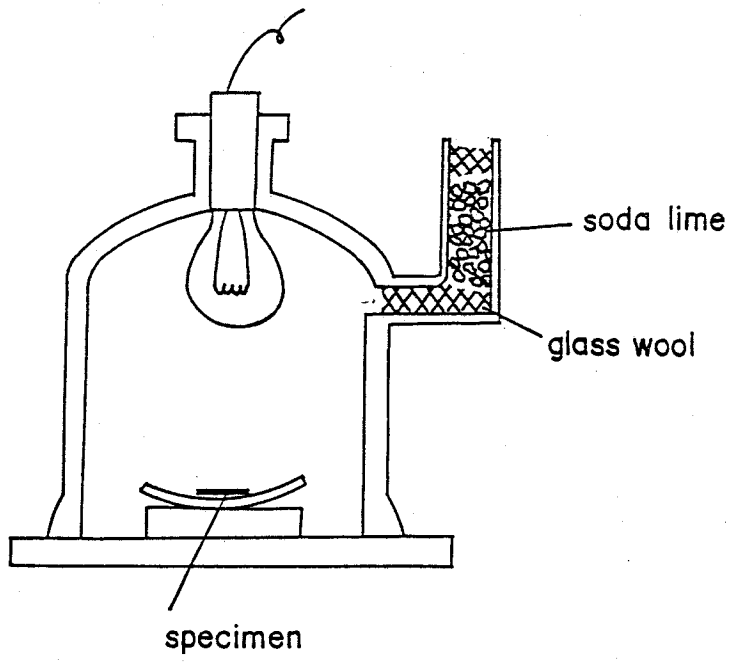

Fig. 2.3 A sketch of the closed vessel for drying liquid drops of $^{57}CoCl_2$ solution

cating that the ^{57}Co atoms were randomly distributed on substitutional sites in the iron matrix and clustering, precipitation, or internal oxidation did not take place.

Table 2.1 shows the typical technical data of ^{57}Co used in the doping. The sample dimensions were $15 \times 15 \times 0.025\ mm^3$. The total amount of ^{57}Co with the radioactivity of 2 mCi correspond to the concentration of 5 at ppm of ^{57}Co in the iron foil of the above dimensions. Taking account of the vaparization of ^{57}Co during the annealing, the concentration of ^{57}Co in the specimen was estimated to be about 3 ~ 4 at ppm.

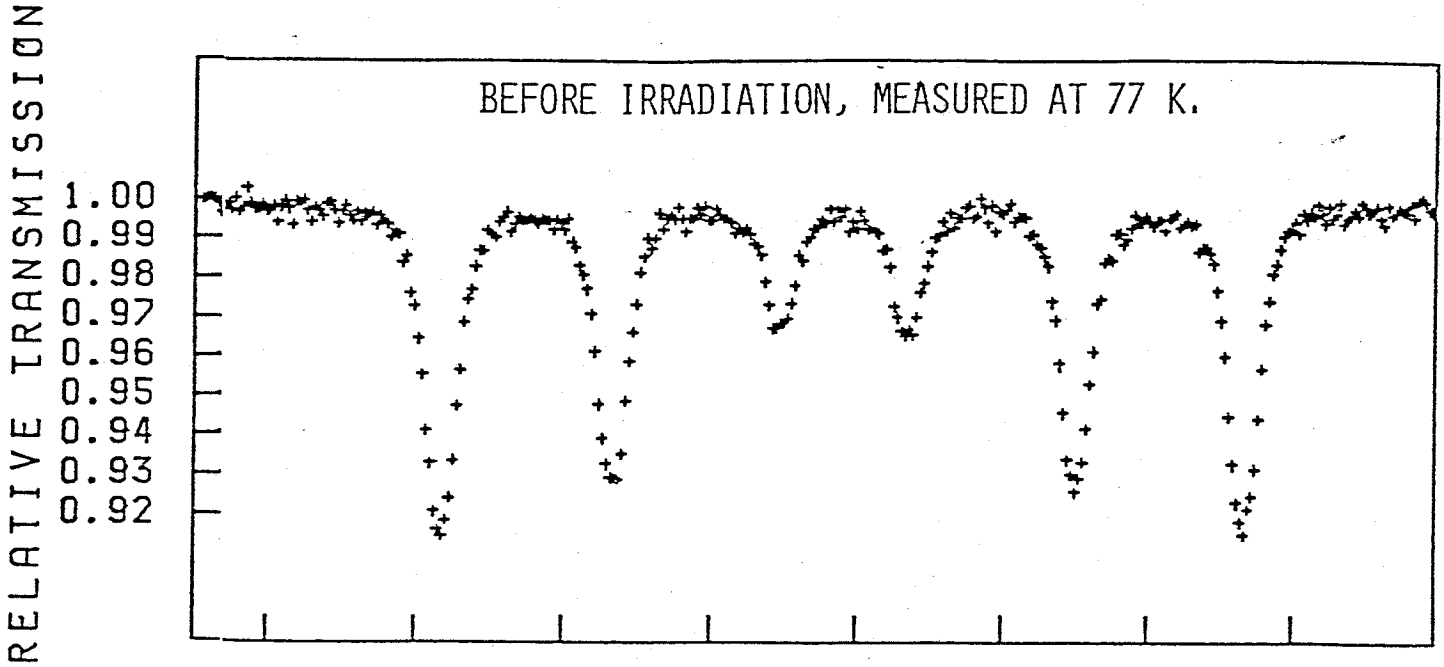

Fig. 2.4 Mössbauer spectrum before irradiation at 77 K of iron dopen with ^{57}Co

Chemical form: $CoCl_2$ in 0.5 N HCl solution	Radiochemical purity: 99 %
Activity: 2m Ci	Radinuclidic purity: 99 % Co-58 0.02 %
Radioactive concentration: 20 mCi/ml	Co-56 0.081 %
Specific activity: > 4 mCi/µg	Volume: 0.1 ml

Table 2.1 Technical data of ^{57}Fe radio-isotope used in the doping.

2.2 Irradiation Techniques

We used three kinds of irradiation techniques; reactor neutron irradiation, LINAC electron irradiation, and self-iron ($^{56}Fe^{+}$, $^{57}Fe^{+}$) irradiation. The neutron and the electron irradiations were performed at Research Reactor Institute of Kyoto University, Kumatori (KUR). The self-ion irradiations were performed at Electrotechnical Laboratory Headquarters, Department of Commerce and Industry, Tsukuba.

2.2.1 Reactor neutron irradiation

Figure 2.5 are the schematic diagrams of the low temperature irradiation facility at KUR; Figure 2.5(a) shows the arrangement of the low temperature loop in the neuclear reactor, KUR-1, and Fig. 2.5(b) a cross section of the low temperature loop. The specimens were put in a capsule made by Aluminum, which is shown in Fib. 2.6 , and the capsule was inserted by using a boat from the bottom of the inlet of the loop and to the top of the loop, where the specimens were irradiated in an atomosphere of refrigerated He gas. The He gas was refrigerated down to 10 K by the refrigerator with the capacity of 30 watts at 10 K . The irradiation temperature during the operation of 5 MW was about 30 K. After irradiation typically for 77 hours, the specimens were took out by dropping down into a liquid nitrogen vessel in the flowing refrigerated He gas at 10 K , transfered to another container, and kept there until the Mössbauer measurements.

The maximum irradiation dose was 6.6×10^{16} fast neutrons/cm^2 and 6.1×10^{17} thermal neutrons/cm^2 with the normal reactor operation cycle for 77 hours. All values of the total dose were summarized in the Table 2.2 .

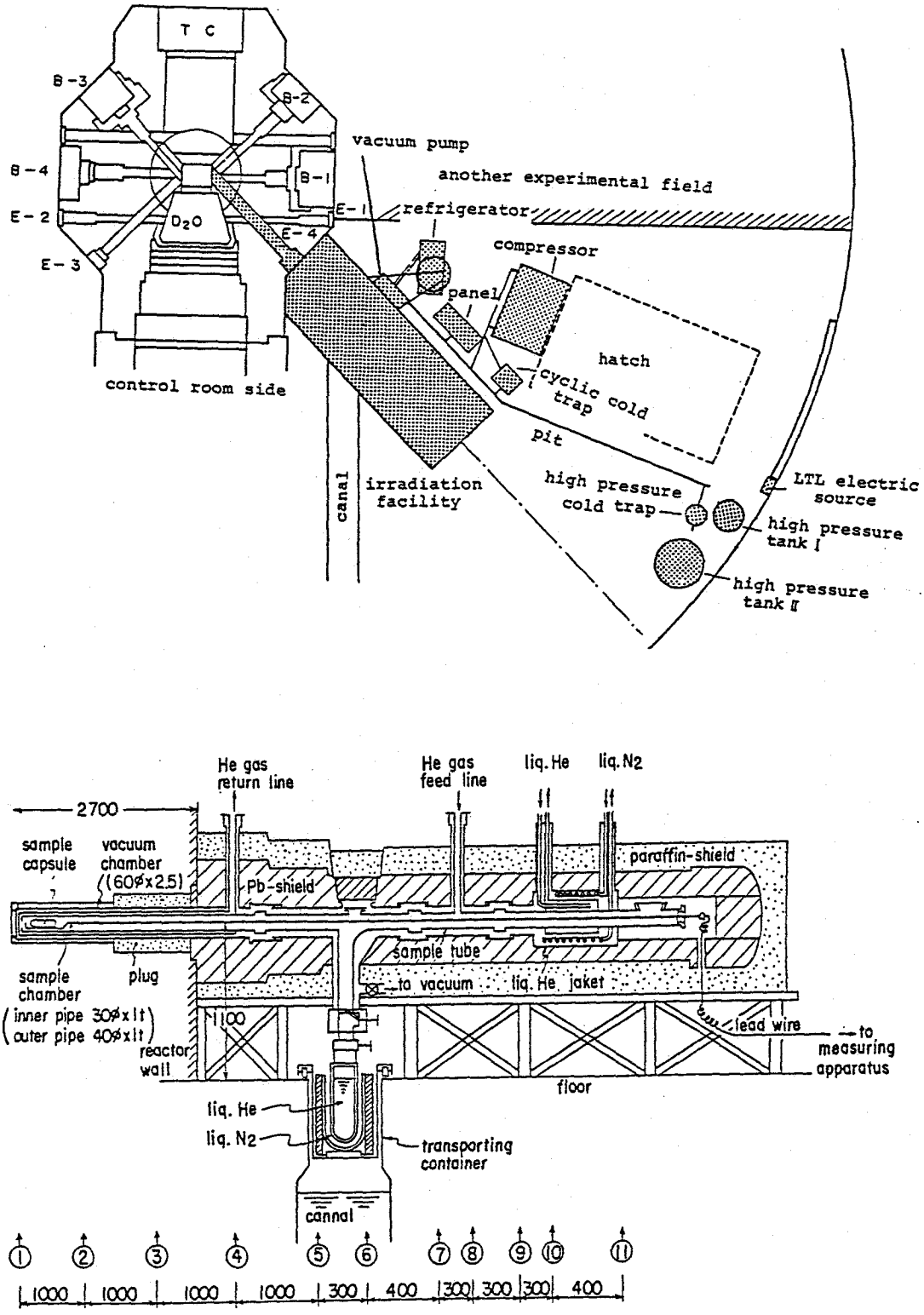

Fig. 2.5 Schematic diagrams of the low temperature neutron irradiation facility at KUR; (a) the ground plan of the low temperature loop, (b) a side cross section of the low temperature loop

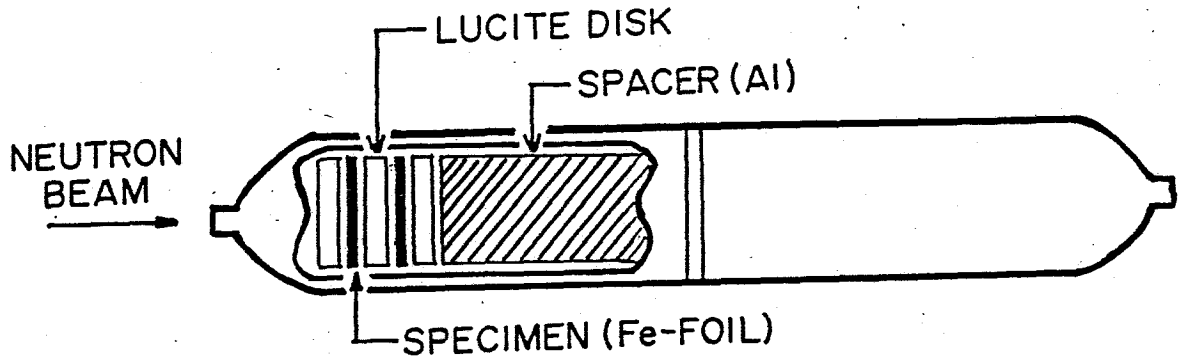

Fig. 2.6 A sketch of specimen capsule for neutron irradiation

NO.		IRRAD. TEMP.	FLUX ($n/cm^2/sec$)	FLUENCE (n/cm^2)	SPECIMENS	MEASUREMENTS
1	n	30 K	2×10^{16}	1.3×10^{11}	Fe doped ^{57}Co	spectrum at 90 K thermal scan (10deg/5min)
2	n	30 K	5×10^{16}	2.6×10^{11}	Fe doped ^{57}Co	spectrum at 4.2 K thermal scan
					Fe	spectrum at 77 K
					Fe-C	spectrum at 77 K
3	n	30 K	5×10^{16}	2.6×10^{11}	Fe doped ^{57}Co (U.H.P)	spectrum at 4.2,77 K thermal scan
					Fe	spectrum at 77 K
4	n	30 K	?	?	Fe-C	**********

Table 2.2 Total dose of neutron irradiations.

2.2.2 LINAC electron irradiation

Linear Accelerator (LINAC) KUR has been designed and constructed as a neutron source prodeced by (γ,n) reaction, but it is available for high energy electron irradiation of materials, too. The acceleration voltage of electrons is variable between 20 and 46 MV. The electrons are accelerated in a series of pulses, of which the pulse width and the number of repetitions are 1 ~ 5 μsec, 1 ~ 100 pulses per second, respectively, and the maximum peak current is 0.5 A. Since the target area against the electron beam is about 10 mm × 10 mm, the electron dose rate on the specimen is about 1.6×10^{18} electrons/cm^2·sec in the macimum. However, this amount of dose rate on the specimen was far beyond the cooling capacity of the cryostat, so that the dose rate was controlled at a certain low level as will be mentioned below.

The low temperature irradiation cryostat in KUR LINAC has been constructed by the groups of Prof. K. Kitajima of the Research Institute for Applied Mechanics, Kyushu University, and Prof. H. Yoshida of KUR [75]. As the irradiation temperature is liquid nitrogen temperature, which is below stage I in pure iron, the irradiation can be performed without allowing the free migration of self-interstitials in pure iron except for a radiation induced diffusion.

Figure 2.7(a) shows a schematic diagram of the chamber and controlling system for liquid nitrogen temperature irradiation, and Fig. 2.7(b) the specimen holder. The specimens were dipped and irradiated in the flowing liquid nitrogen supplied from the liquid nitrogen vessel at the outside of the target room; the liquid nitrogen is transfered from the tank 1, kept for a while in the tank 2, and fed to the cryostat as shown in the figure (a), in

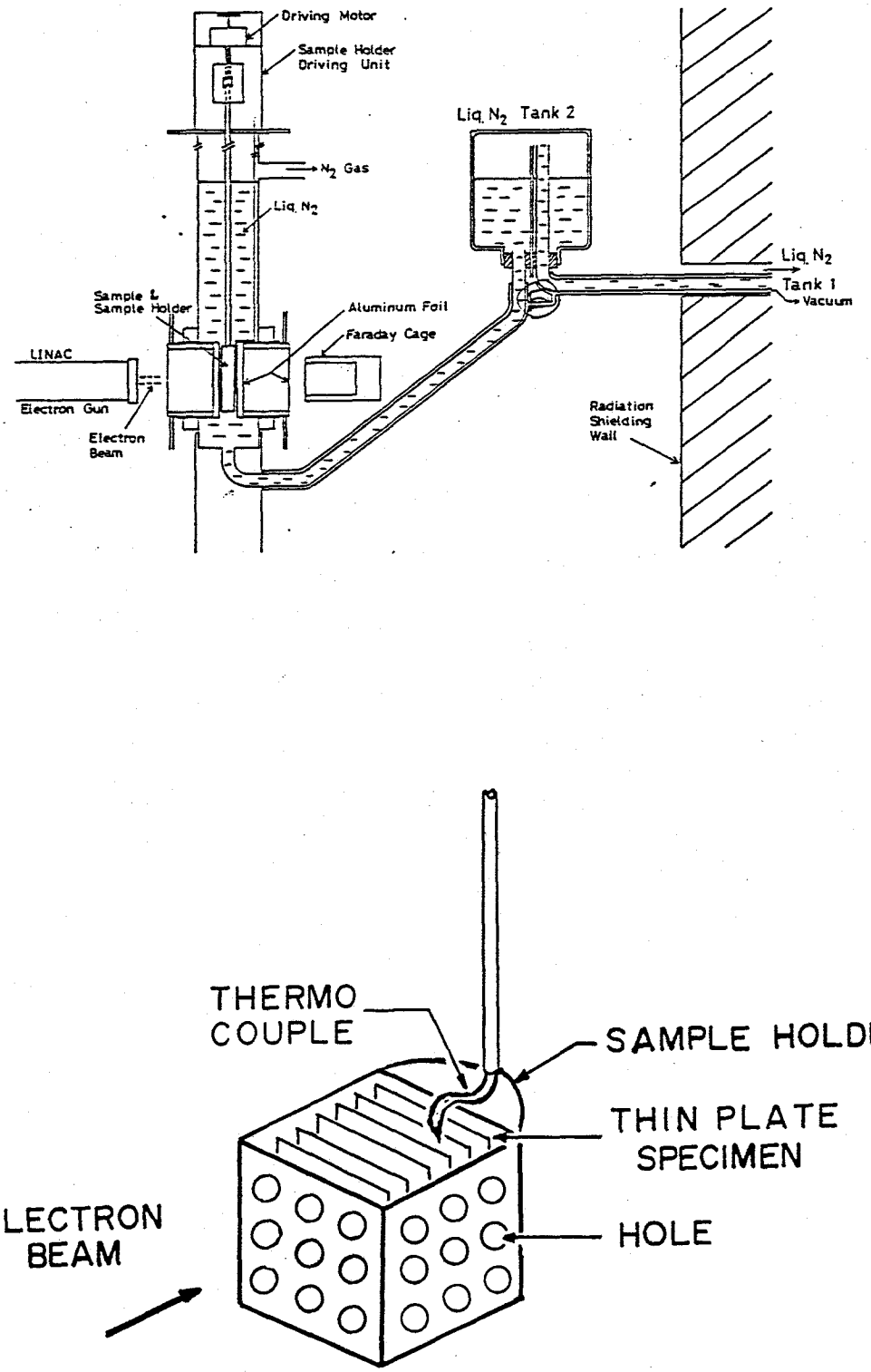

Fig. 2.7 Schematic diagrams of the low temperature electron irradiation system, LINAC at KUR; (a) the target chamber and controlling system for liquid nitrogen temperature irradiation, (b) the specimen holder

order to keep the liqid nitrogen level during irradiation above the specimen bolder in the irradiation chamber. The temperature at the points denoted by Roman letters in Fig. 2.7(a) were monitored and indicated in the controll romm during irradiation so as to controll the amount of flowing liquid nitrogen. The irradiation temperature of the specimens was measured by using a copper constantan thermocouple which was spot-welded on the monitor specimen.

Table 2.3 shows the irradiation conditions of LINAC emploed in the present experiment. The electron energy was so high that the electron penetration depth reached to the order of 1 cm and, therefore, it was possible to irradiate many specimens at the same time by using a multi-specimen holder as in Fig. 2.7(b). The sample dimension used in the LINAC electron irradiation were typically $12 \times 12 \times 0.025\ mm^3$. The electron fluence was monitored by the sum of the currents which flowed from the ground to the cryostat and the Faraday cage. All values of the total dose are summarized in the Table 2.4 .

After the irradiation, the specimen holder was taken out of the cryostat by transfering to a small liquid nitrogen backet, disintegrated in liquid nitrogen, and then the specimens were kept in the liquid nitrogen vessel until the Mössbauer measurements.

Accelerated Energy	28 MeV	Irradiation Times	30 hours
Repitition Times	30 pps	Irradiation Temperature	80 K
Pulse Width	3 usec	Resultant Dose Rate	1.0×10^{17} e/cm^2.sec
Peak Current	180 mA		

Table. 2.3 Condition in LINAC irradiation

NO.		IRRAD. TEMP.	FLUX ($e/cm^2/sec$)	FLUENCE (e/cm^2)	SPECIMENS	MEASUREMENTS
1	e^-	77 K	2×10^{18}	1.9×10^{13}	Fe	spectrum at 90 K
2	e^-	77 K	2×10^{18}	1.9×10^{13}	Fe doped ^{57}Co	spectrum at 77 K
						thermal scan
					Fe	spectrum at 77 K
3	e^-	77 K	2×10^{18}	1.9×10^{13}	Fe doped ^{57}Co (U.H.P)	spectrum at 4.2,77 K
					Fe doped ^{57}Co	spectrum at 77 K
					Fe	spectrum at 77 K
					Fe doped ^{57}Co	thermal scan (10deg/5min)

Table 2.4 Total doses of electron irradiations

2.2.3. Ion implanter self-ion irradiation

The Cockrofr-Walton type ion accelerator in the Electrotechnical Labaratory, Tsukuba, shown in Fig. 2.8, was used for the self-ion irradiation. This accelerator is ususally used as the ion-implanter, by which many kinds of donor or acceptor ions are implanted into semiconductors in the basic and applied studies for the development of various electronic devices.

The ion energy is variable from 30 to 400 keV, and the ion fluence, which depends on the conditions of the ion source, is about 0.05 to 3.0 μA . The ion source were natural Fe foils and $^{57}Fe_2O_3$ powder for the $^{56}Fe^+$ irradiation and $^{57}Fe^+$ irradiation, respectively. The ion energy of Fe^+ was 200 keV, which corresponds to the projected range of 550 A according to the calculation by the E-DEP-I computer program [69]. The ions in the state of plasma in a source chamber are taken out with the energy of 30 keV, and the ions are separated by the mass separator, accelerated up to 200 keV, and deflected in a phase shifting Lissarfous's figure in order to get the homogeneous ion density on the specimen surface. After monitoring the profile and the fluence of the ion beam, the ions are introduced to the specimen for irradiation. The beam size is 16 mm in diameter. The resolution in mass separation was high enough to separate $^{57}Fe^+$ ions from $^{56}Fe^+$ ions.
The sample chamber was evacuated to a vacuum of $5.0 \sim 10.0 \times 10^{-7}$ Pa by turbomolecular pump. Accordingly, the oil free atmosphere was obtained and the effect of contamination by carbon during irradiation was negligible.

The specimen holders made of oxygen freee copper for irradiation are shown in Fig. 2.9 . Figure 2.9(a) that for the specimens of

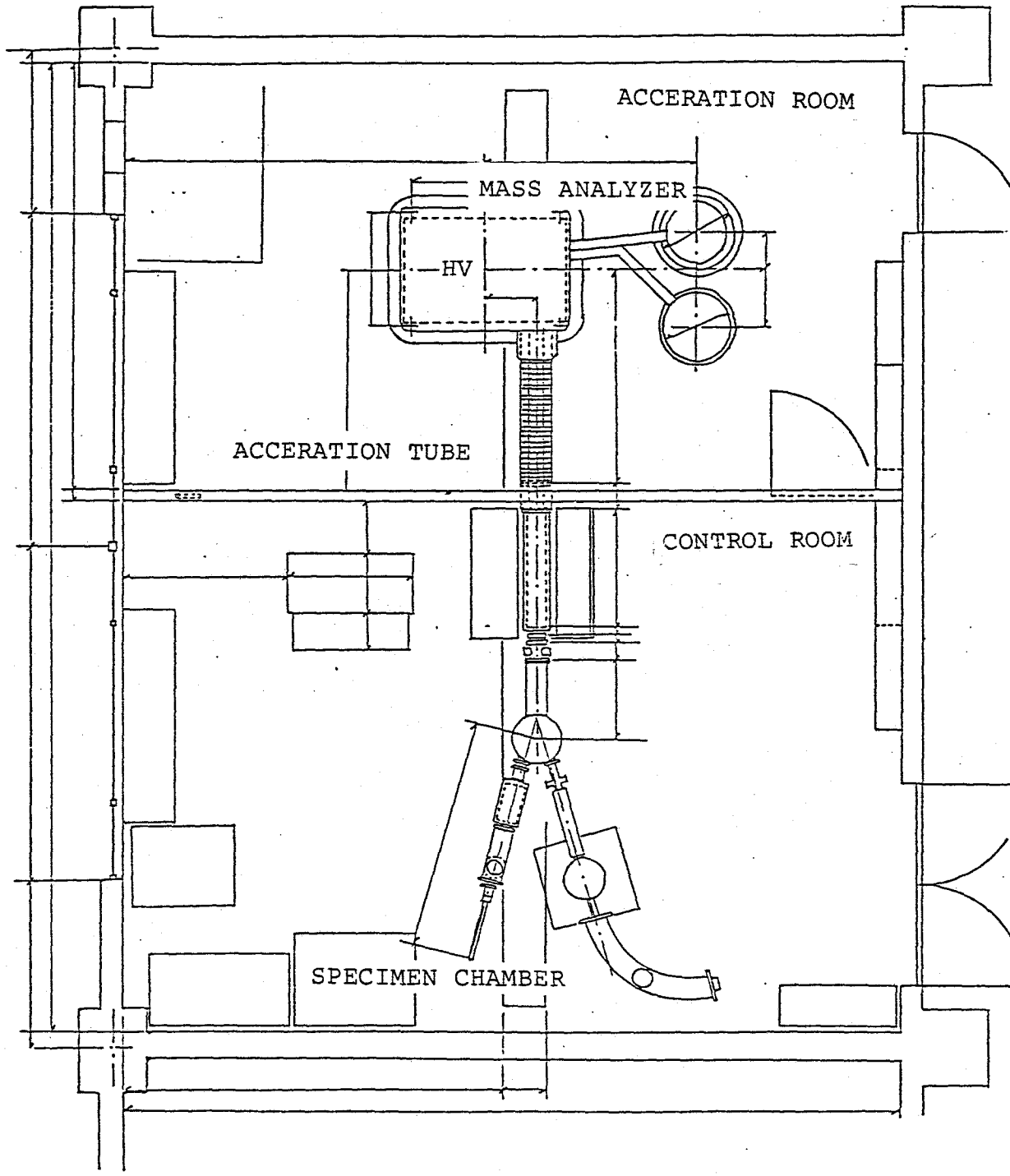

Fig. 2.8 Crockroft-Walton type ion accelerator in the Electrotechnical Laboratory, Tsukuba

electron microscopy. The holder block was attached to another copper block with small screws and the assembly was set in the irradiation chamber. The exchange of the specimens was easily done through the pre-evacuation chamber. The machine shut down time for the specimen exchange was typically 1 hour.
The irradiation temperature was room temperature, but a small increase of the temperature of the specimen holder was observed after irraditaion. The specimen temperature could not be measured directly because of the generation of the noise in the thermocouple EMT due to the stray current during irradiation. The average irradiation fluence, the irradiation flux, the temperature of the specimen holder after irradiation, the projectile and the specimens are summarized in Table 2.5 .

After irradiation, the specimens were taken out from the holder and kept in an evacuated container before the Mössbauer spectroscopy and electron microscopy. No induced activity was observed after irradiations.

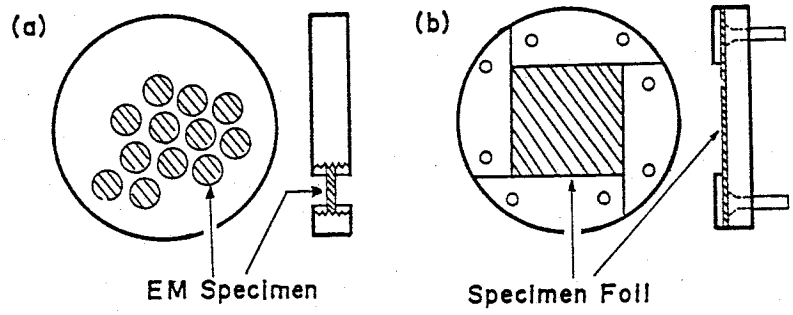

Fig. 2.9 Sketch of the specimen holders of self-ion irradiation at room temperature; (a) for Mössbauer measurement, (b) for electron microscope observation

NO.	MEASUREMENTS	ION	FLUX (IONS/cm^2/sec)	FLUENCE (IONS/cm^2)	dpa	FINAL TEMP.
1	EM	$^{56}Fe^+$	1.4×10^{15}	1.0×10^{15}	4	----
2	EM	$^{57}Fe^+$	3.0×10^{11}	5.0×10^{14}	2	33°C
3	EM	$^{57}Fe^+$	2.8×10^{11}	1.0×10^{14}	0.4	25°C
4	Möss.	$^{56}Fe^+$	8.8×10^{12}	5.0×10^{16}	250	52°C
5	Möss.	$^{57}Fe^+$	8.6×10^{12}	4.6×10^{12}	180	48°C

Table 2.5 Total doses of self-ion irradiation.

2.3 Mössbauer Measurements

Classifying roughly as shown in the left hand side of Fig. 2.10 , two different Mössbauer techniques were used in the present investigation; one is the measurement of the Mössbauer spectrum and the other the thermal scanning as will be explained below. The spectrum measurement is further classified into the transmission method and the scattering method, and, more precisely speaking, the transmission method can be applied to the source experiment and the absorber experiment accordint to the kind of the specimen, the source specimen or the absorber specimen, as are seen in the upper right of the diagram. This classification is also applicable to the thermal scan method. But, the scattering method is not suitable for thermal scan since the counter is not always susceptible to the temperature change. The scattering method for the spectral measurement was used only for the absorber specimen irradiated by self-ions.

This section is devided into four parts dealing separately with the transmission method for the measurement of the Mössbauer spectrum, the scattering method by using conversion electrons, the

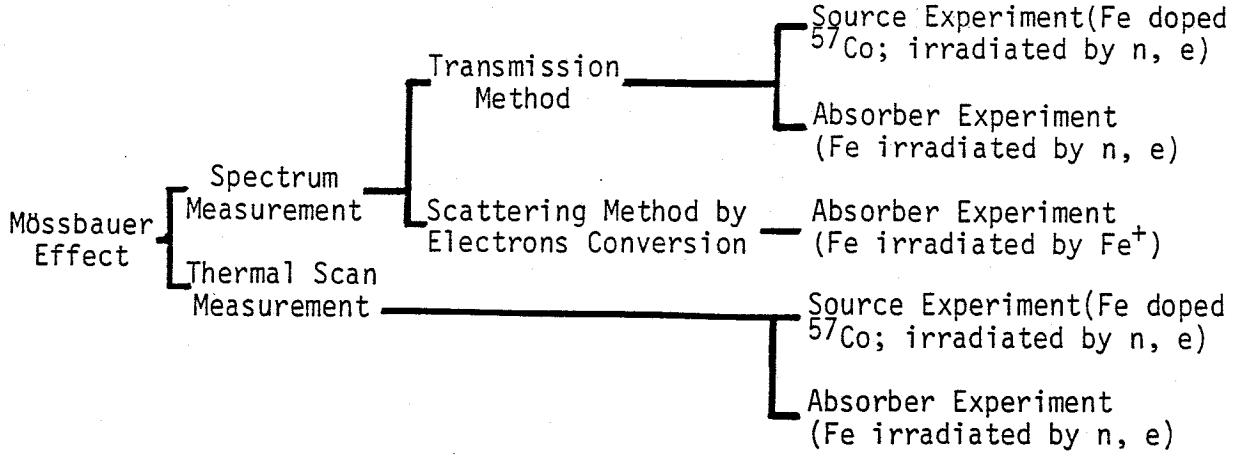

Fig. 2.10 Diagram of various methods for the measurement of Mössbauer effect

thermal scan method, and the temperature control and heat treatment techniques. All measurements using the specimens irradiated with neutrons, electrons were performed at KUR because the specimens were radioactive after the irradiations.

2.3.1. Transmission method for the measurement of Mössbauer spectrum

2.3.1.a) General methods for gamma-ray detection and velocity-drive system

A large number of literatures on the Mössbauer equipments are available today [31-35]. Therefore, the principle of the Mössbauer spectrometer used in this investigation is briefly described below. A block diagram illustrating the principle of the equipment is given in Fig. 2.11 . The source emitting Mössbauer γ-quantums, shown in the right bottom of the diagram, is moved relative to the absorber by using a drive system in the absorber experiment in order to impart an additional Doppler velocity to the γ-quantums. In the source experiment in the present study, the source stands still in the cryostat and the absorber is moved relative to the source. The γ-rays are resonantly absorbed by the Mössbauer nuclide in the absorber during transmitting it, and the number of unaffected γ-rays is counted by a proportional counter.

The velocity transducer consists of the rigidly connected driving and pick-up coil moving in a homogeneous magnetic field. The transducer is driven in the constant acceleration mode at about 6 Hz with a symmetric sawtooth current so as to minimize the difference between the reference signals and the induced pick-up signals by using a negative feedback system.

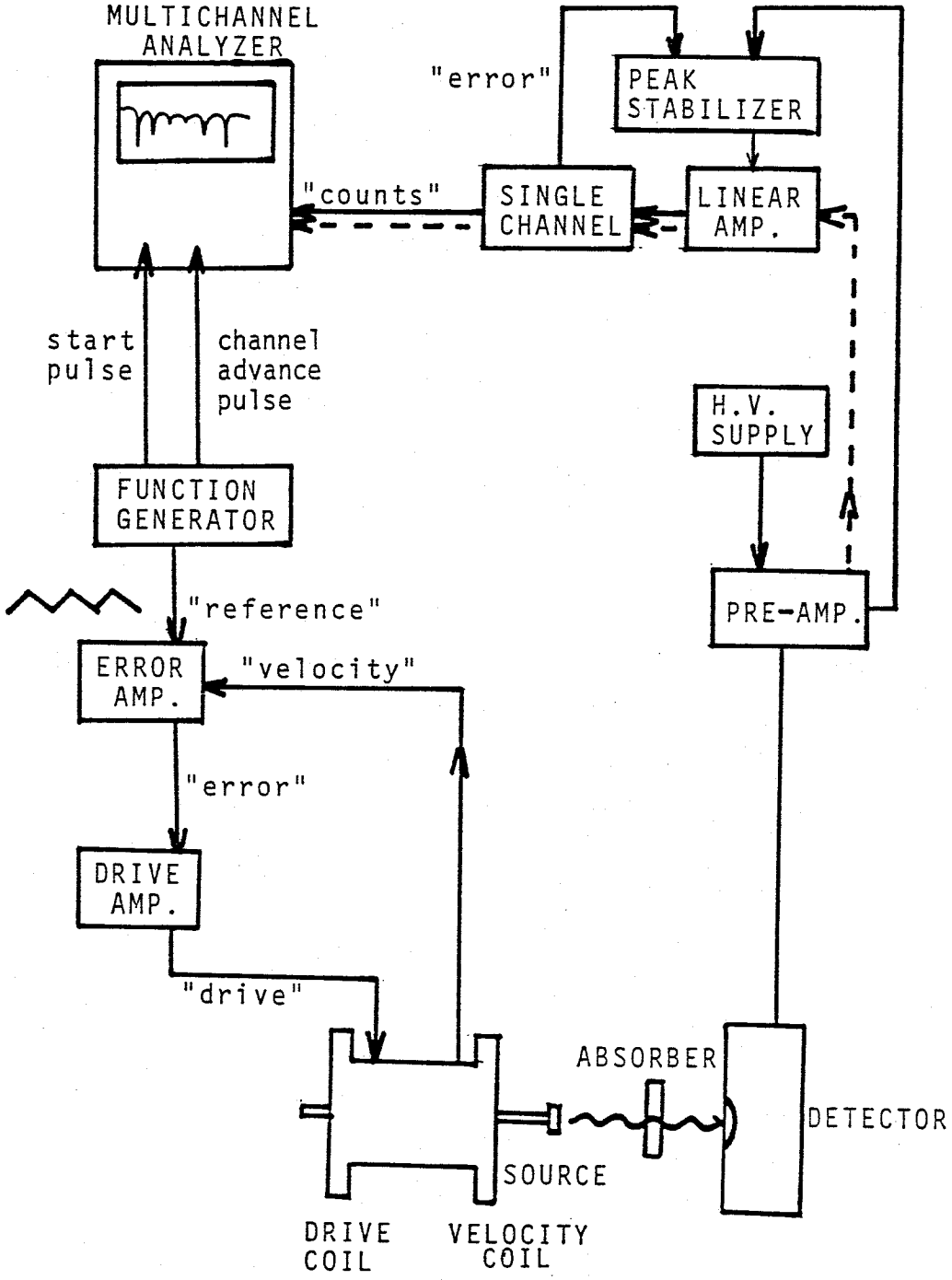

Fig. 2.11 Block diagram illustrating the principle of Mössbauer measurement

The 14.4 keV γ-ray is detected by a 2-in.-diameter Xenon-filled proportional counter coupled to a preamplifier. Further pulse counting and handling was done with a peak-stabilizer, a linear-amplifier and a single-channel analyzer, which are illustrated in the upper right of the figure. The stabilizer plays an important role for the precision comparison of the total resonance areas of different Mössbauer spectra or the measurement of the changes in the count-rate, in which it is required to keep a constant signal -to- noise ratio during the measurement. A detailed description the stabilizer will be given later.

The detected counts are stored in a multichannel analyzer with 1024 channels. The synchronization of the channel number selection in the multichannel analyzer with the transducer velocity is performed by using the start pulse and the channel-advance pulse from the function generator, which is, at the same time, used for the control of the transducer movement.

2.3.1.b Source experiments

Figure 2.12 shows the schematic block diagram of the measurement equipment for the transmission Mössbauer spectrum in the source experiment. During each measurement the velocity of the absorber was checked by measuring simultaneously the Mössbauer spectrum of a ^{57}Co-in-Rh source mounted on the other end of the drive axis, so that the drift of zero point and velocity scale during measurement was precisely monitored. The drift definitely disturves the analysis by subtracting Mössbauer spectrum before annealing from that after annealing as will be mentioned in §2.4 . Two kinds of the absorber were used in taking the transmission Mössbauer spectra; stainless steel foil with 25 μm thickness and natural Fe foil with

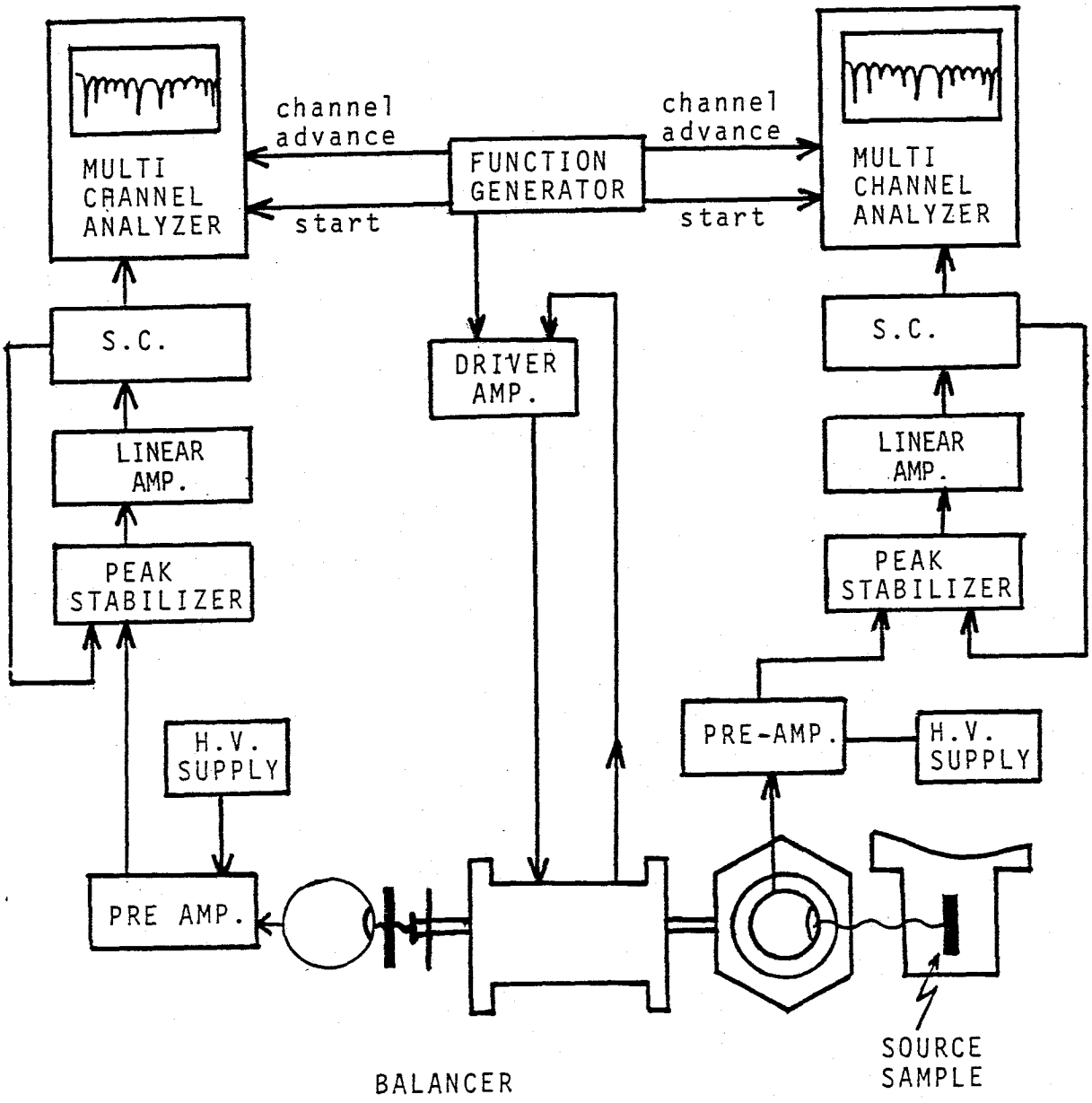

Fig. 2.12 Block diagram of the measurement system for the transmission Mössbauer spectrum in the source experiment

20 μm thickness. The distance between the absorber and the source specimen in the cryostat was about 10 cm.

The 14.4 keV γ-ray was detected by a 2-in.-diameter Xenon-filled proportional counter with a bias high voltage of 2500 V. The source specimen was put between lucite disks with 1 mm thickness, and the absorber between lucite disk and myler sheet in order to reduce the intensity of the low energy X-rays. Figure 2.13 shows a typical gamma-ray spectrum of the source specimen irradiated by neutrons, as obtained through the resonant absorber of the stainless steel foil. The 14.4 keV gamma-ray is clearly visible, its signal-to-background ratio being of the order of 6:1, so that the increase of the background just after the neutron irradiation was negligibly small. Then, the comparisons of the total resonance area before and after irradiation become possible as will be discussed later.

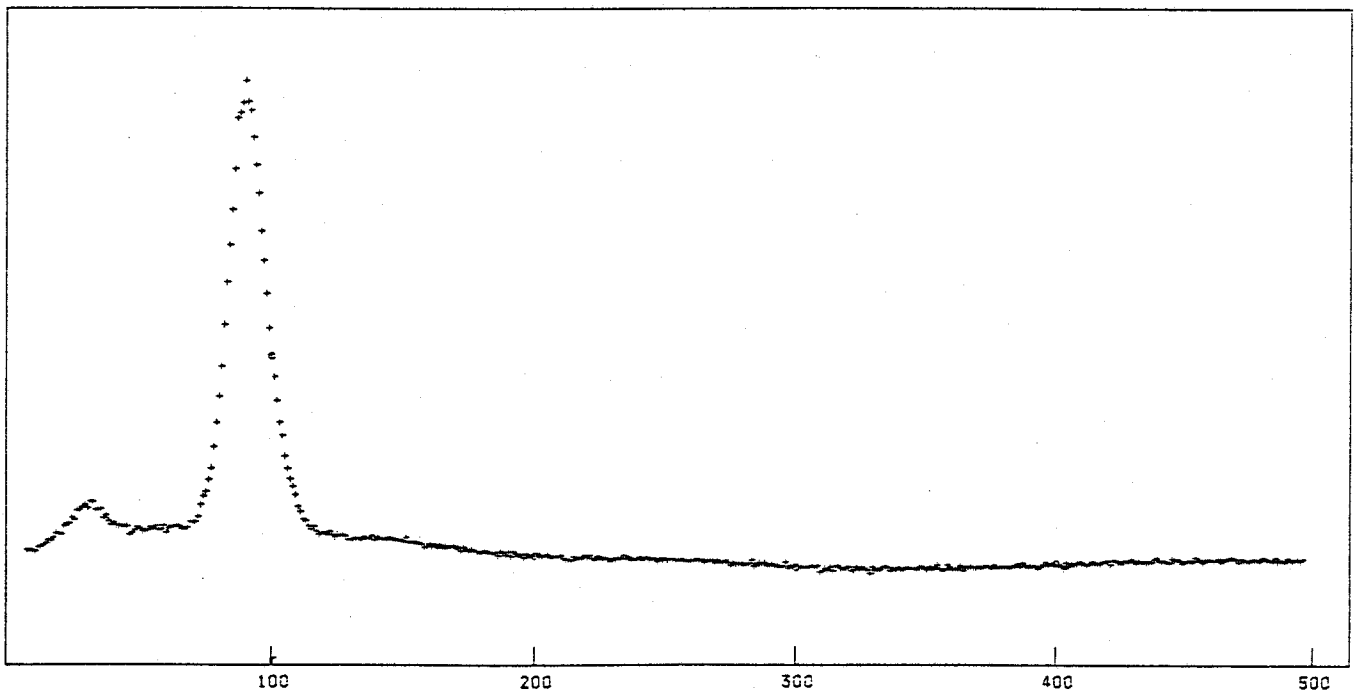

Fig. 2.13 Typical γ-ray spectrum of ^{57}Co in Fe through stainless steel absorber

The absorber was attached on an absorber holder as shown in Fig. 2.12 . Not to perturb the regular smooth vibration of the transducer, the holder was made of a light Aluminum frame with 1 mm thickness, and a lead plate was mounted as a balancer on the other end of the drive axis, close to the ^{57}Co-in-Rh calibration source. The full width at half maximum (FWHM) of the spectrum, obtained from a 25 μm thick pure Fe foil absorber by using the ^{57}Co-in-Rh source , was about 0.41 mm/sec.

An unfolded Mössbauer spectrum of the ^{57}Co-in-Fe source with an stainless steel absorber taken by the symmetried sawtooth driving mode is given in Fig. 2.14 . The Mössbauer spectrum was measured twice in one period of the triangular wave, and two folded up about the center axis of the whole figure so as to cancel the parabolic background originated from the relative motion between the source and the absorber. Only the folded spectra will be used in the following sections in this paper.

2.3.1.(c) Absorber experiments

The block diagram of the transmission method in the absorber experiment have already been shown in Fig. 2.12. The 30 mCi ^{57}Co-in-Rh standard source was given the Doppler motion relative to the absorber specimen in the cryostat. The typical value of the FWHM was 0.353 mm/sec for the pure Fe foil absorber with 25 μm thickness measured at room temperature. Details of the technique for the measurements of the Mössbauer spectra in the absorber experiment were simmilar to those of the source experiment already described before.

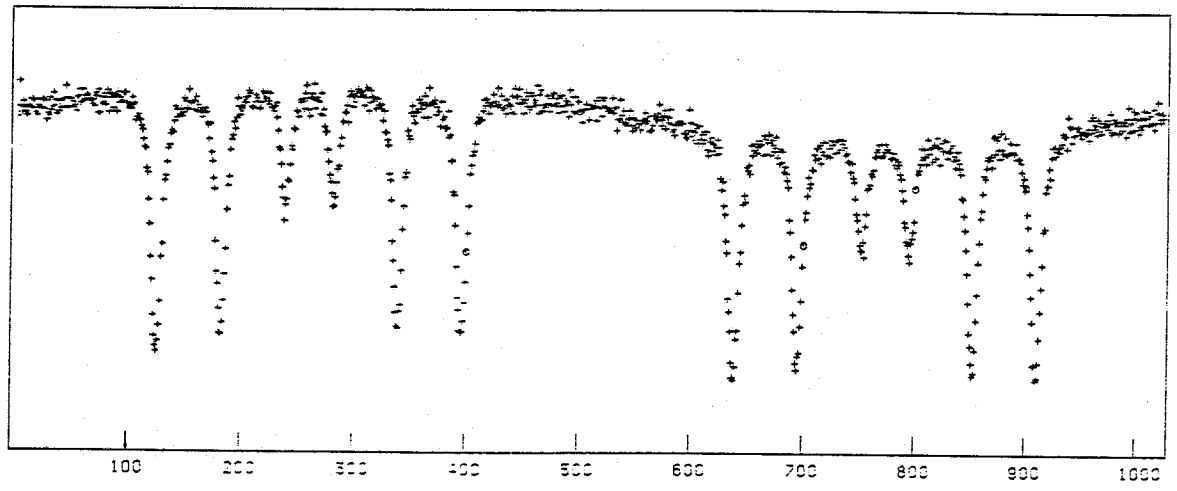

Fig. 2.14 Unfolded Mössbauer spectrum of the ^{57}Co-in-Fe source with an stainless steel absorber

2.3.2. Scattering method by conversion electrons

In the transmission method, the unaffected γ-rays after transmitting through the absorber are counted as a function of the relative velocity or Doppler velocity between the source and absorber. On the other hand, in the scattering method, the number of the conversion electrons, or the subsequently emitted Auger electrons are detected. Conversion electrons were emitted by the nuclear conversion process after the nuclear resonance absorption by the Mössbauer γ-ray. Re-emission of X-rays and γ-ray excitaion are also available for the measurement, although they were not used in the present investigation. The absorber nuclei of ^{57}Fe excited by the Mössbauer γ-rays from the source will be transmuted into the ground state by the way of the re-emission of gamma rays (10%) and conversion electrons, where the internal conversion co-

efficicent is $\alpha = \omega_e/\omega_\gamma = 8.2$ * . The internal conversion processes are due to the direct electro-magnetic interations between nucleus and arbital electrons; 7.3 keV, 13.6 keV, and 14.3 keV conversion electrons are emitted from the K-shell (79%), L-shell (8%), and L-shell(2%) respectively. The conversion electrons are accompanied by 5.5 keV K-LL Auger electrons (63%), 0.53 keV L-MM Auger electrons (6%) and 6.4 keV X-rays (28%) [76]. The scattering method is especially suitable for the investigation of surface layer, surface reactions, or implantation reactions including the defect productions, because of the small range of low energy electrons in solids, for instance, only about 1000 A in iron metals for 6 keV Auger electrons of Fe.

In order to defect these radiations, a He/ C_4H_{10} quenching gas filled proportional counter shown in Fig. 2.15 ** was used at a bias voltage of 1000 V. The resonant γ-rays from a moving source enter it, and penetrate the absorber specimen on the backwall of the counter. The backward re-emitted electrons are detected in a 2π geometry. The typical energy spectrum obtained from this counter is given in Fig. 2.16, and the schematic diagram of the spectrum measurement system for hte scattering method in Fig. 2. 17 . After selecting the energy range as shown in Fig. 2.13, the count rate per channel was 500 counts/min·channel. The spectrum

---

* The total transition probability is given by $\omega = \omega_e + \omega_\gamma$, where the transition probabilities for emission of gamma rays and conversion electrons are ω_γ and ω_e respectively.

** The counter was made by Dr. s. Nasu

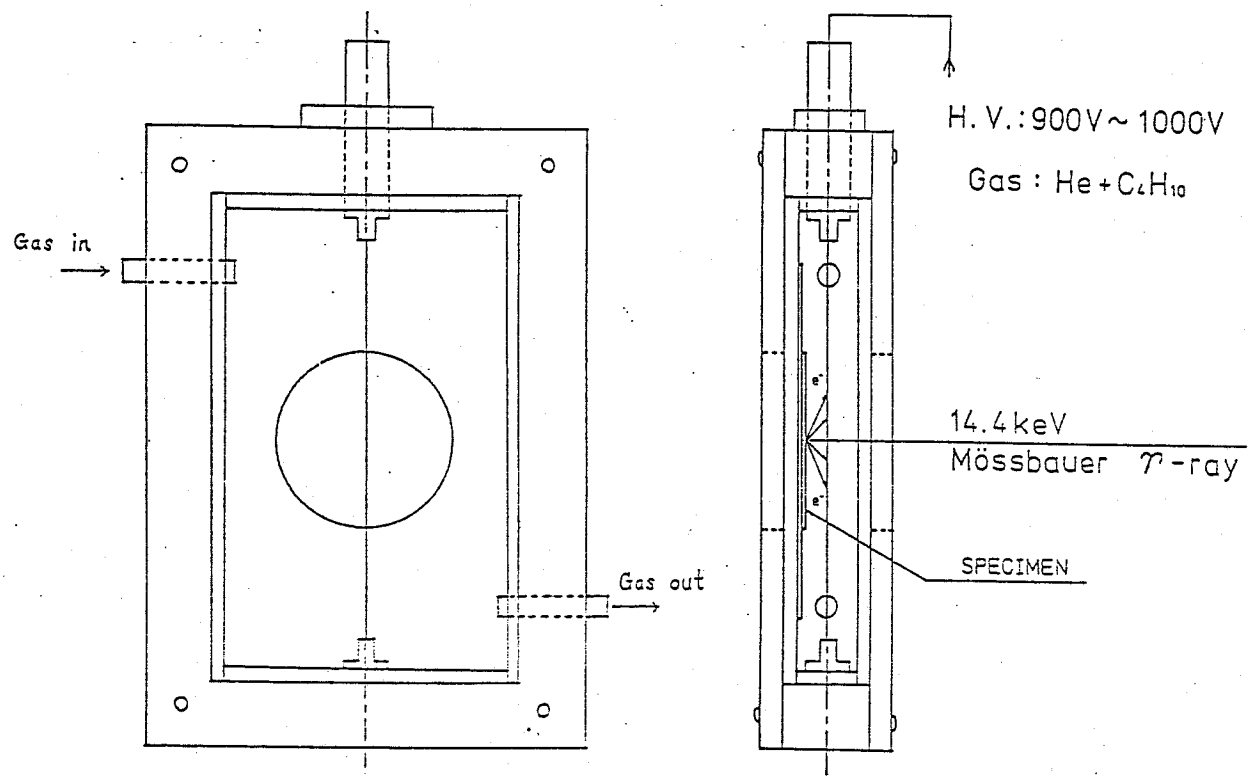

Fig. 2.15 A sketch of gas-flow-type proportional counter

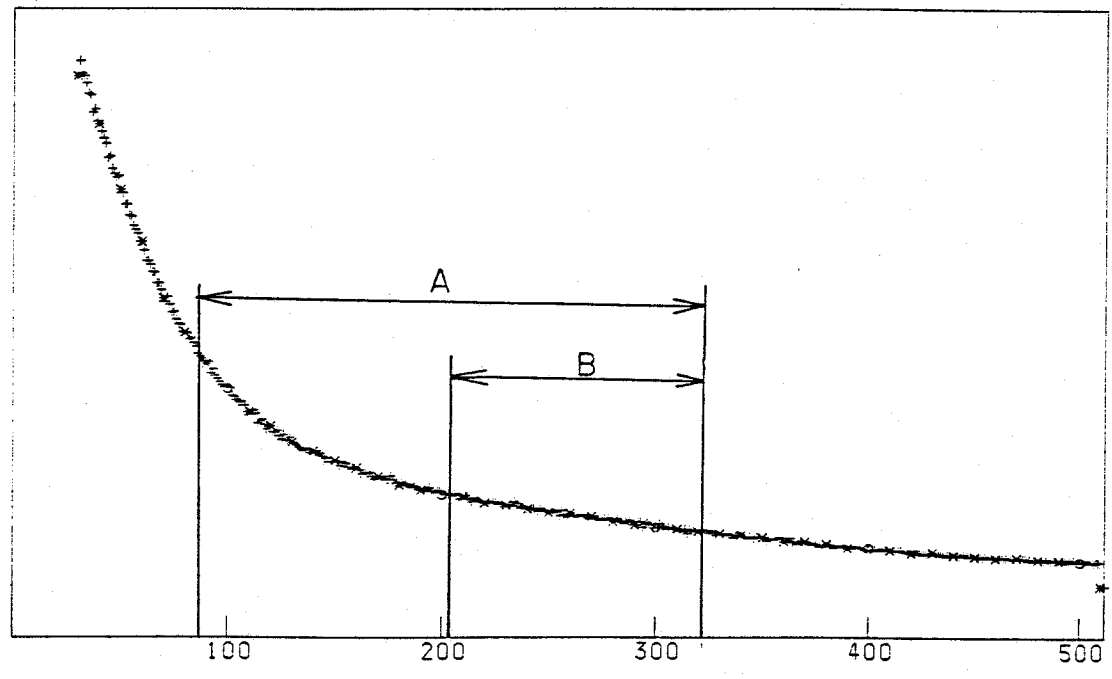

Fig. 2.16 A typical energy spectrum of gas-flow-type proportional counter

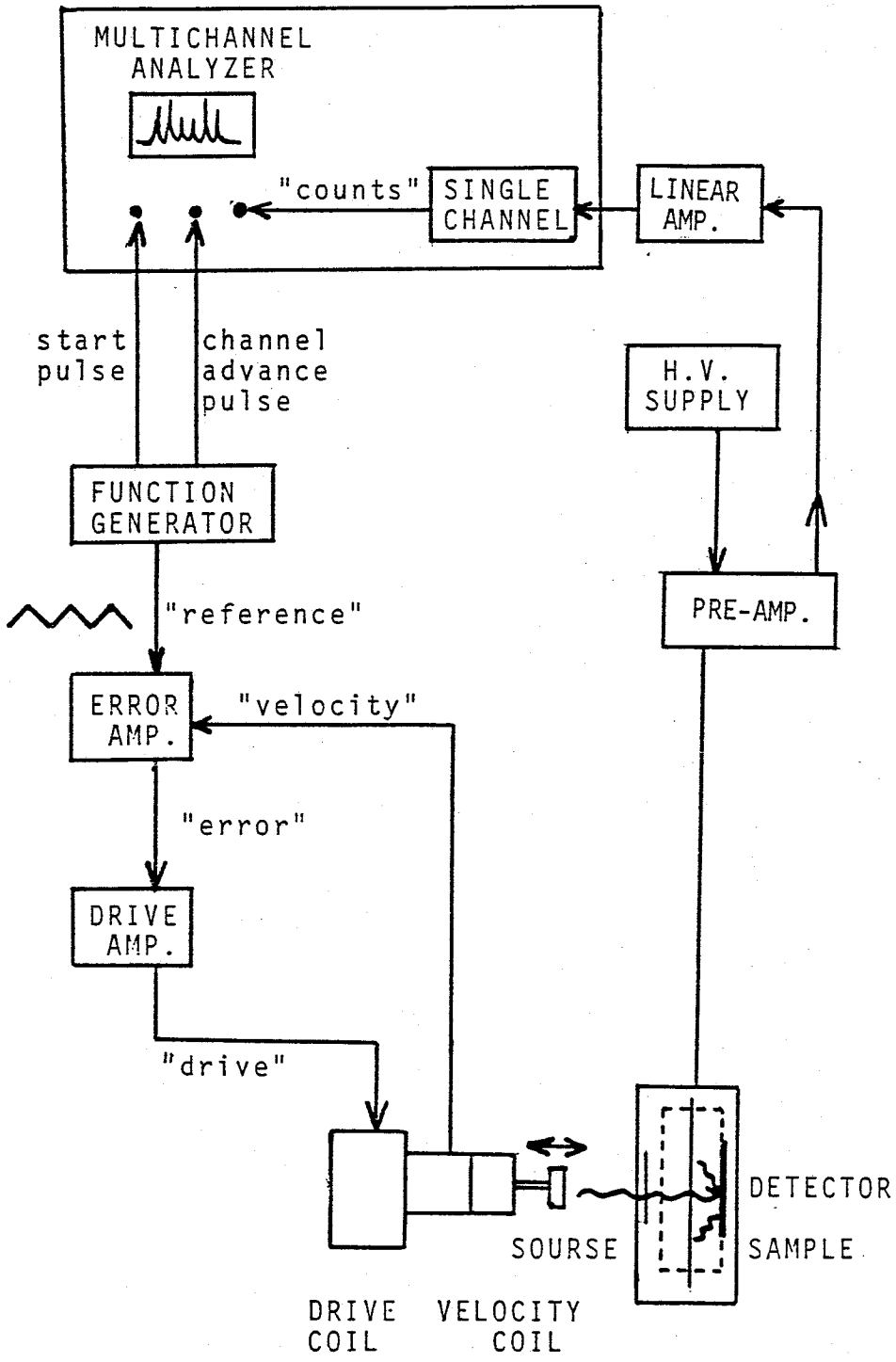

Fig. 2.17 Schematic diagram of scattering measurement system

measurements were done by using the asymmetric sawtooth driving mode, and the number of channels of the multi-channel analyzer was 512. The correction of parabolic back ground was necessary to obtain the exact Mössbauer spectrum because of the asymmetric driving mode. The conversion electron method was very useful in the case of the self-ion irradiation experiment, since the projected range of the latter was as short as the above mentioned electron range. Precise comparison and selection of the ranges will be discussed later.

2.3.3. Thermal scan method

The principle of thermal scan method is to precisely measure and follow the count rates at zero velocity as a function of the annealing temperatures or the measuring temperatures, as is already mentioned in the §1.6 . This paragraph is devided into two parts dealing with the static measurements during isochronal annealings, and the dynamical measurements during continuously increasing the specimen temperature.

2.3.3.(a) Static measurement during isochronal annalings

In the static measurements of the thermal scan method, the counts per 1000 sec were measured at 77 K before and after the successive annealings at each isochronal annealing temperature. At different annealing temperatures, different defect motions are expected to take place and change the count rate. 77 K is supposed to be less than the temperature where the interstitial-migration can occur. Nevertheless, the local motions of the ^{57}Co atoms around defects or some kinds of dynamical motions of them could occur even at this temperature. Accordingly, the changes in the count rate

many include the information about what kinds of reactions of ^{57}Co atoms with defects will take place as a results of reactions with defects after the annealings at various temperatures, and in addition, what kinds of local motions will occur around the ^{57}Co-defect complexes. Two absorbers at 77 K and at room temperature were used at the same time as shown in Fig. 2.18 , in order to monitor simultaneously the changes in the number of the ^{57}Co atoms unperturbed and perturbed by defects, respectively. Details of the changes in the count rate by using the two absorbers will be discussed later chapter.

The experimental procedure of the static thermal scan measurements is as follows. First, the spectrum measurement of the specimen after the irradiation is done, in the second, the two absorbers are set at the positions shown in Fig. 2.18 , and in the third, the counts per 1000 sec through the two absorbers are measured for five times. The measured values are averaged by omitting the maximum and minimum values. The isochronal annealing at a desired temperature is done by lifting the specimen holder from the bottom to the middle part of the cryostat. After the annealing period of 5 minutes at that temperature, the specimen holder is reset on the bottom plate of the specimen chamber and the counts per 1000 sec. are measured for five times. These cycles are repeated at each annealing temperature and the spectrum measurements are also done after four or five annealing steps.

The count rate is very sensitive to both the instability of the instruments and the changes of the geometrical configuration between the source, the absorber and the detector. The instabilities of the counting system are due to the changes in the high voltage supply of the proportional counter, and the gain drift in the

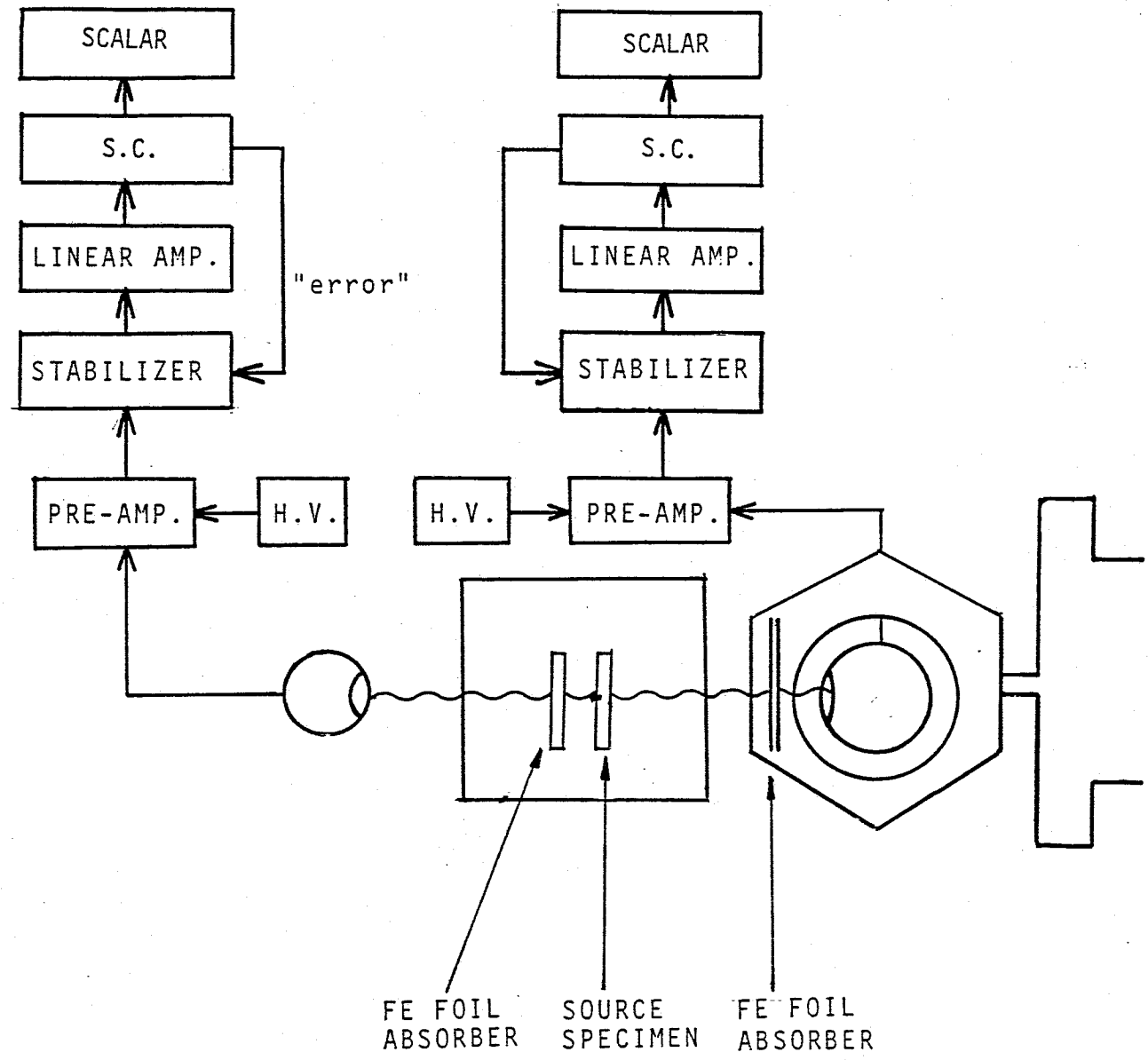

Fig. 2.18 Schematic diagram of the static thermal scan method

linear amplifier and/or the pre-amplifier. These changes originate mainly in the variations of the electric power source. The gain drifts also arise from the intermissions of counting, which are invitable in the isochronal annealing treatments of the specimen. For the correction of the drifts, a peak stabilizer * was used as shown in the upper parts of Fig. 2.15 . It consists of three parts; a voltage-controlled-gain amplifier, error detector and $1/2 \cdot \Delta E$ discriminator. The timing single channel analyzer and the $1/2 \cdot \Delta E$ discriminator in the peak stabilizer make up a single channel analyzer with a split window as is shown in Fig. 2.19 . A shift of energy spectrum due to a gain drift is corrected by equalizing the half area, S_A, on the left side to the half area, S_B, on the right side of the energy peak. Then, the number of the γ-rays with an energy in the range ΔE is kept constant for a long time during the annealings unless the cource or the absorber is changed. The changes of the counts arise only from the natural decay of ^{57}Co, the geometrical changes during the annealings, the statistical error, and the rearrangements of defects-^{57}Co complexes in

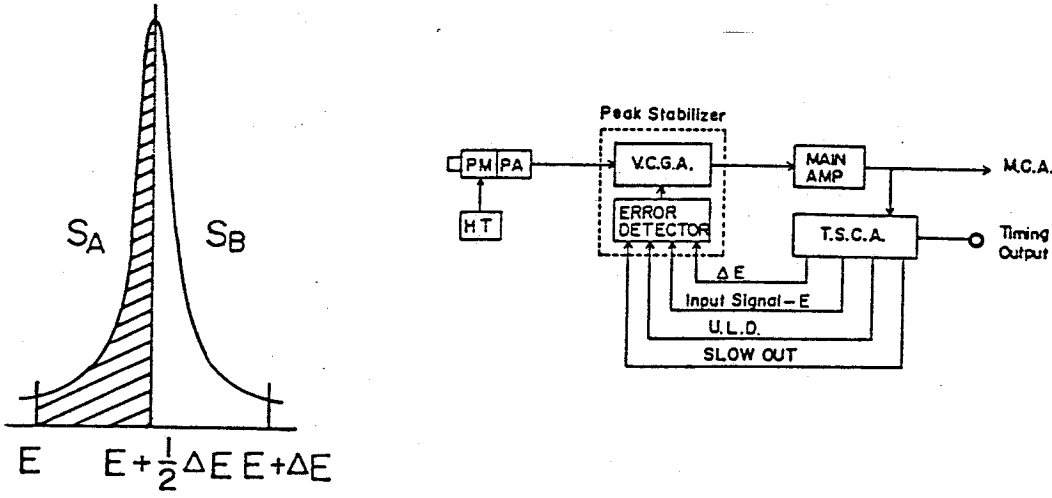

Fig. 2.19 Working principle of peak stabilizer with two energy windows

---

* The stabilizer was designed and made by Mr. S. Uehara of KUR.

the spectrum, the last of which is the object of the presint study. Detailed descriptions about the peak stabilizer are given in the reference [77] .

The geometrical configuration of the source, the absorber and the detector strongly affect the count rate/ Nevertheless, it is too difficult to reset the specimen holder at the "same" position for the measurements after each annealing. After the up-down, resettings of the specimen holder and measuring the count rate repeatedly, the error of the count rate due to the geometrical change of the specimen after the annealings, was evaluated to be less than 0.5 % . Another origin of the errors could be condensations of ice on the surface of the specimen or some other part of the cryostat in the path of gamma rays during the annealing or measurement. However, the specimen chamber of the cryostat id always evacuated during the measurements and, after each annaling, it is filled with pure He gas for a short time in order to rapidly cool the specimen to the measuring temperature. Accordingly, the effect of "ice" on the count rate is thought to be negligibly small.

Since the life time of ^{57}Co is 270 days and the annealing cycle is 2 hours, the magnitude of the changes of the count rate during one cycle of annealing due to the natural decay of ^{57}Co is about $10^6 \times \exp(-2/270 \times 24) \approx 300$, which is far less than the value of statistical error, ≈ 3000. Considering all the origins of the errors discribed in the above, the magnitude of the total error in measuing the counts for 3000 sec is estimated to be about 0.7 % , where the total counts was about 10^6.

2.3.3.(b) Dynamical measurements in thermal scan method

In the dynamical thermal scan method, the counts are measured as a function of the specimen temperature during continuous heating. In this meghod, not only the local motions of ^{57}Co atoms around defects byt also the long range migration of ^{57}Co atoms could be detected as a result of the change in the Debye-Waller factor. For instance, the long range migration of ^{57}Co atom by a vacancy mechanism may be expected to increase the count rate, that is to reduce the resonance absorption, due to the decrease in the Debye-Waller factor depending on the jump frequency of the ^{57}Fe atom and its life time before emitting the Mössbauer γ-ray to be measured. Accordingly, the changes in the count rate during increasing the specimen temperature may give the ingormation about the recovery stages and mechanisms of defects. Detailed discussion will be given in a later chapter.

As the first trial of the dynamical thermal scan method, the specimen temperature was increased by the spontaneous evaporation of liquid nitrogen in the cryostat combined to the continuous counting of gamma rays through the natural Fe foil absorber, which was placed in the specimen holder together with the ^{57}Co-doped-Fe source as shown in Fig. 2.20 . Either the absorber specimen or the source specimen was irradiated and measured. The heating-rate of the specimen was about 0.1 degree per minute. The counts were stored in the multichannel analyzer in which the channel advancing was done by every 200 seconds. As the first step of the measurement, both the counts and the specimen temperature were recorded as a function of time as shown in Fig. 2.20 . The two data were coupled together, and the counts were plotted as a function of the specimen temperature. Although the dynamical measurement is

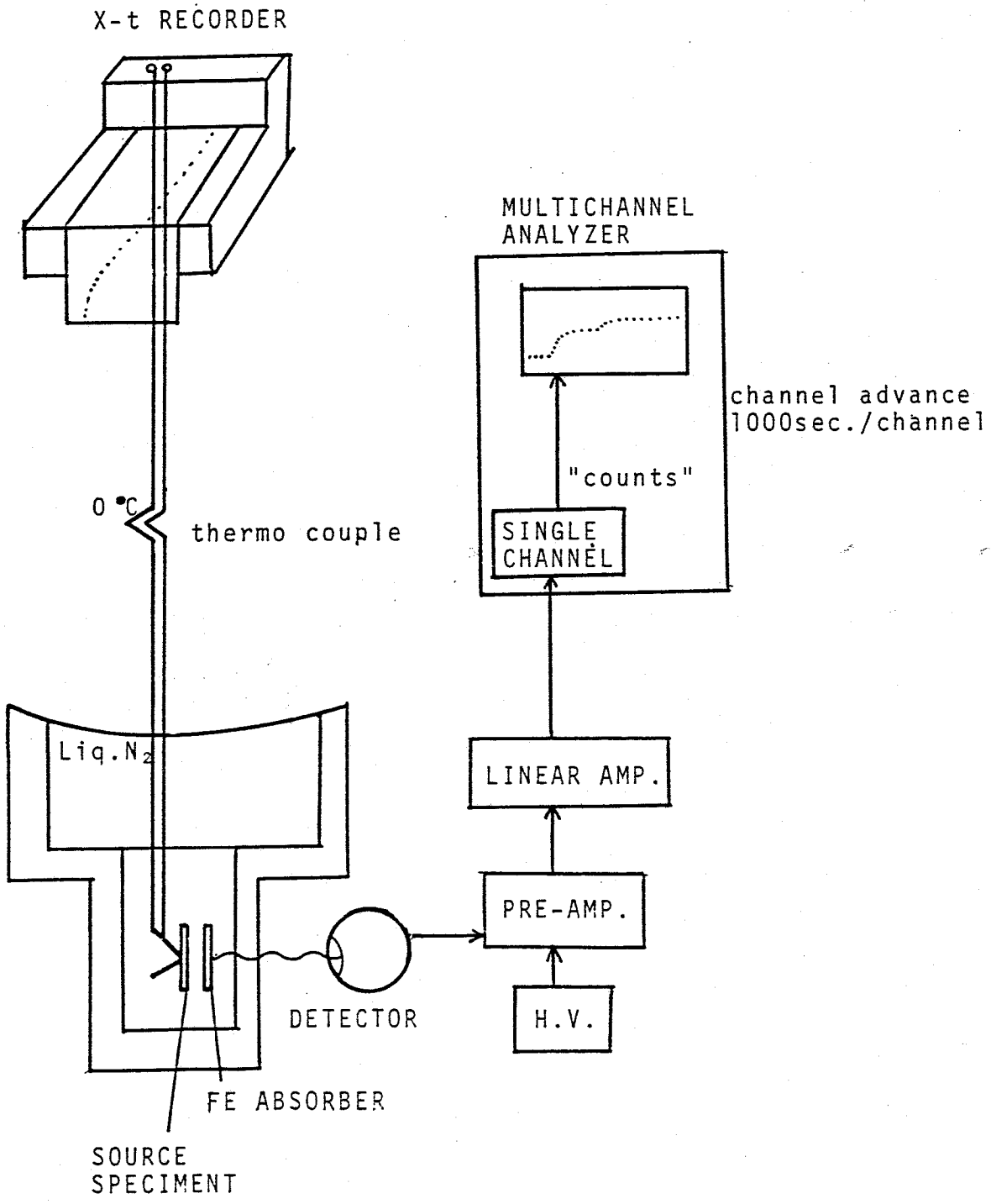

Fig. 2.20 Schematic diagram of the dynamical thermal scan method

supposed to be very sensitive and useful to idendify the recovery stages and mechanisms, it is sometimes susceptible to miscellaneous disturbances of outer origins, for instance a disturbence by a condensed thin film of liquid nitrogen or oxygen on the surface, and the measurement is difficult. An example of the measurement will be shown later.

2.3.4. Temperature control and heat treatment techniques

Figure 2.21(a) and (b) show the top-roading type cryostat for the measurement of Mössbauer spectrum and thermal scanning, and the specimen holder with a small electric heater for annealing, respectively. The measurements in the cryostat were done at liquid nitrogen temperature except for the dynamical thermal scan method. The cryostat was always evacuated by a powerful diffusion and mechanical pump, even disturbing a desirable vibrations free en-

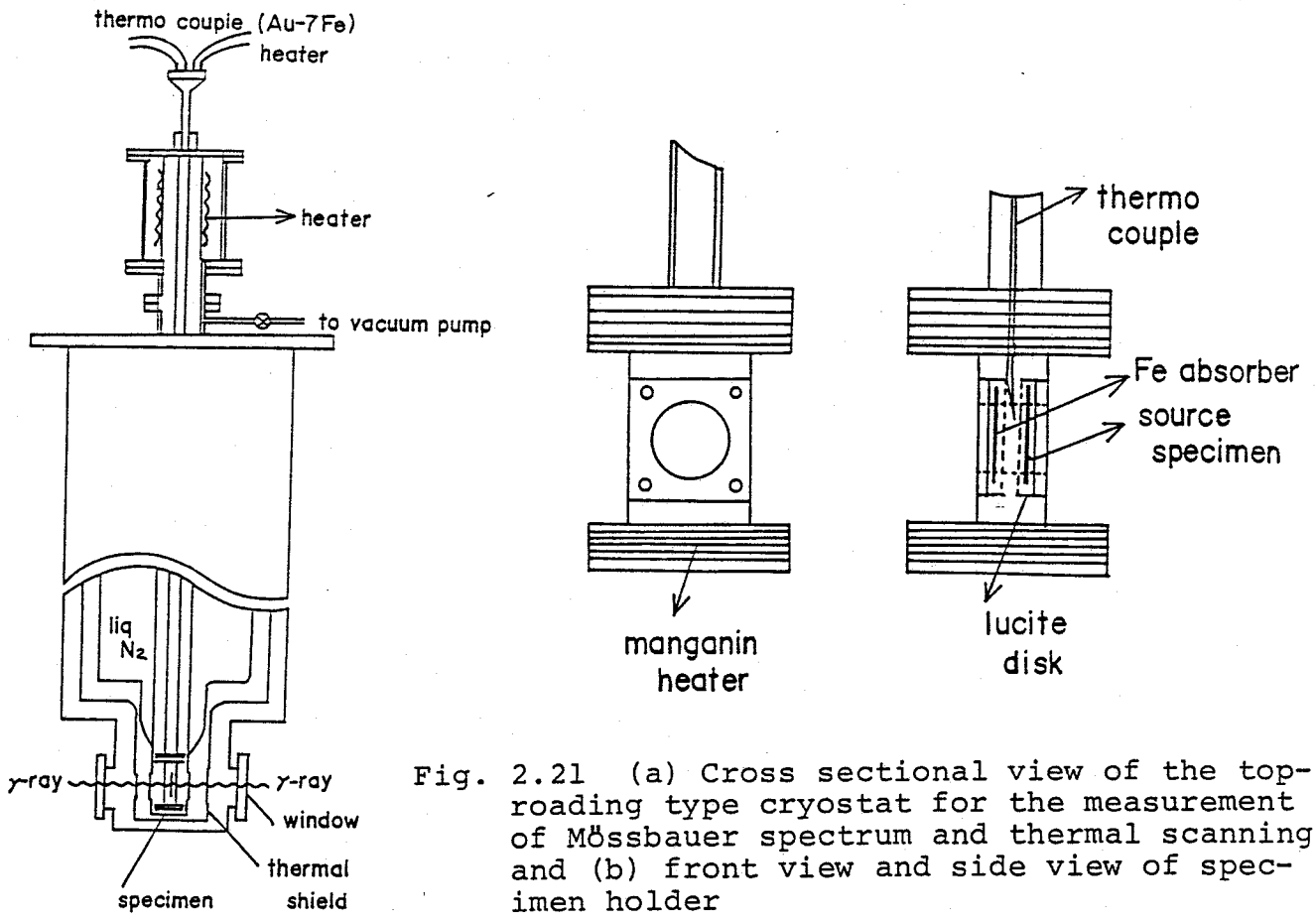

Fig. 2.21 (a) Cross sectional view of the top-roading type cryostat for the measurement of Mössbauer spectrum and thermal scanning, and (b) front view and side view of specimen holder

vironment, because the measurement of the annealing experiment needed a long time, about two months. The specimen holder was a light bobbin mede of Aluminum, which had a small heat capacity. A manganin-wire with 0.7 mm diameter was used for the heater, of which electrical power was about 15 Watt. The specimen temperature was monitored by a Au-Au7Fe thermocouple attached to the specimen holder, as in shown in Fig. 2.21(b) .

After the irradiation at low temperature, the specimen was put between lucite disks with 1 mm thickness in the specimen holder in liquid nitrogen, and transferred from the liquid nitrogen vessel to the cryostat as fast as possible. The increase of the specimen temperature during the transfer did not exceed 10 degrees, which was monitored by the specimen holder thermocouple.

The annealings below room temperature were done by lifting the holder from the bottom part of the specimen chamber to the middle part and heating up by the manganin heater in vacuum by manual operations. The rate of temperature increase was about 10 degrees per minute, and the annealing period at a desired temperature was 5 minutes. After the annealing, the specimen was rapidly cooled down to the measurement temperature by filling He fas into the specimen chamber. The coolingrate was about 40 deg/min.

For the annealings above room temperature up to 470 K, silicon oil bath was used as the first trial. The specimen was removed from the holder, and annealed in the oil for 5 minutes. After cleaning with Acetone, it was reset in the holder. Above the room temperature, only the measurements of the Mössbauer spectra were done and the thermal scan measurements were not performed because it was impossible to set the specimen at the "same" position.

The Mössbauer spectra at 4,2 K were measured in another cryostat, which is shown in Fig. 2.22(a) . The specimen was put between lucite disks in the copper holder, as in Fig. 2.22(b), and transferred quickly from the liquid nitrogen vessel into the attachment in the cryostat, which was already cooled down to liquid nitrogen temperature.

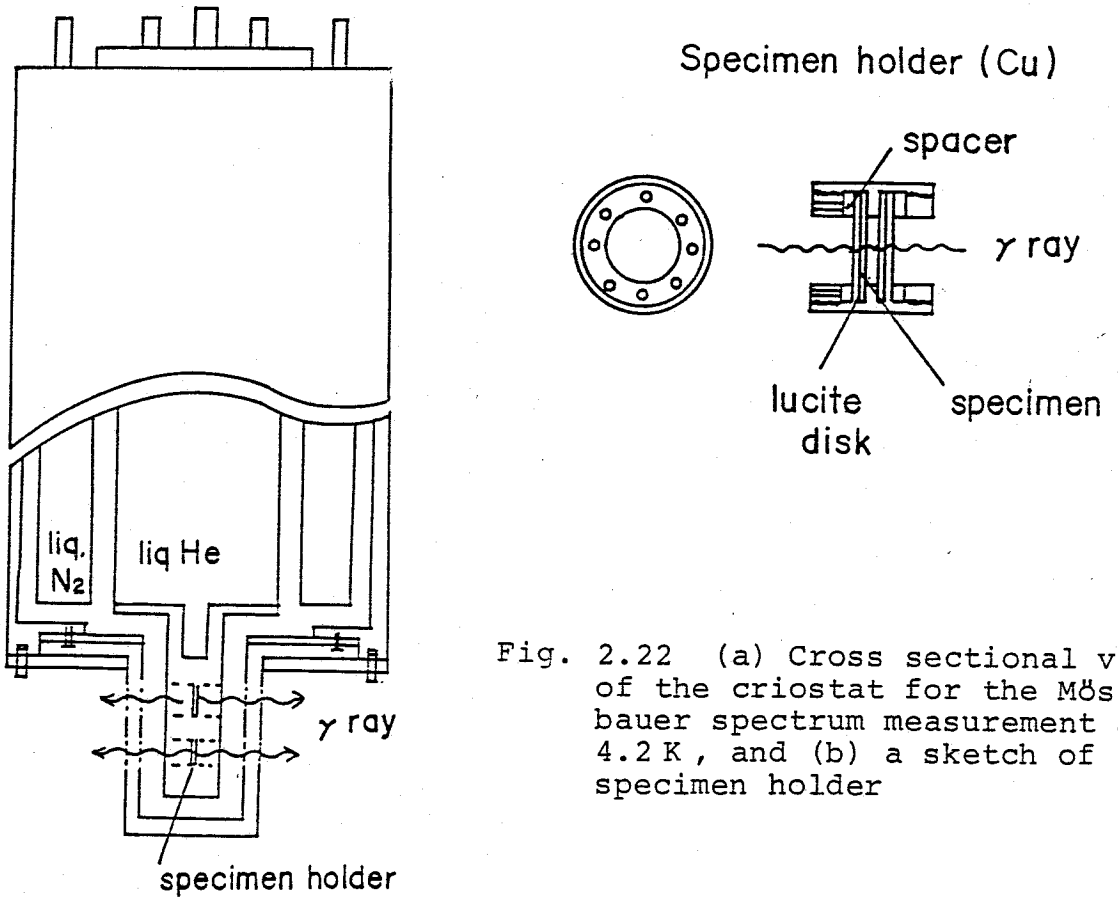

Fig. 2.22 (a) Cross sectional view of the criostat for the Mössbauer spectrum measurement at 4.2 K , and (b) a sketch of specimen holder

2.4 Analysis of Mössbauer Spectrum

The numerical data of Mössbauer spectrum from the multichannel analyzer were memorized using a data tape and/or a mini-floppy-disk as a media, and processed in a form acceptable by the computer system, as shown in Fig. 2.23 . For the accurate determination of the Mössbauer parameters, such as the internal field, the full width at half maximum, the isomer shift, the electric field gradient, and the absorption intensity, it is necessary to do a computer fitting. Futhermore, in order to investigate more precisely the differences in the Mössbauer spectra before and after irradiation or annealing, the subtraction analysis is useful because of its high sensitibity to the small changes in the spectra. In the following description, first, the principles of the computer fitting analysis will be given, and, secondly, the subtraction analysis will be explained.

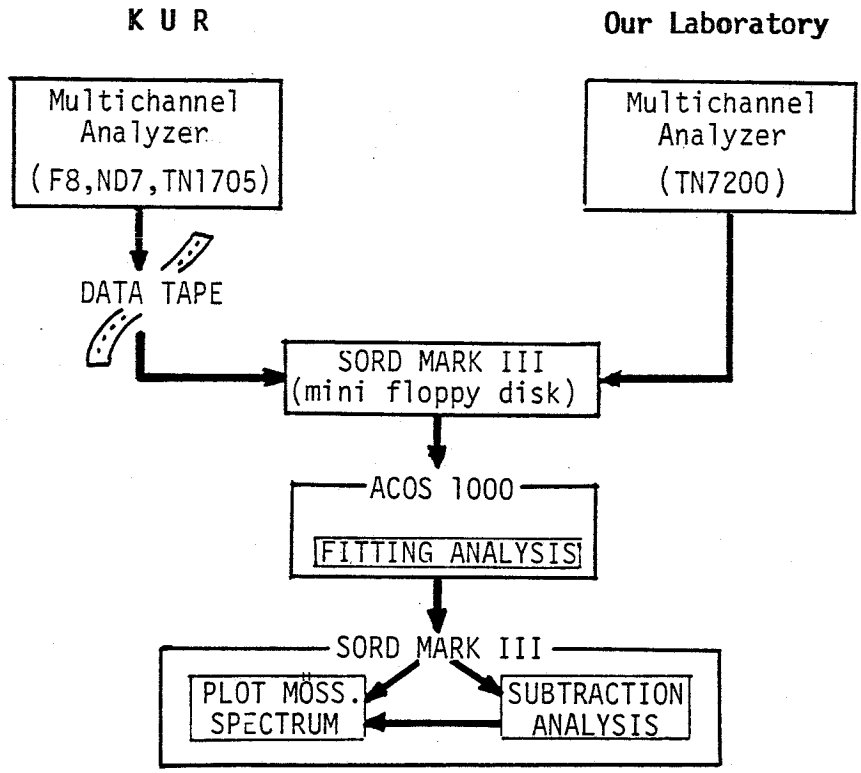

Fig. 2.23 Flow chart of analysis of Mössbauer data

2.4.1. Fitting analysis

Least-squares fitting by the sum of the Lorentzian lines is often used in the detailed analysis of the Mössbauer spectrum. The so-called cosine smearing effect due to the oppler energy shift, which is given by $\Delta E = E_0 \cdot \frac{v_0}{c} \cos\theta$, where E_0 is the photon energy, and θ an angle between the wave vector of an emitted photon and the direction of the relative velocity v_0 , leads to the asymmetric deviation of the Mössbauer Lorentzian line. Nevertheless, the effect was negligibly small in our experimental geometry, as is shown in the section 2.3.1 . It was actually ensured by the measurement of the Mössbauer spectrum of the unirradiated source specimen. On the other hand, the thickness effect associated with the transmission integral, as is already discussed in the section 1.3 , is also thought to lead to the deviation from the Lorentzian line, but it was again found experimentally not to distort the Lorentz shape of the spectrum. Accordingly, the fitting analysis was done by using the sum of the unmodified Lorentzian lines in this investigation as will be mentioned below.

In the least-squares fitting, the hteoretical profile of the Mössbauer spectrum must be determined so as to minimize the weighted mean square deviation χ^2,

$$\chi^2 = \sum_{i=1}^{512} \frac{1}{\sigma_i^2} (Y_i^{th} - Y_i^{ex})^2 \qquad (2.1)$$

where Y_i^{ex} and $\sigma_i^2 = Y_i^{ex}$ are the experimental data and the square of the statistical variation of the counts in the i-th channel of the multichannel analyzer corresponding to a velocity range v_i to $v_i + \Delta v_i$, respectively. In the investigation on the ferromagnetic iron, Y_i^{th} is represented by the sum of the six Lorentzian lines which are mainly originaged from the nuclear magnetic

hyperfine interation, as is already mentioned before.

$$Y_i^{th} = Y_{BG}^{th} - \sum_{\alpha=1}^{n} \sum_{j=1}^{6} \frac{W_j^{\alpha}}{\left(E_j^{\alpha} - \frac{v_i}{c} E_0 \right)^2} \qquad (2.2)$$

where Y_{BG}^{th} is the counts off-resonance position, i.e. the backbround, W_j^{α}, E_j^{α}, and Γ_j^{α} are the absorption intensity, the position, and the full width at half maximum of the j-th line in the α-th six line component, respectively. The minimization procedure of χ^2 used in our computer program mainly consists of the expansion of Lorentz function to the polynomial expression,which was first made by W. Kündig [78] and developed later by others. The program enables us to change fix any variables with special limitations during the computer fitting process. For instance, the intensity ratios of the six lines of all α's components, $W_1^{\alpha} = W_2^{\alpha} = W_3^{\alpha}$, can be taken as a common variable and changed for the fitting. Such a limitation is necessary for the fitting analysis of Mössbauer spectrum of magnetic materials because the spin orientations of all the different components are expected to be equal in a magnetic domain. In this investigation, only one or two, exeptionaly three, six-line-components were used and good results of spectrum fitting were obtained.

2.4.4. Subtraction analysis

The subtraction analysis of the different Mössbauer spectra is a useful method for the detection of the small changes hidden in the broad and unresolved spectrum. Nevertheless, it is a difficult technique because for that purpose the high stability in the driving system and the constant signal-to-noise ratio in the counting system required for a long time in the measurement. Accordingly, the drifts in the velocity scale, the center position

of Mössbauer spectrum, and the energy spectrum must be monitored during the measurement, that are already mentioned before.

The calibration factor, which means the energy range per channel in each measurement, mm/sec/channel, and the center position of the Mössbauer spectrum of pure Fe at room temperature were measured by a calibration source and an iron absorber attached on the other side of the driver system as shown in Fig. 2.12 . In the subtraction analysis, differential spectrum was obtained by subtracting the spectrum after irradiation from that before irradiation, or the spectrum after annealing from that before annealing, taking account of the changes in the calibration factors and the center positions of the two spectra. For the correction of the changes in the calibration factor and the center position, the numerical data of one Mössbauer spectrum was modified by the linear interpolation so as to equalize the calibration factor and the center position to those of the other spectrum. After the subtractions, the difference spectra were plotted with the same scales as those of the relative transmission and the velocity of the original Mössbauer spectra.

3. EXPERIMENTAL RESULTS

3.1 Neutron Irradiation

As the first trial of a search for the "defect lines" in the Mössbauer spectrum of the irradiated pure iron foils, the specimens irradiated with reactor neutrons at 30 K were investigated by the various methods already mentioned before. In this section, the results from the source and the absorber experiments will be given separately. As before mentioned, the iron specimens with two different levels of purity were prepared. One was about 500 in the resistivity ratio $R_{300K}/R_{4.2K}$ (RRR_H) and the other was higher than 5000. Most of the irradiation experiments mentioned below were preformed by using the former specimens, and for the final neutron irradiation experiment the latter was carefully used. Although clear defect lines in the Mössbauer spectra were not observed as they were in both experiments, the characteristic changes in the Mössbauer parameters, especially by using the subtraction method, and those in the count rate at zero velocity, i.e., in the thermal scanning, during the isochronal annealing treatments were observed in the cource experiment. In addition, in the absorber experiment, noticiable changes were also found in the subtraction spectra after the annealings.

3.3.3 Source experiment

3.3.1(a) Comparison between the Mössbauer spectra before and after irradiation

The Mössbauer spectrum of the ^{57}Co-doped-Fe source specimen at 77 K before irradiation showed a perfect six line profile, as shown in Fig. 3.1(a), indicating that all ^{57}Co atoms were randomly distributed on the substitutional sites of Fe matrix, and that precipitates of

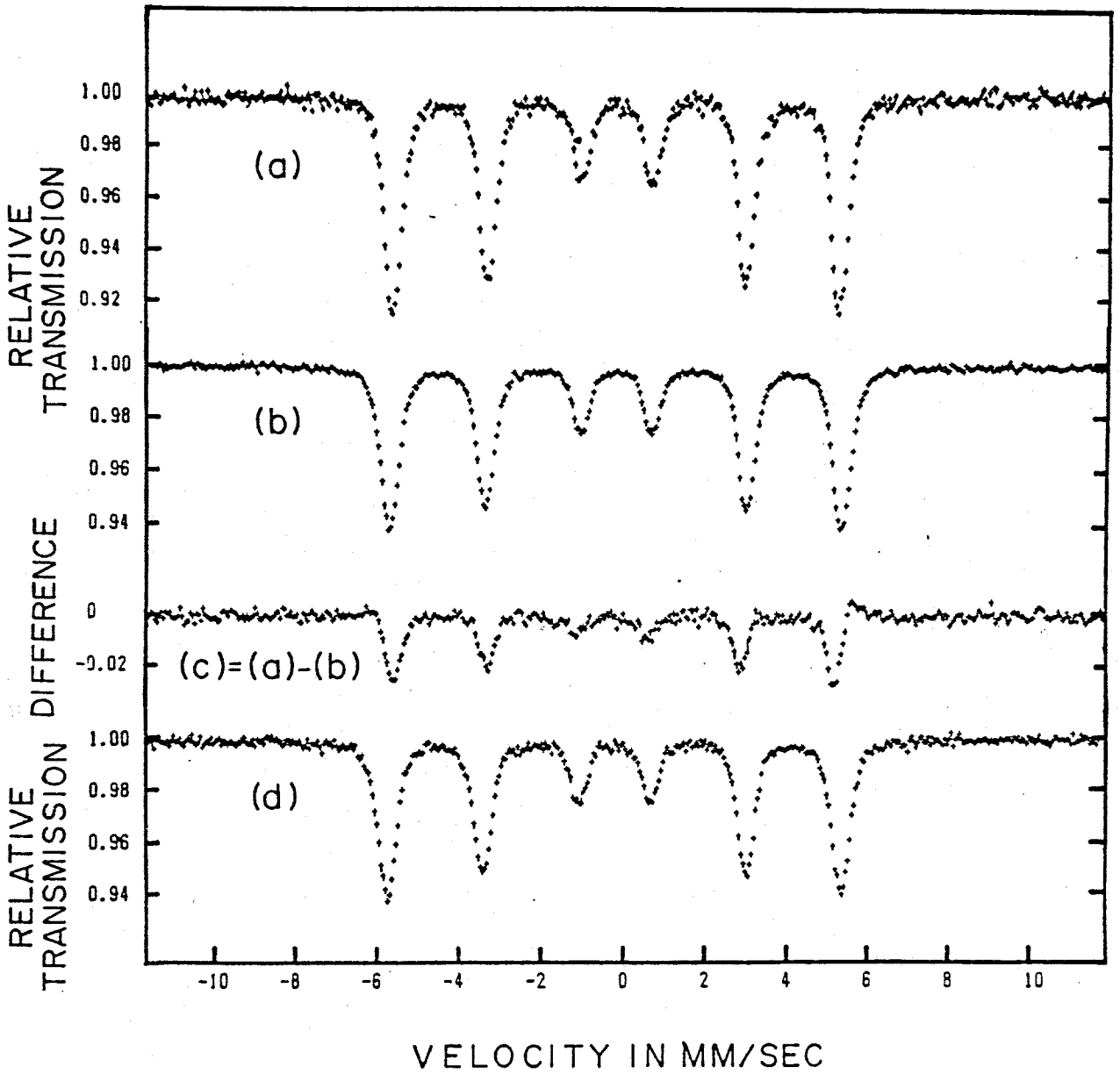

Fig. 3.1

FE DOPED WITH ^{57}Co IRRADIATED BY NEUTRONS AT 30 K

(A) BEFORE IRRADIATION, MEASURED AT 77 K.

(B) AFTER IRRADIATION, MEASURED AT 77 K.

(C) SUBTRACTION ; (A) - (B)

(D) AFTER IRRADIATION, MEASURED AT 4.2 K.

Co atoms of which the hyperfine field was reported to be 325 kOe and 315 kOe for the fcc and the hcp precipitates, respectively [79], did not exist in the specimen. The average hyperfine field and the full width at half maximum (FWHM), 340 ± 1 kOe and 0.45 ± 0.01 mm/sec respectively, were obtained from the fitting analysis by using a set of six Lorentzian lines. The magnitude of the average hyperfine field was slightly larger than that of pure iron, 338 kOe [80]. The origin of the larger hyperfine field is not clear, but it is conceivable that the existence of other Co atoms before the decay to ^{57}Fe increases the hyperfine field of Fe atom the average spontaneous magnitization in Fe-Co system increases linearly with the increasing concentration of Co atoms up to 25 at.%Co [81].

After the irradiation with a total dose of 5×10^{16} n/cm^2, the total resonance area of the Mössbauer spectrum at 77 K decreased, and the new components with a higher hyperfine field and a positibe isomer shift appeared, as in Fig. 3.1(b). Although the new components was not well resolved from the unperturbed component, the differences can be clearly seen in the subtraction spectrum as is shown in Fig. 3.1(c). Since the spectrum after irradiation was subtracted from that before irradiation, the negative components in the subtraction spectrum means the disappeared components, and the positibe components the newly appeared components during irradiation. The average hyperfine field and the full width at half maximum (FWHM) were 343 ± 1 kOe and 0.50 ± 0.01 mm/sec, respectively, which were a little larger than those before irradiation, corresponding to the appearance of the new components after irradiation.

The Mössbauer spectrum taken at 4.2 K immeadiately after irradiation is given in Fig. 3.1(d). The total resonance area of the spectrum was nearly equal to that at 77 K after irradiation, which may show

the formation of a region after irradiation, where the Debye-Waller factor is too small to be detected even at 4.2 K . The average hyperfine field of 345 ± 1 kOe was also larger than that of pure Fe at 4.2 K , 339 kOe [80]. It will be explained later after discussing the annealing processes of defects. All Mössbauer parameters obtained from the spectra before and after irradiation are summarized in Table 3.1 . The magnitudes of the changes in the Mössbauer parameters before and after irradiation were different from one trial to another, but the same tendencies were observed; the total resonance area decreased, the hyperfine field increased, and the FWHM increased, after irradiation. The experimental error of the total resonance area was evaluated as less than 5 % from the measurements of the spectra after remounting the same specimen, but the differences between the three specimens are much larger than that. It may be attributed to the differences in the total doses of neutrons arising from the fluctuations in the irradiation conditions in the reactor, or ununiformity in the concentration distribution of ^{57}Co atoms dopes into Fe foils; the total dose was not measured directly during every irradiation, but estimated from the calibration values as a function of the specimen position in the irradiation chamber, which were measured during the reactor operation with 5 MW by K. Atobe et al.[82].

It is difficult to understand from the above data what kinds of defects were introduced by the low temperature neutron irradiation and how they contributed to the increase in the hyperfine field and the decrease in the total resonance area. To solve these problems, the annealing experiments were necessary and helpful, the details of which will be mentioned in the following sections.

3.1.1(b) Isochronal annealing experiments

NO.		AREA RATIO A_{after}/A_{before}	H_{int} (kOe)	FWHM (mm/sec)	δ (mm/sec)	eqQ (mm/sec)	I_2/I_1	I_3/I_1
1	before irrad. 77K	------	--------	--------	--------	--------	---------	--------
	after irrad. 77K		343.4(5)	0.516(8)	-0.11(1)	-0.003(3)	0.936(10)	0.389(8)
2	before irrad. 77K	0.9512	339.7(5)	0.454(8)	-0.12(5)	-0.002(4)	0.822(12)	0.362(10)
	after irrad. 77K		343.4(5)	0.497(6)	-0.15(2)	-0.003(5)	0.808(10)	0.353(7)
	after irrad. 4.2K	------	344.7(4)	0.488(7)	-0.16(2)	-0.001(9)	0.804(10)	0.350(9)
3	before irrad. 77K	0.9185	338.5(6)	0.466(9)	-0.12(3)	-0.000(3)	0.844(10)	0.373(7)
	after irrad. 77K		339.2(3)	0.467(8)	-0.12(2)	-0.001(3)	0.873(11)	0.437(9)
	after irrad. 4.2K	0.9300	340.1(2)	0.480(8)	-0.13(2)	-0.002(4)	0.827(16)	0.389(13)

Table 3.1 Mössbauer parameters of the spectra before and after neutron irradiation

In order to clarify the recovery behavior of the point defects introduced by the low temperature irraditaion and to give explanations to all the changes after irradiation and after annealing, the isochronal annealing experiment was done on the specimen irradiated by neutrons with a total dose of 2×10^{16} n/cm^2. Figure 3.2(a) and (b) show the Mössbauer spectra measured at 77 K and their subtraction spectra during the isochronal annealings of which the stepwise annealing rate was 5 min/10 deg. The difference spectra were obtained by successively subtracting the spectrum before each annealing from that after the annealing. Clear defect lines were not observed in all spectra, but remarkable changes in both the total resonance area and the profile of the spectrum occured after the annealings at 110, 270, 320, 370, and 470 K, as are more clearly seen in the subtraction spectra in ig. 3.2(b). The total resonance area of the spectrum, (a), the average hyperfine field, (b), the average FWHM, (c), the average electric field gradient, (d), and the average center shift of the spectrum, (e), are plotted in Fig. 3.3 as the functions of the annealing temperatures. The values of the tatal resonance area were normalized by that before the annealings. The others were obtained from the fitting analysis using a set of six Lorentzian lines. After the annealings at 110 K and 270 K, which seem to correspond to the recovery stage of self-interstitial and vacancy, respectively, the total resonance area stepwise increased. The average hyperfine field and the FWHM decreased at the 110 K annealing stage, in parallel with the changes in the subtraction spectrum; it was found by the fitting analysis of the subtraction spectra using two sets of Lorentzian lines that the component with the hyperfine field of 357 kOe disappeared and a new component with that of 335 kOe appeared. Futhermore, after the 270 K annealing, new components

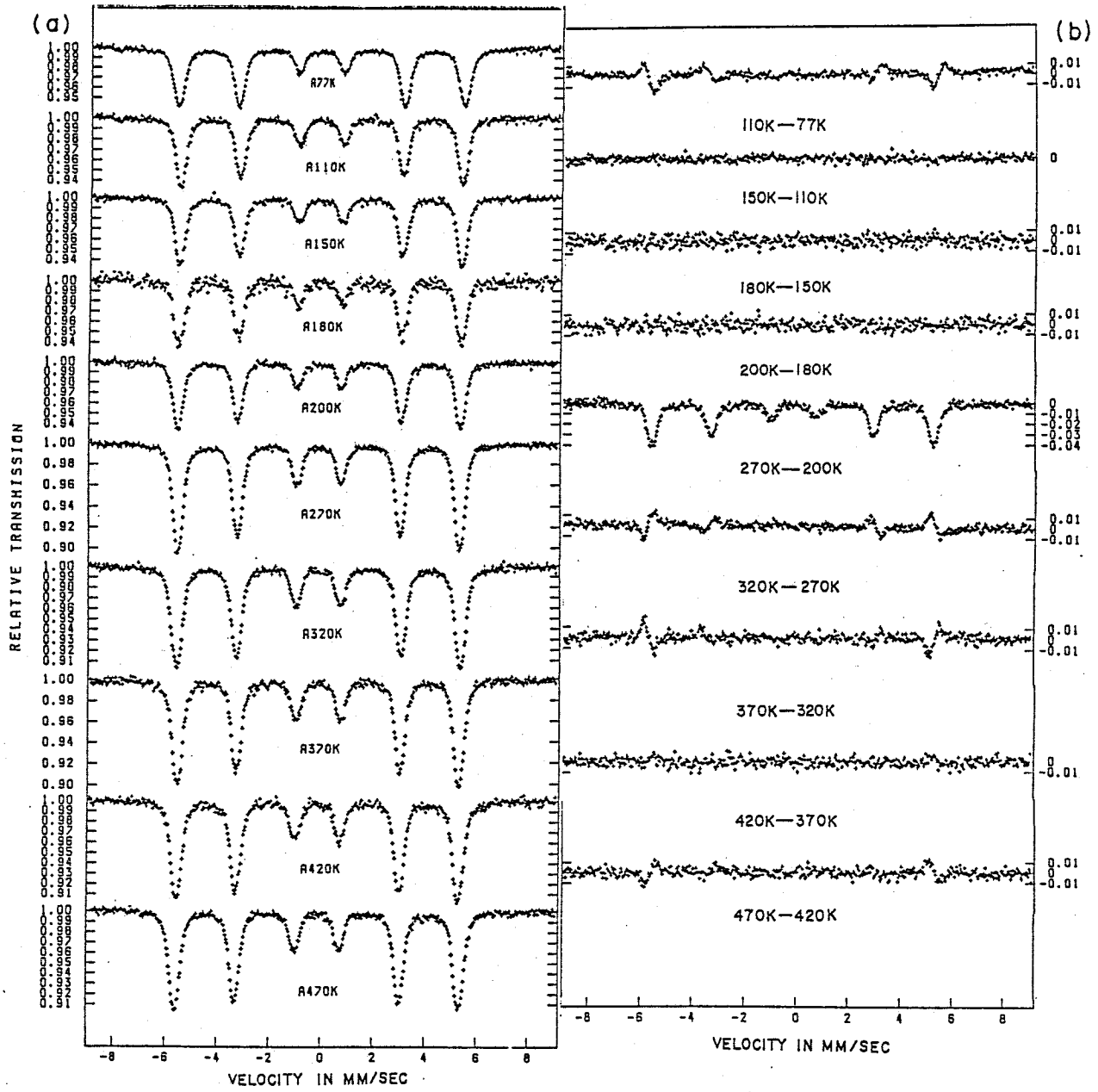

Fig. 3.2 Mössbauer spectra taken at 77 K during isochronal annealings and their successive subtractions

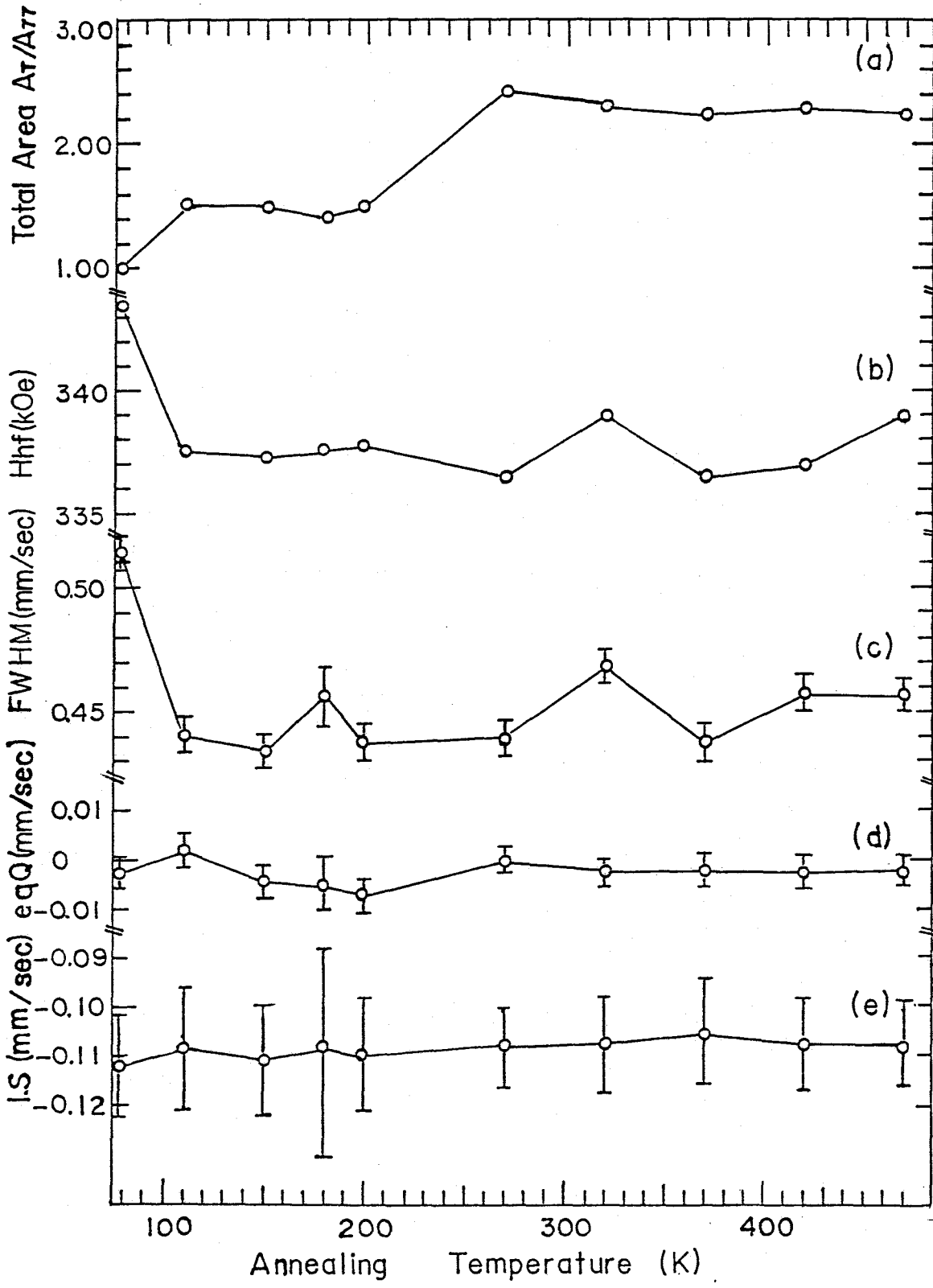

Fig. 3.3 Mössbauer parameters during isochronal annealings as the functions of the annealing temperature; (a) total resonance area, (b) the average hyperfine field, (c) the FWHM, (d) the electric quadrupole splitting, and (e) the isomer shift

with 328 and 341 kOe appeared. These changes were peculiar since the appearance of the new components, especially the last two, were always associated with large recoveries of the total resonance area. They could, therefore, arise from dissociations of defects complixes of which the Debye-Waller factor was too small to be detected in the Mössbauer spectrum before each annealing. In addition, after the 320 K annealing, the component with the hyperfine field of 330 kOe disappeared and that of 352 kOe appeared. After the 370 K annealing, the 352 kOe component disappeared again the 328 kOe component appeared. A similar change took place between 370 and 470 K ; the component of 349 kOe emerged at the sacrifice of the 349 kOe component, as is seen in the lower part of Fig. 3.2(b). During the annealings between 320 K and 470 K , the total resonance area was kipe nearly constant.

The above changes are thought to be originated from various reactions between the ^{57}Co atoms, the other impurities and the defects introduced by the low temperature irradiation, associating and dissociating with each other at various temperatures. Detailed discussions will be given later concerning with the two components fitting analysis, and the assignments for the above components appeared and disappeared during the annealings will be given too.

3.1.1(c) Static thermal scan measurements

For the more precise investigations on the various reactions between ^{57}Co atoms, the other impurities, and point defects during the above isochronal annealing treatments, the static thermal scan measurements were done in parallel on the same specimen. The narmalized counts per 1000 sec through the Fe absorber at room

temperatures in Fig. 3.4 . The count rate first decreased at arround 110 K , corresponding to the first increase in the total resonance area already described in the above paragraph (see Fig. 3.3(a)). After the large up-and-down changes between 110 K and 190 K , it decreased remarkably accompanied by the small up-and-down changes between 190 K and 270 K , corresponding to the increase in the total resonance area in Fig. 3.3(a) . In this case, the peak stabilizer described before was not used, so the error arising from the drifts in the counting system might be included in the data. Nevertheless, parallel tendencies of annealing stages appeared in the changes of the Mössbauer spectra, and another thermal scan measurement using the peak stabilizer confirmed these changes in the count rate includings the up-and-down behavior.

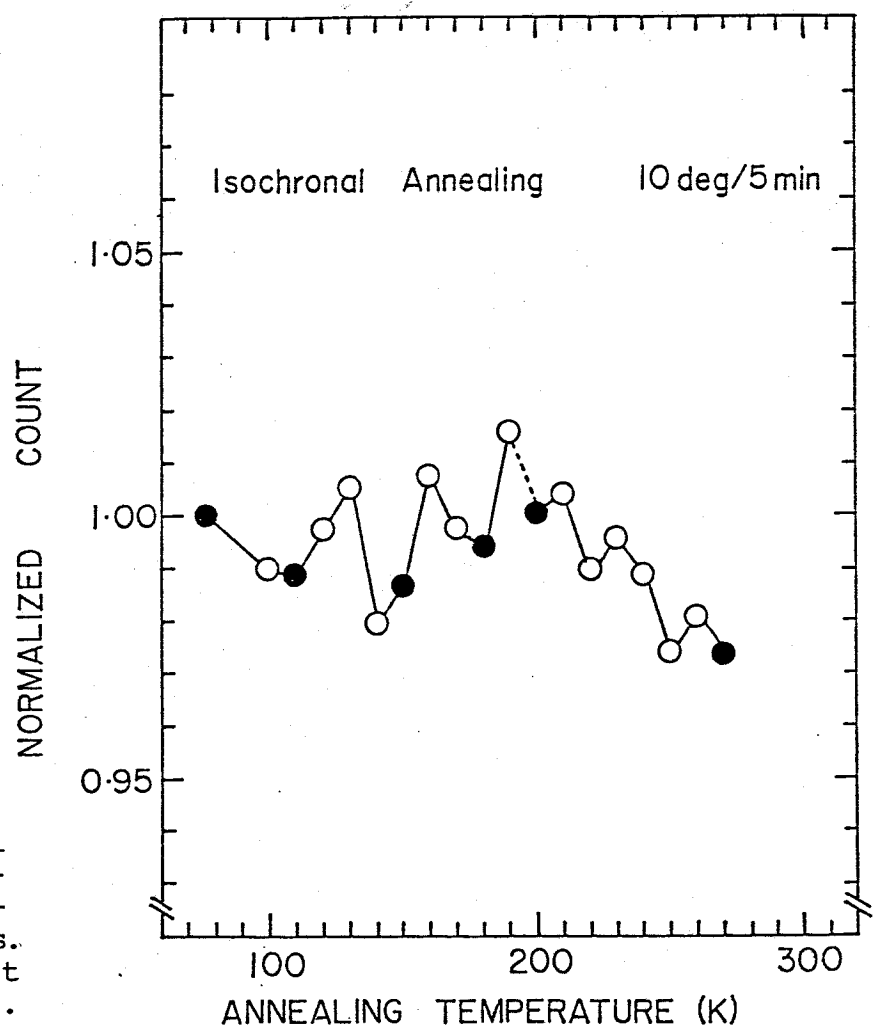

Fig. 3.4 Static thermal scanning with ^{57}Co-doped-Fe source irradiated by neutrons. The absorber was kept at room temperature.

3.1.1(d) Source experiment on super-purity iron

Figure 3.5 shows another result of the static thermal scan measurement in which the ultra high pure foil with $RRR_H = 5000$ was used and the peak stabilizer was attached to the counting system. The upper curve in the figure shows the result from the Fe absorber at 77 K, and the lower one from that at room temperature. Roughly speaking, three annealing stages were observed in the curves, which were clearly seen in the counts through the absorber at room temperature; first, the stage at around 110 K, secondarily, at around 150 K, and, in the third, between 180 K and 280 K. The last stage around 190 K, 220 K, and 260 K. These stage agree well with those in iron reported by many authors [4,10,24,28], as was already discussed in the section 1.2, and, according to the classification accepted in general, they are named the stage I, the stage II, and the stage III in the order of the annealing temperatures respectively. The differences between this result and that obtained from the first trial described in the above, are remarkable especially in the stage II which is thought to be closely related to the assiciation and dissociation process of the interstitials and impurities, like carbon. Accordingly, these differences seem to arise from the difference in impurity concentration between the specimens with $RRR_H = 500$ and the super-pure specimen with $RRR_H = 5000$. On the other hand, after the small changes below 230 K in the curve obtained from the absorber at 77 K, a drastic decrease in the counts was observed at around 250 K. Since the decrease in the counts means the increase of the resonant absorption, the number of ^{57}Fe atoms which decayd from ^{57}Co, and came into the same circumstances as pure Fe atoms unperturbed by defects at 77 K must have increased at 250 K. Such a chnge could be induced by the dissociation of

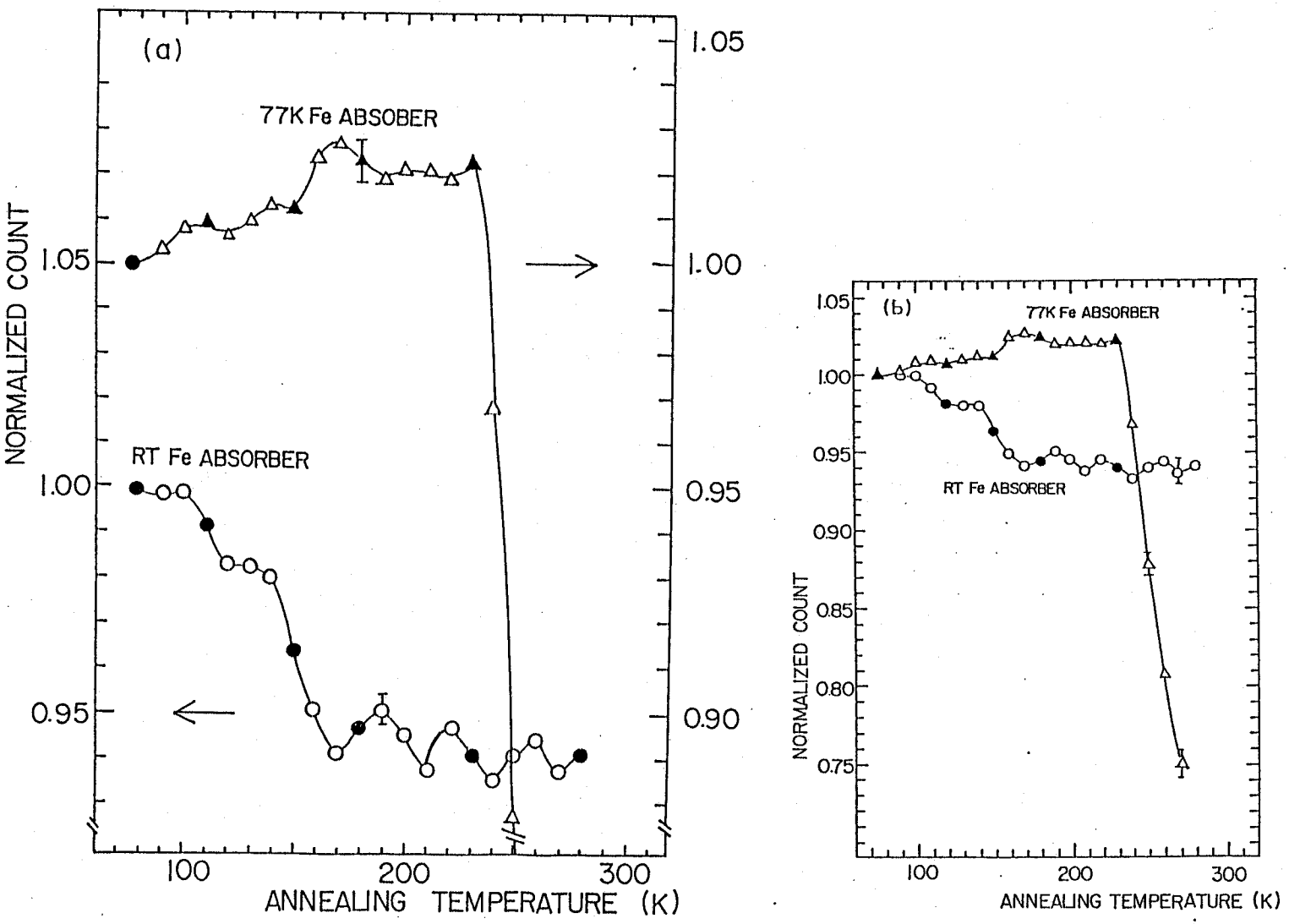

Fig. 3.5 Static thermal scanning with super Fe doped with ^{57}Co. The Fe absorbers were kept at room temperature and 77 K.

the Co-defects complexes. Likewise, the small jerky increases up to 230 K in the counts through the absorber at 77 K could be interpreted as the increase in the number of Co atoms associating gradually with defects during the recovery of defects.

Figure 3.6(a) and (b) show the Mössbauer spectra of the high purity iron during the above isochronal annealing experiment and the succesive subtraction spectra, respectively. The Mössbauer fitting parameters obtained by these spectra are plotted as the functions of the annealing temperature as shown in Fig. 3.7 . The total resonance area increased stepwise both after the 110 K and 280 K annealings, but the magnitudes of the increases are different from those of the low purity iron as in Fig. 3.3(a); the increase at around 280 K is smaller than that in the low purity iron. The decrease in the count rate mentioned above was not so large between 200 and 270 K as shown in Fig. 3.5(b) compared with that of the low purity, too. The reason why the area did not increase so larger than that in the low purity iron is not clear, but the trapping of vacancies by the impurity atoms, like carbon, might affect the increase of the total resonance area. The average hyperfine field and the FWHM decreased after the 110 K annealing, increased up to around 150 K , and redecreased at 230 K ; these changes are very similar to that of the low purity iron as in Fig. 3.3(b). The changes of the average hyperfine field and the FWHM are slightly different, especially at stage II, from those of the low purity iron corresponding the difference in the count rates. Detailed discussions will be given later concerning the difference in the purity.

3.1.2 Absorber experiments

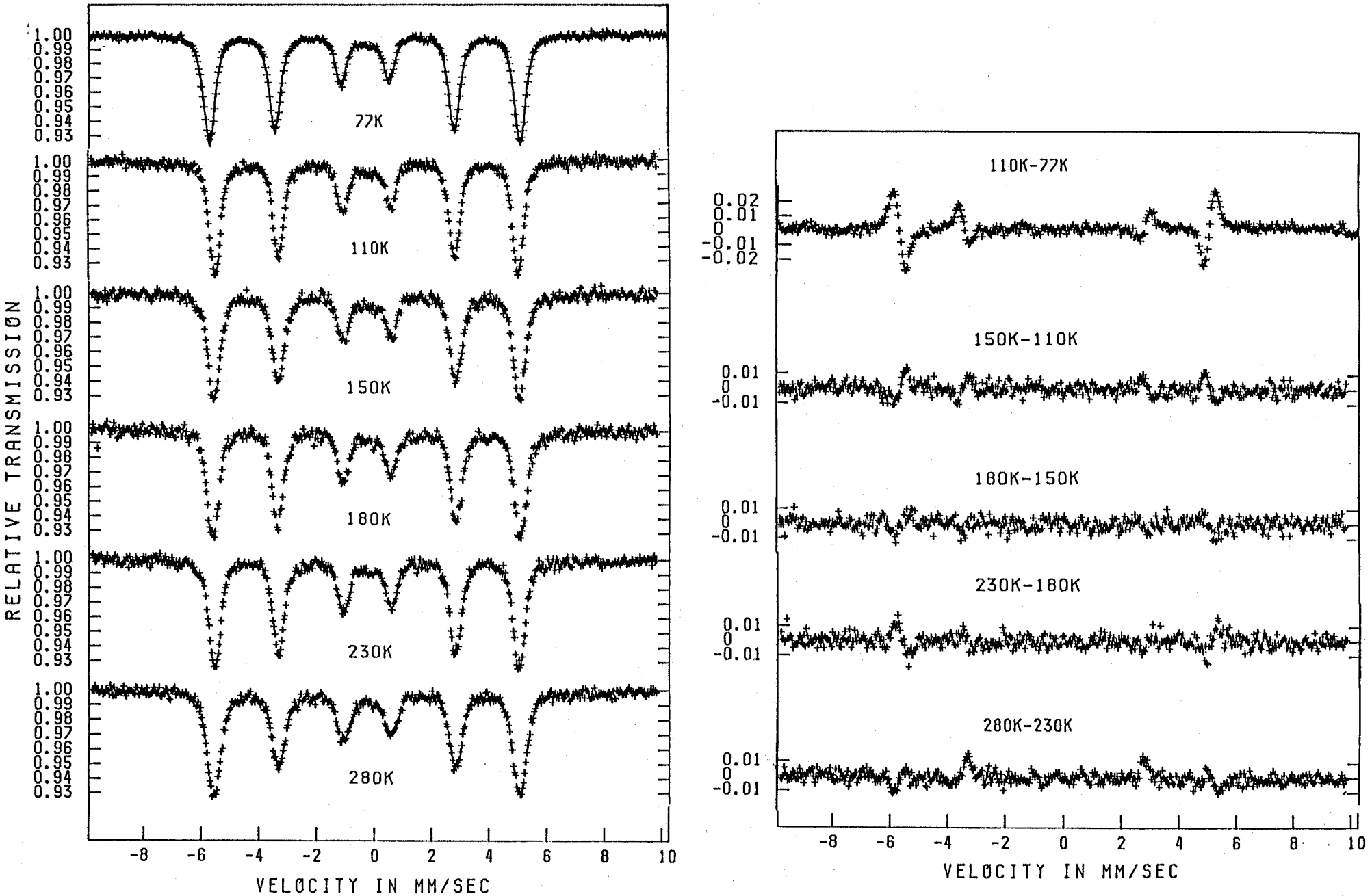

Fig. 3.6 Mössbauer emission spectra of super pure Fe with ^{57}Co during isochronal annealings and their successive subtractions.

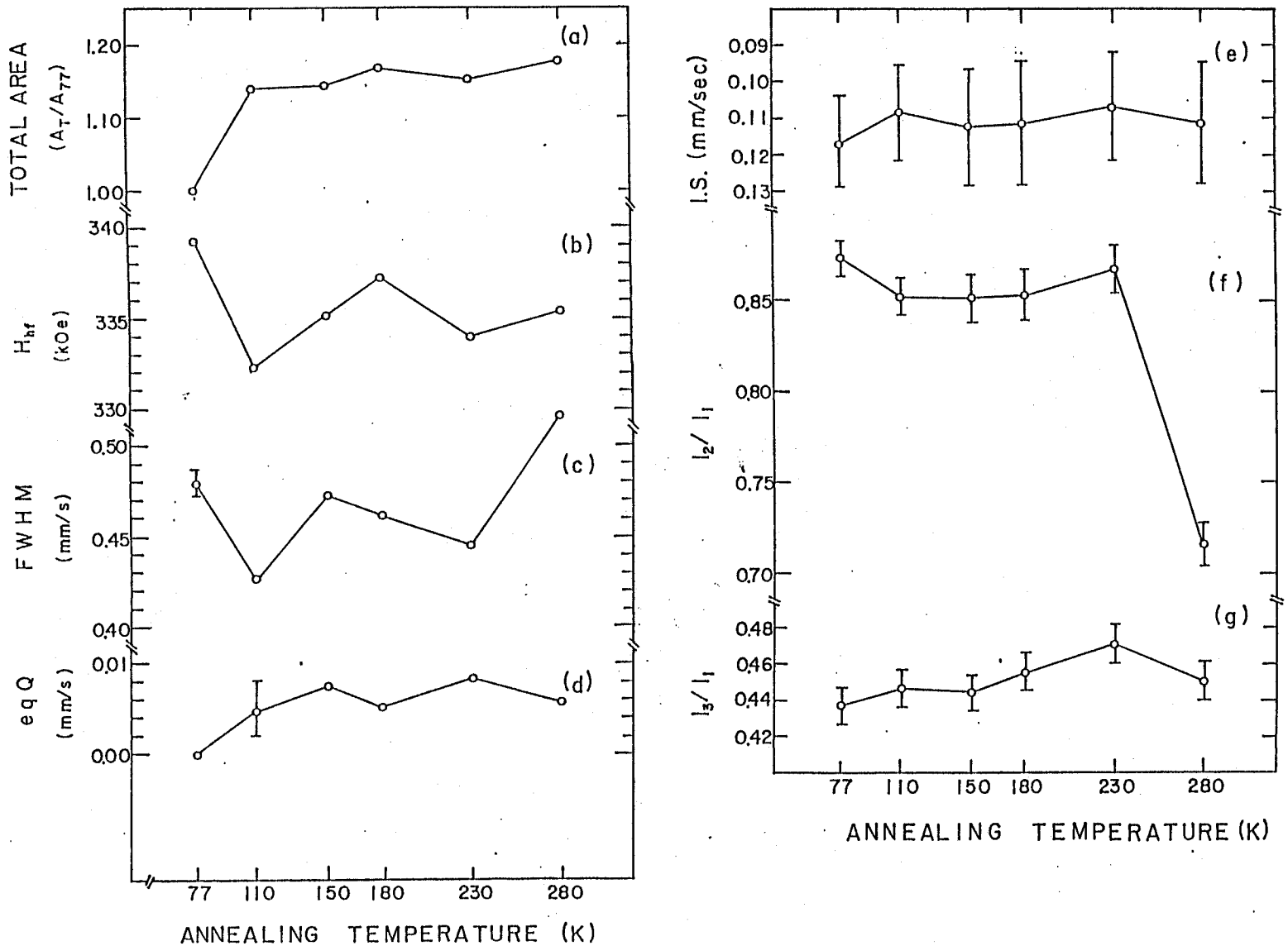

Fig. 3.7 Mössbauer parameters as the functions of the isochronal annealing temperature.

In the absorber experiments, the sensitivity to detect the defects may be smaller than the source experiments because no special interaction between the prove atoms of ^{57}Fe and radiation produced defects is expected. Nevertheless, the reactions of the prove atoms with point defect during the irraditaion and the annealings are thought to be more simple and understandable than those in the source experiment, in which the ^{57}Co source atoms react with deects as impurities in pure iron matrix and, in addition, it is necessary to take into account of the after effects of the decay processes of ^{57}Co atom.

For the comparison with the source experiments mentioned before, the absorber Fe specimen with $RRR_H = 500$ was irradiated at 30 K by neutrons with a total dose of 5×10^{16} n/cm^2, and the Mössbauer spectra were measured at 77 K after the irradiation, (a), and after the annealing at room temperature for one hour, (b), as shown in Fig. 3.8 . The average hyperfine field and the full width at half maximum (FWHM) were 339 ± 1 kOe and 0.37 ± 0.01 mm/sec after irradiation and 336 ± 1 kOe and 0.37 ± 0.01 mm/sec after the annealing at room temperature, respectively. The decrease in the average hyperfine field is clearly seen in the subtraction spectrum shown in Fig. 3.7(c), and the tendency of the changes of the hyperfine field by irradiation and anneling are the same as those of the source experiment. On the other hand, the total resonance area decreased a little after the annealing at room temperature, which is opposite to that observed in the source experiment mentioned in the last paragraph.

In order to see more precisely the changes of the area before and after the annealings until room temperature, an isochronal annealing experiment with stepwise heating with a heating rate of 5 min/

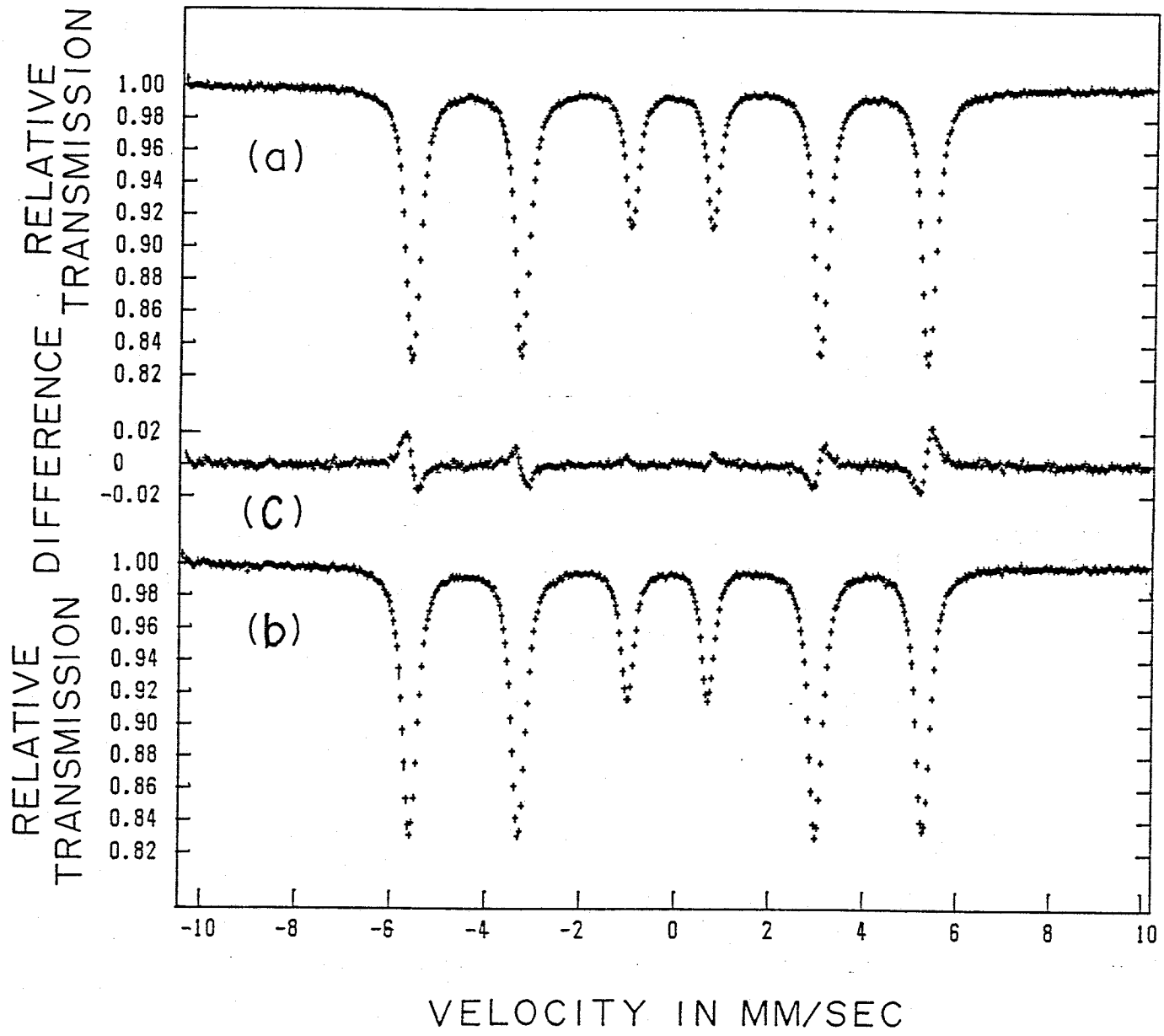

Fig. 3.8 Mössbauer absorption spectra taken at 77 K as irradiated, (a), after the annealing at room temperature, (b), and their subtraction, (c).

50 deg. was done by usint another specimen after the same neutron dose as the above one. Figure 3.9 shows the Mössbauer spectra at 77 K during the annealings and their subtraction spectra. The latter are plotted between two successive Mössbauer spectra, of which the lower one, the spectrum often each annealing, was subtracted from the upper one before the annealing. The lowest is the subtraction spectrum between the 260 K annealed and as irrdiated spectrum. As the second lowest subtraction spectrum shows, the total resonance area decreased remarkably after the annealing at 260 K , but the average hyperfine field, 336 ± 1 kOe, was kept constant. The reason why the average hyperfine field did not decrease at any stages of the annealings in this run, differing from the other neutron irradiation is thought to arise from an experimental failure such that the heating-up of the specimen could have occured by a mishandling during the transfer of it from the liquid nitrogen vessel to the cryostat. However, the specimen temperature rise was supposed not to be higher than 100 K since the spectrum changed at 110 K annealing as is indicated in the uppermost subtraction spectrum. Accordingly, the decrease in the hyperfine field, which was observed in the before mentioned first absorber experiment, may have occured belo 110 K as well as in the source experiment.

The total resonance area, (a), the FWHM, (b), the average hyperfine field, (c), the isomer shift, (d), the electric field gradient, (e), and the peak intensity ratios of I_2/I_1 and I_3/I_1 , (f), are plotted as the functions of the annealing temperature in Fig. 3.10. In the figure are plotted the same parameters for other specimens obtained from the absorber experiment by electron irradiation, which will be mentioned and discussed in the later sections.

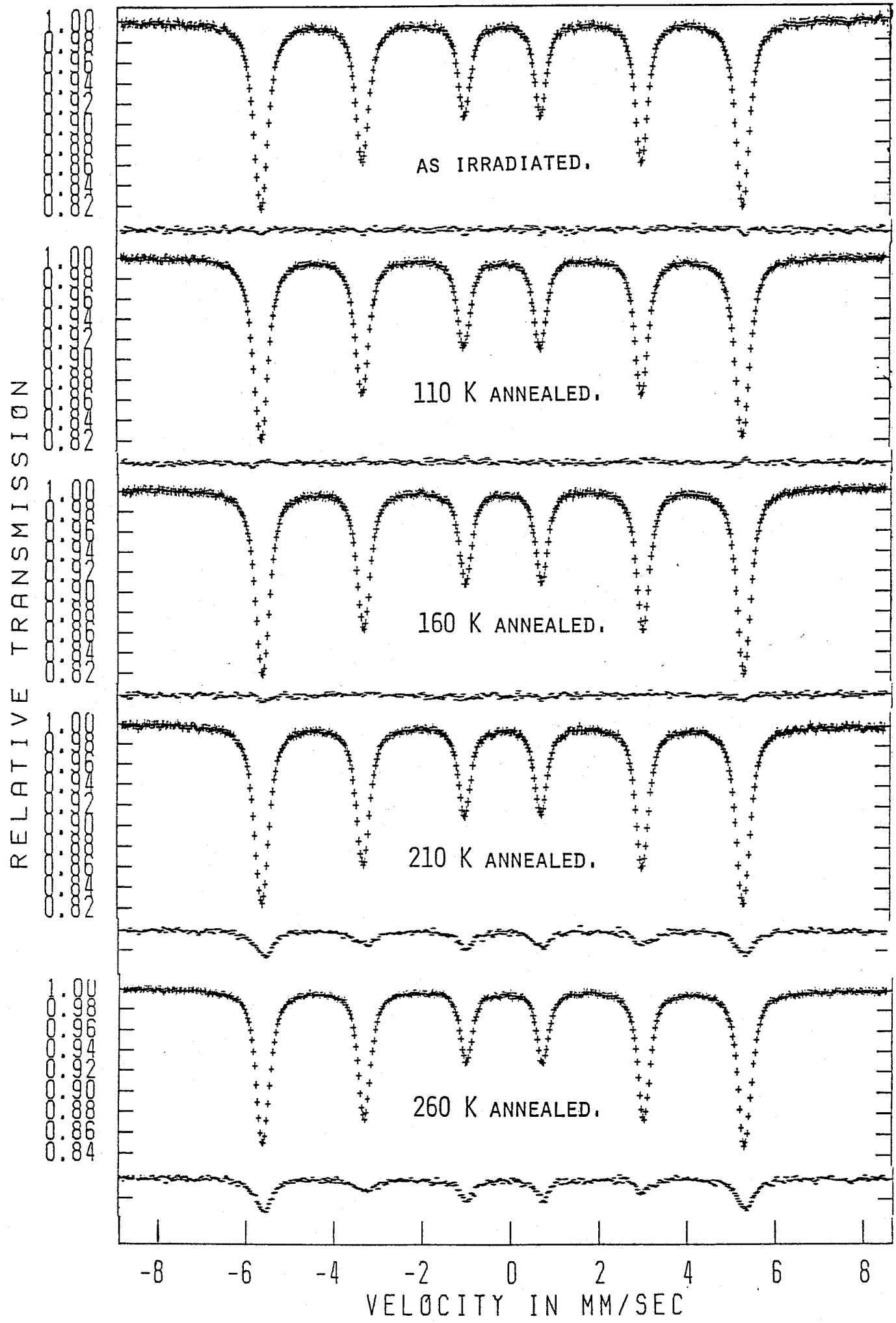

Fig. 3.9 Mössbauer absorption spectra during the sichronal annealings and their subtractions

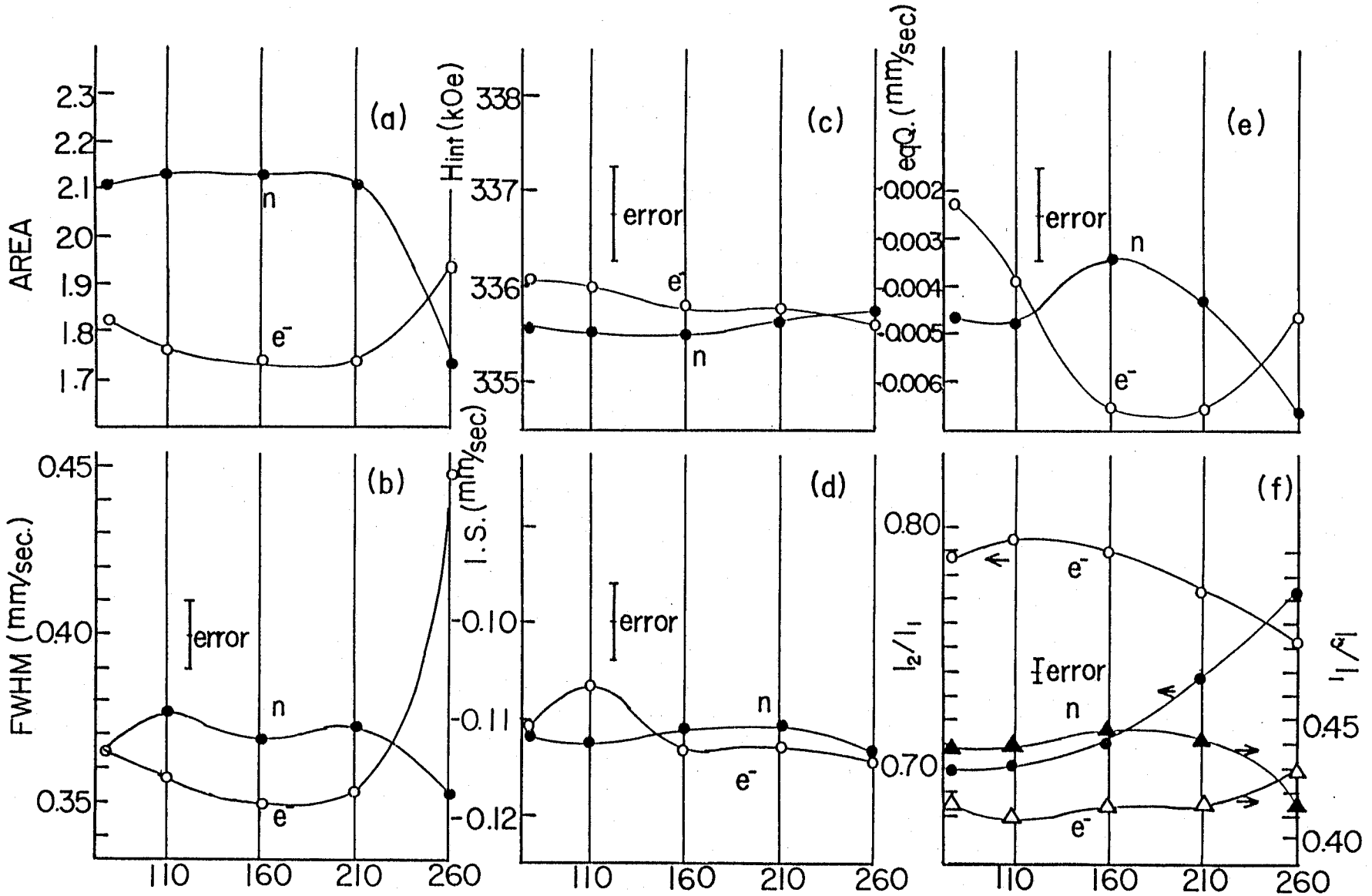

Fig. 3.10 Mössbauer parameters as the functions of the annealing temperatures; (a) total resonance area, (b) FWHM, (c) average hyperfine field, (d) isomer shift, (e) electric quadrupole effect, and (f) the peak intensity ratios of I_2/I_1 and I_3/I_1.

As for the neutron irradiation experiment, changes of the peak intensity tatios and the total resonance area are most striking among others. The large monotonous increase in I_2/I_1 and decrease in I_3/I_1 above 160 K, as shown in (f), may be originated from either the changes in the spin orientations in the foil specimen, or the appearance or disappearance of a component with a slightly different hyperfine field. The inclination of the atomic spins from the random orientation to the direction parallel to the surface of the specimen, i.e. perpendicular to the direction of the gamma rays will increase the peak ratio of I_2/I_1 and decrease that of I_3/I_1; when a new component with a hyperfine field slightly different from that of unperturbed iron appears after annealing, the first peak depth will be reduced more pronouncedly than the second and third one. To identify the origins, the partial resonance area ratios to tha total resonance area of the first, (a), second, (b), and third peak, (c), were obtained from the fitting parameters, and are shown by A_1/A_0, A_2/A_0, and A_3/A_0 respectively in Fig. 3.11 . The total resonance area, A_0, calculated from the fitting parameters is also plotted in (d) of the figure. The second peak area increases above 110 K, corresponding to the decrease in the first and the third peak areas. Accordingly, the atomic spins in the neytron irradiated specimen are thought to include gradually to the direction of the surface of the specimen during the annealings. The reason why the inclination of the atomic spins occured is not yet clear, but the existence of the defects introduced by the irradiation seems to affect the magnetic damain structures. Any appreciable change of the peak area ratio, A_3/A_1, is not expected from the spin orientation change, and, therefore, uncorrelated irregular changes of A_1/A_0 and A_3/A_0 are probably not essential but from the experimental errors.

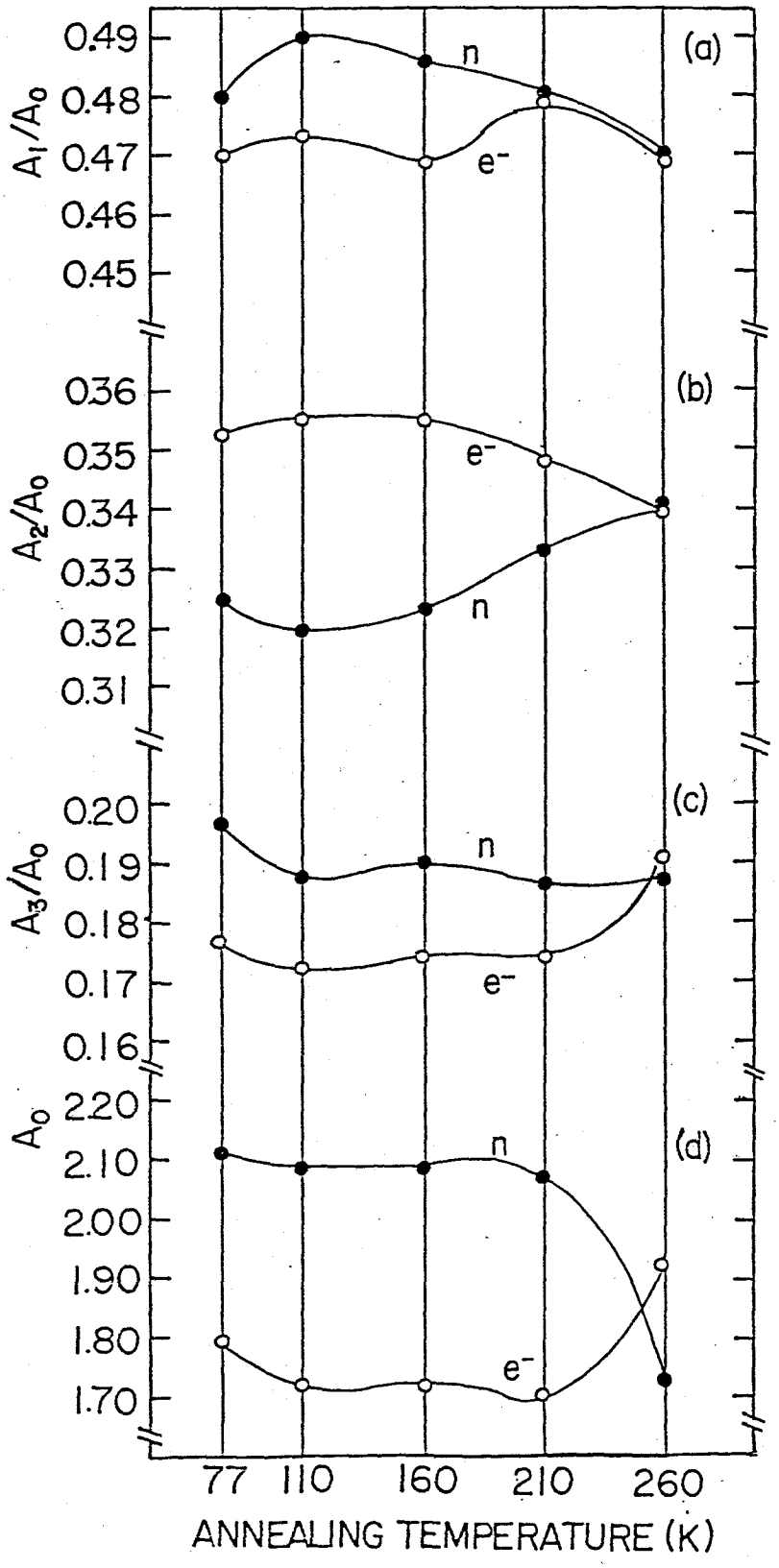

Fig. 3.11 Areal intensity ratios of A_1/A_0, (a), A_2/A_0, (b), and A_3/A_0, (c) and calculated total resonance area, (d).

The magnitude of the decrease in the total resonance area after the 260 K annealing seem to be larger than that expected from the concentration of defects, less than 0.1 at.% , and in addition, the change of the area in this absorber experiment has a opposite tendency to that in the source experiment already mentioned before; in the source experiments, the total resonance area increased remarkably after the 270 K annealing. Futher discussions , taking account of the difference of the positions of the prove atoms between the source and absorber will be developed in later sections and comparisons between the neutron and the electron irradiation will also be given there.

3.2 Electron Irradiation

As the second trial of the search for the "defect lines" in the Mössbauer spectrum, the specimens irradiated with LINAC electrons at 80 K were investigated by the method similar to those employed in the neutron irradiation experiment. In this section, the results of the source experiment, the absorber experiment, and the dynamical thermal scan measurement after electron irradiation will be described in this order. The high purity iron specimens with the resistivity ratio, $R_{300K}/R_{4.2K}$ (RRR_H), of about 5000 were used for the source experiment, and those with $RRR_H = 500$ for the absorber experiment and the dynamical measurement. Although clear defect lines in the spectra were not observed as they are, the Mössbauer parameters and the subtraction spectra changed as well as in the case of neutron-irradiation. But, the chracteristic of the changes are quite different, probably arising from the difference in the defect distributions between the neutron and electron irradiation case.

3.2.1 Source experiments

Only the Mössbauer spectra taken below 180 K annealings and their subtractions are given in Fig. 3.12(a) and (b) respectively. The annealings were not done above 190 K because the specimen temperature was accidentally increased during the measurement of the Mössbauer spectrum after the 180 K annealing. After the irradiation with a total dose of 4×10^{18} e^-/cm^2, the total resonance area decreased a little, and a new component with the hyperfine field lower than that at 77 K before irradiation and a negative isomer shift appeared, as is clearly seen in the subtraction spectra in the upper most part of the figure (b). The average hyperfine

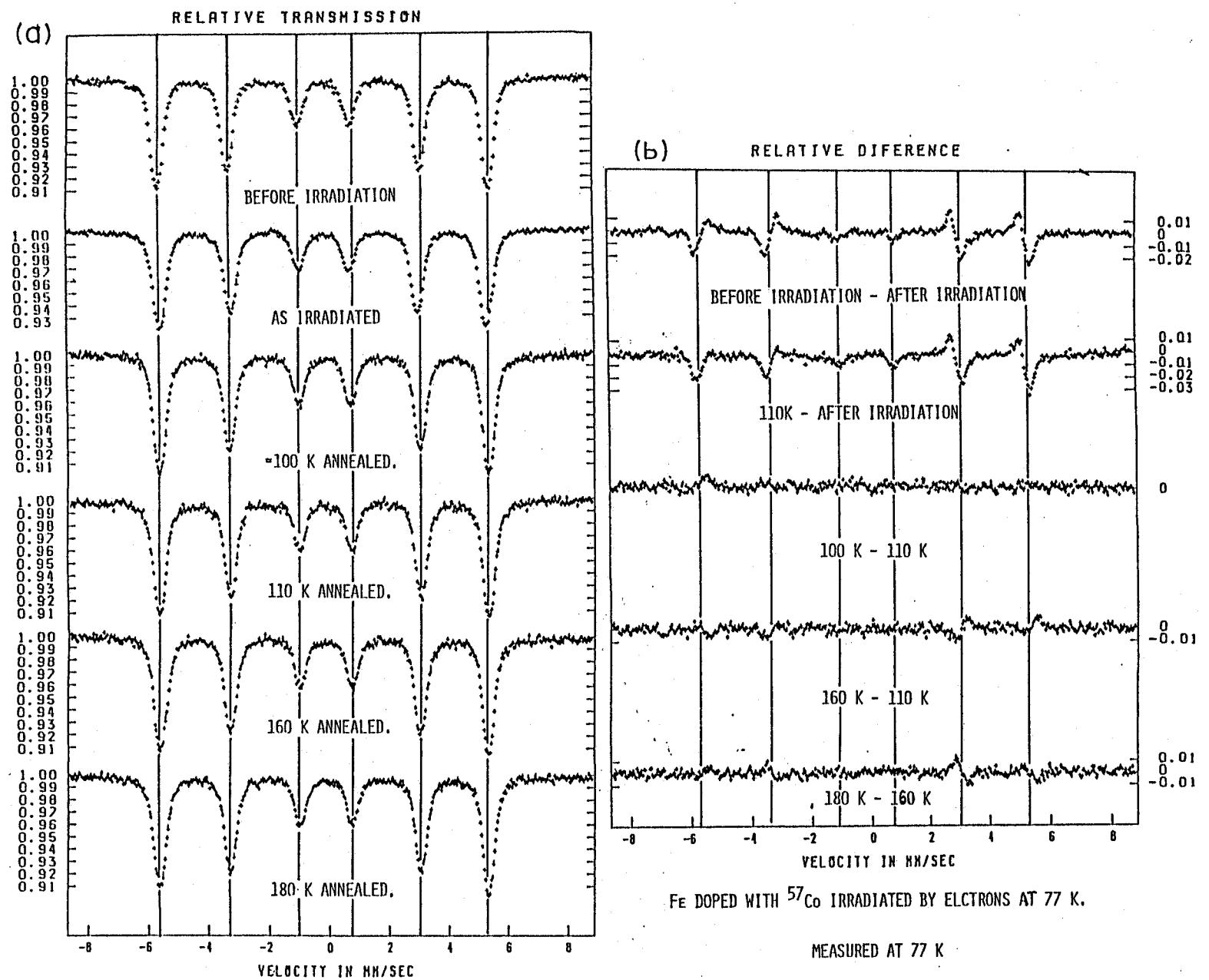

Fig. 3.12 Mössbauer emission spectra of the electron irradiated ^{57}Co-in-Fe source taken at 77 K before and after isochronal annealings, (a), and their subtractions, (b).

fields and the full widths at half maximum (FWHM) are 338 ± 1 kOe and 0.46 ± 0.01 mm/sec before irradiation and 335 ± 1 kOe and 0.47 ± 0.01 mm/sec after irradiation, respectively.

For the comparisons between the neutron and the electron irradiated specimens measured at both 77 K and 4.2 K just after irradiations, the Mössbauer spectra of the former were subtracted from the latter as shown in Fig. 3.13 ; the left ones are the spectra at 77 K before irradiation and their subtraction, the middle ones those at 77 K after irraditaion, and the right ones those at 4.2 K after irradiation. Mössbauer parameters obtained from these spectra are summarized in Table 3.2 . The decrease in the total resonance area after neutron irradiation is larger than that after electron irradiation, and the increment of the area by lowering the temperature from 77 K to 4.2 K is larger in the electron irradiated specimen than in the neutron irradiated one. The average hyperfine field increased after the neutron irradiation, but decreased after the electron irradiation. Although the differences between the electron and the neutron irradiation can be pronouncedly seen in the subtraction spectra at 77 K , they do not appear appreciably at 4.2 K . These interesting results may be originated from the difference of the defect distribution between them detailed discussion will be given later.

Figure 3.14 shows the normalized counts per 3000 sec. at zero velocity through the Fe absorber at 77 K , (a), and toom temperature, (b), as the functions of the annealing temperature. The former increased remarkably between 110 and 160 K after the small up-and-down changes around 100 K , indicating that the ^{57}Co atoms on the unperturbed sites in the Fe matriz were trapped gradually by the mobile defects during the annealings between them. On the

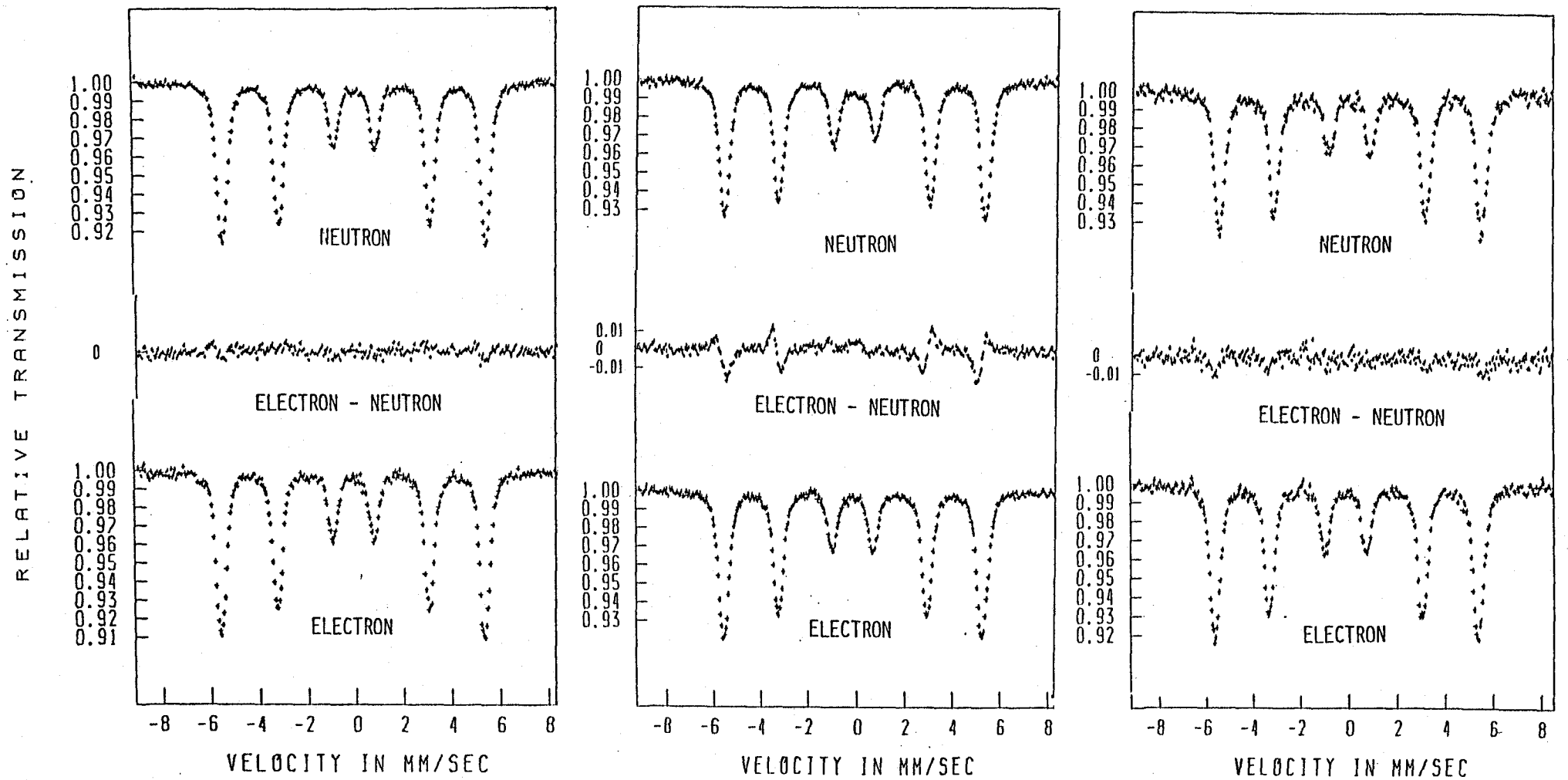

Fig. 3.13 Comparison at 77 K between neutron and electron irradiated source specimen before irradiation, (a), after irradiation, (b), and at 4,2 K after irradiation, (c).

NO.		AREA RATIO A_{after}/A_{before}	H_{int} (kOe)	FWHM (mm/sec)	δ (mm/sec)	eqQ (mm/sec)	I_2/I_1	I_3/I_1
3	before irrad. 77K	0.9245	338.5(6)	0.466(9)	-0.12(3)	-0.001(3)	0.844(10)	0.373(7)
	after irrad. 77K		335.2(2)	0.471(8)	-0.12(2)	-0.002(4)	0.817(16)	0.394(10)
	after irrad. 4.2K	0.9777	339.4(4)	0.473(9)	-0.13(2)	-0.002(5)	0.788(13)	0.362(11)

Table 3.2 Mössbauer parameters of the spectra before and after electron irraditaion

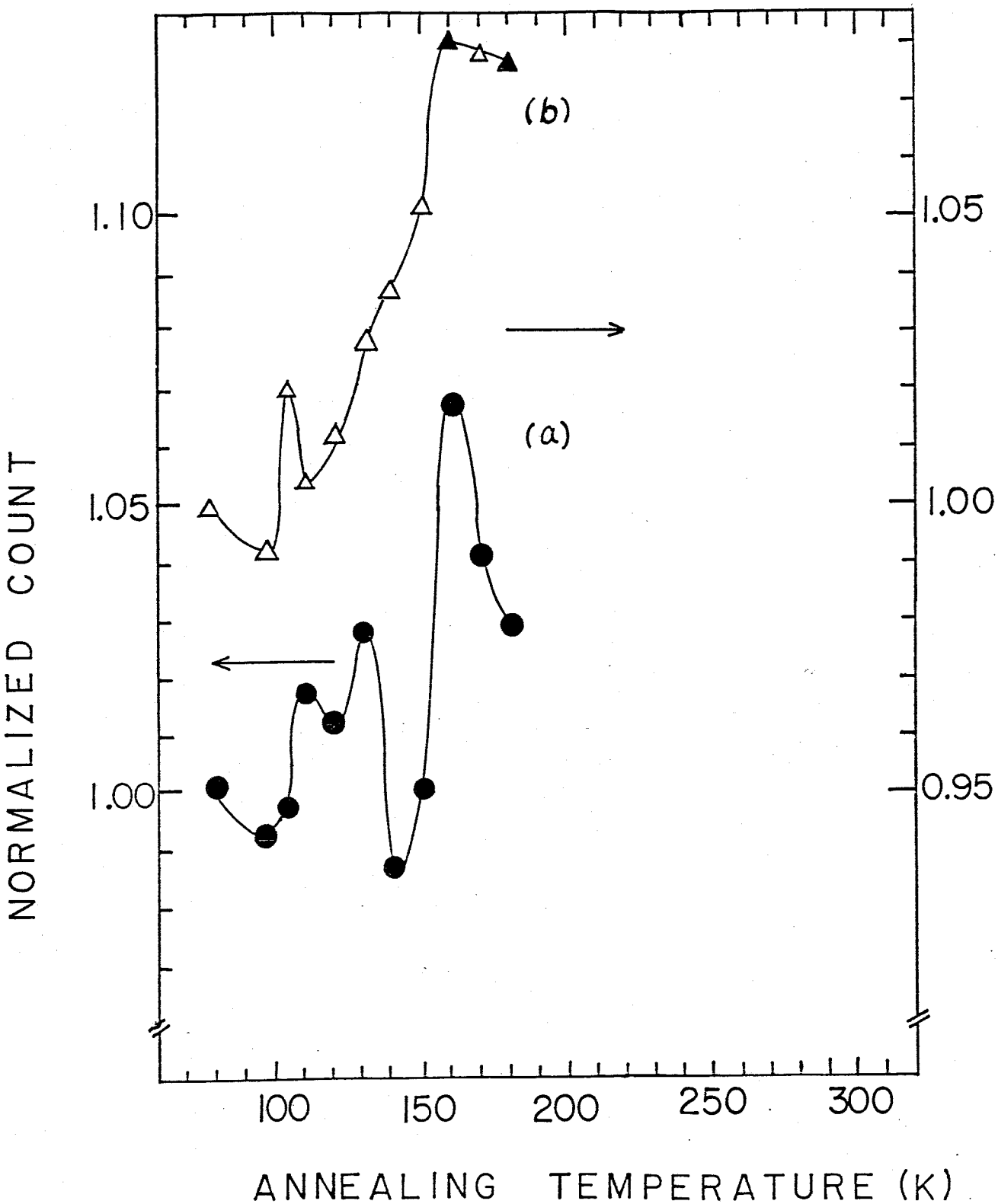

Fig. 4.14 Static thermal scanning curve on electron irradiated source specimen. The absorbers at 77 K, (a), and room temperature, (b), were used.

other hand, the latter increased and decreased repeatedly up to the 180 K annaling depending on the hyperfine interactions in the comploxes. This suggests the association and dissociation process of the ^{57}Co atoms-defects complexes.

The Mössbauer parameters after the isochronal annealing experiment with the step-up rate of 10 deg./5 min ,which were obtained from the fitting analysis using a set of six Lorentzian lines, are given in Fig. 3.15 as the functions of the annealing temperatures; the total resonance area is in the figure (a). the FWHM in (b), the average hyperfine field in (c), the isomer shift in (d), the electric field gradient in (e), and peak intensity ratios of I_2/I_1 in (f). The parameters at the 270 K annealing were obtained from the spectrum of the specimen after accidentally heated up to 270 K during the measurement. The Mössbauer spectrum at the 90 K annealing was obtained only after transfering the specimen from the Helium cryostat to the top-roading type cruostat for the isochronal annealing experiment, but it shows a profile different from the spectrum before transfering, as is shown in the second upper subtraction spectrum in Fig. 3.12(b). This means that the radiation produced defects extensively moved and internal structure of the specimen was changed. However, the count rate at zero velocity changed clearly after the 90 K annealing as Fig. 3.13 shows, and the Mössbauer parameters, i.e. the total resonance area, and the FWHM, also changed after the 110 K annealing as Fig. 3.14 shows, so that the specimen temperature during the transfer was thought not to increase up to 90 K . The total resonance area in (a) of the figure increased after the 90 K annealing, and decreased a little between 90 K and 180 K . The area at 270 K was not able to be obtained because of the change in the measurement condition of

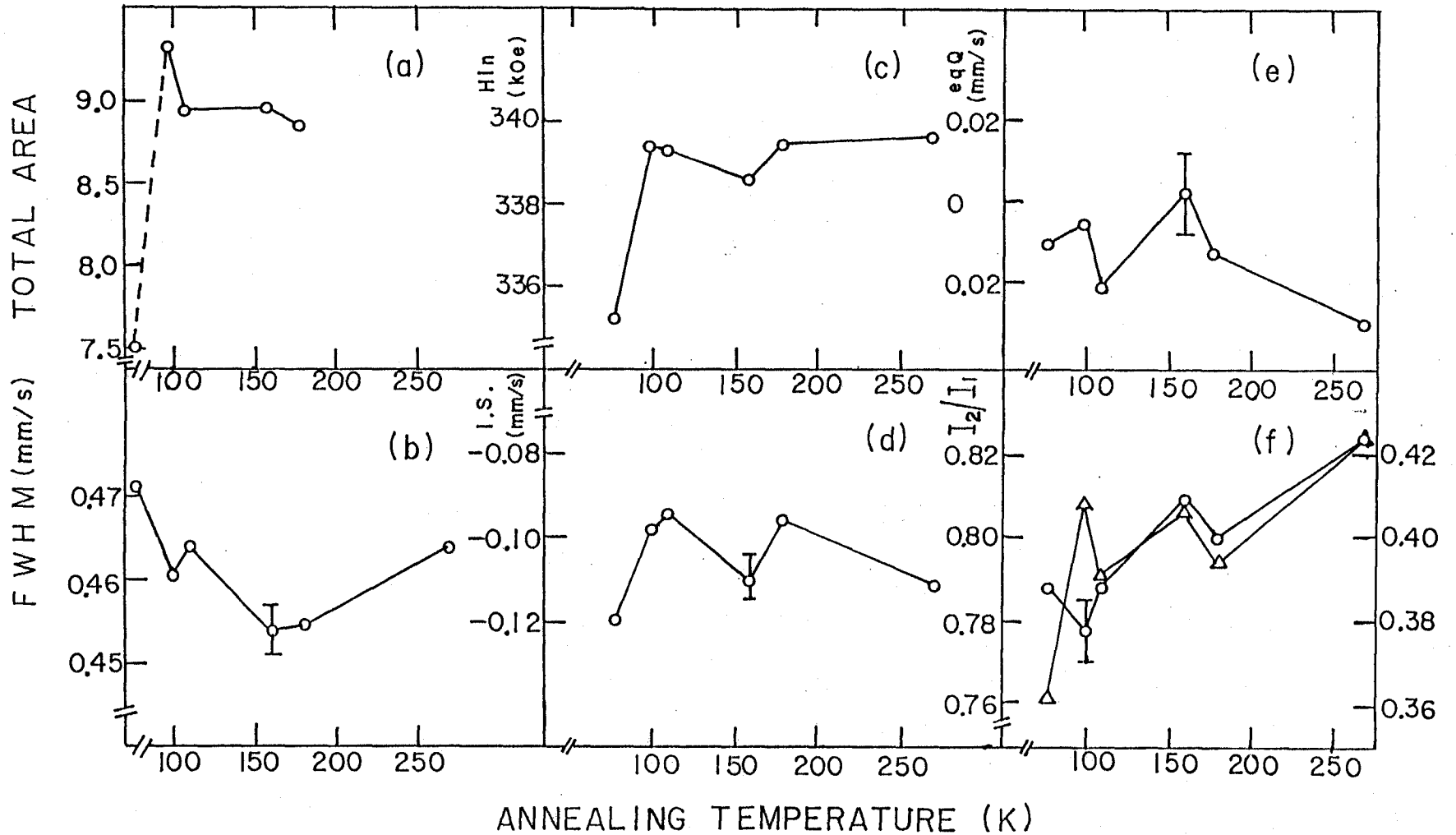

Fig. 3.15 Mössbauer fitting parameters during isochronal annealings; (a) total resonance area, (b) FWHM, (c) average hyperfine field, (d) isomer shift, (e) electric quadrupole effect, and (f) peak intensity ratios of I_2/I_1 and I_3/I_1.

the gamma-ray detection. The average hyperfine field increased from 335.2 to 339.4 kOe after the 90 K annealing, decreased slightly at 160 K, and reincreased to the value of 339.4 kOe. The average isomer shift changed more pronouncedly than that in the neutron irradiated specimen, as is seen in the subtraction spectra in (b) of Fig. 3.12; after the 160 K annealing, a component with a positive isomer shift to that of the unirradiated specimen disappeared and a new component with negative one appeared, roughly corresponding to the increase in the count rate at 160 K compared with that at 110 K as is shown in Fig. 3.14(b), and after the 180 K annealing, tha latter component disappeared and with a positive one appeared, corresponding to the decrease in the count rate through the absorber at room temperature between 160 K and 180 K.

The recovery behavior of the count rate and the fitting parameters during the isochronal annalings below the stage II are quite different from those in the nwutron-irradiated source specimen as mentioned before. Especially, the magnitude of the increase in the count rate through the absorber at 77 K is much larger than that in the neutron irradiation as in Fig. 3.5, and the increase in the average hyperfine field is opposite to that in the neutron irradiation. These differences may be originated from the difference in the defect distribution in the Fe matrix just after irradiation; the neutron irradiation is thought to introduce a cascade damage, the distribution of which is well localized so that the distances between the ^{57}Co atom and the defects are larger than those in the electron irradiation which is thought to introduce a uniform Frenkel-pair defects. Accordingly, the probability of reaction of the defects with the ^{57}Co atoms durinf the annealings is much larger in the electron irradiation than that in the neutron irradiation, so that the magnitude of the increase in the

count rate is expectee to be larger in the former than that in the latter. The reason why the different distribution of defects products the different hyperfine fields is not clear, the theoretical calculation is neccesary to solve the problem.

3.2.2 Absorber experiment

The absorber experiment is thought to have both a merit and a demerit discussed before; the reactions of the prove atoms with the defects are simple, but the sensitivity to detect the perturbations by defects is small. In the neutron-irradiated Fe absorber, appreciable changes in the total resonance area, the average hyperfine field, and the peak intensity ratios were observed, as were shown before.

Figure 3.16 shows the Mössbauer spectra of the Fe absorber taken at 77 K , which was irradiated by LINAC electrons with a total dose of 4×10^{18} e^-/cm^2; the spectrum as irradiated is in (a), after the annealing at room temperature (b), and their subtraction spectra (c). The subtraction spectrum was obtained by subtracting the spectrum before the annealing from that after the annealing, in which the remarkable decrease in the peak intensity of I_2/I_1 and the disappearance of a small broad component can be seen after the annealing. The average hyperfine field and the FWHM are 337.5 ± 0.5 kOe and o.375 ± 0.005 mm/sec before the annealing, and 337.1 ± 0.5 kOe and 0.367 ± 0.005 mm/sec after the annealing, respectively. The peak intensities of I_2/I_1 and I_3/I_1 are 0.965 and 0.444 before the annealing, and 0.777 and 0.440, respectively. For further investigations, the isochronal annealing experiment of the steps of 50 deg./5 min was performed. The Mössbauer spectra and their subtraction spectra are given in Fig. 3.17. The subtraction pro-

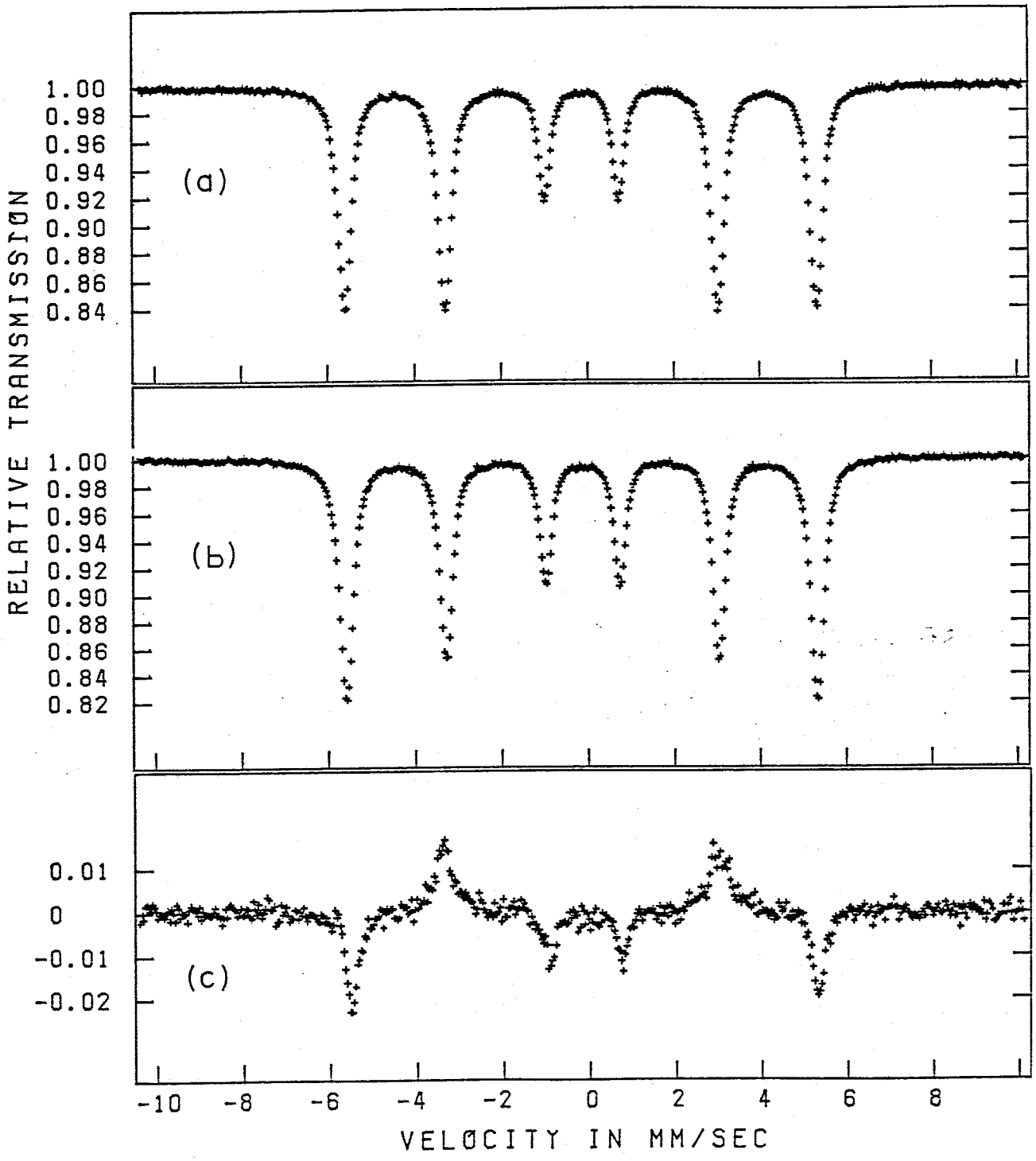

Fig. 3.16 Mössbauer absorption spectrum of electron irradiated Fe measured at 77 K as irradiated, (a), after the annealing at room temperature, (b), and their subtraction spectrum, (c).

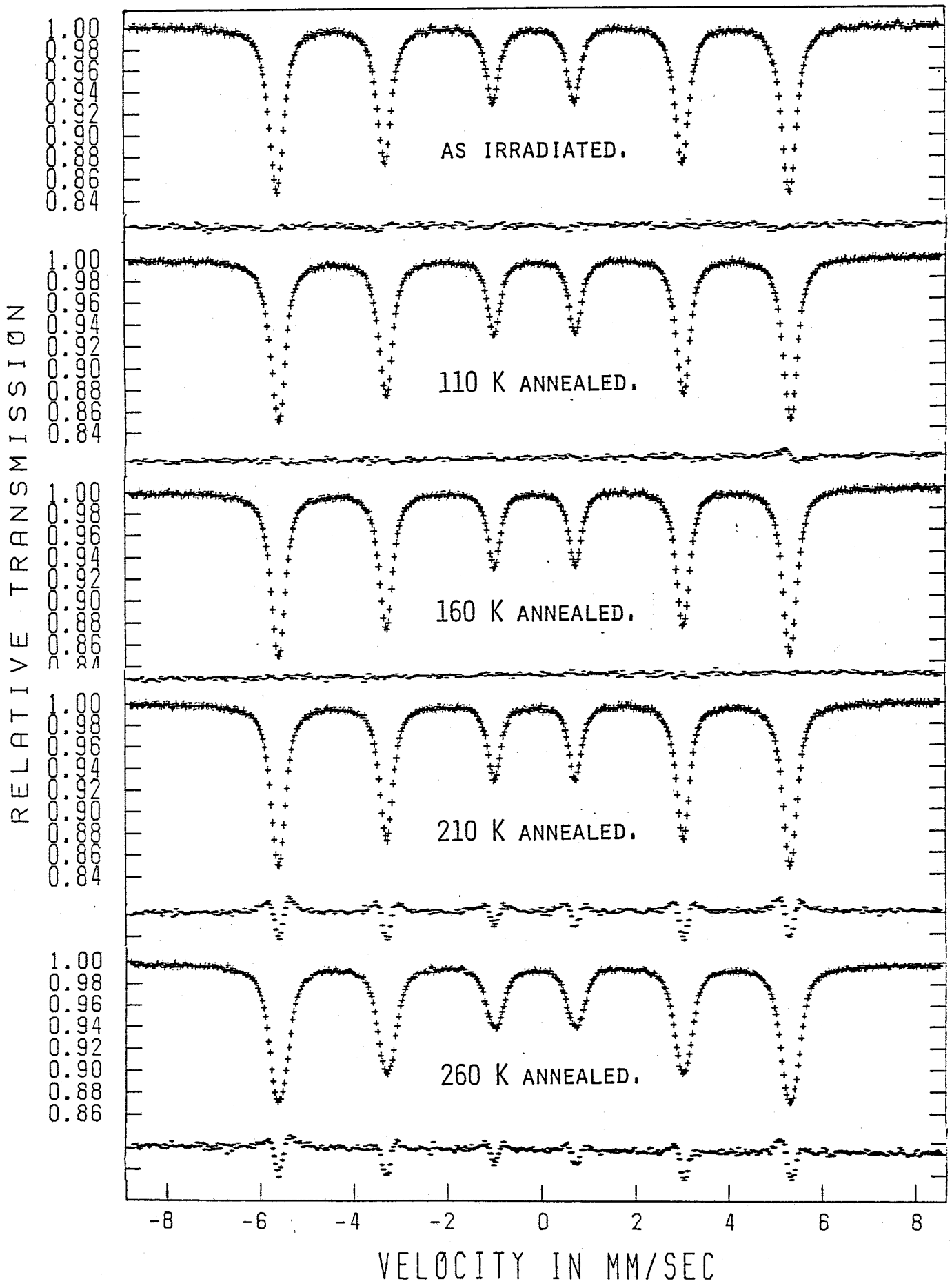

Fig. 3.17 Mössbauer absorption spectra measured at 77 K during the isochronal annealings and their subtractions.

cedures are the same as in teh isochronal annealing experiment using the neutron-irradiated-Fe absorber, and the Mössbauer spectra and their subtractions are shown in Fig. 3.9 . All Mössbauer parameters obtained from this isochronal annealing experiment are already given in Figs. 3.10 and 3.11 together with those from the neutron irradiation experiment. Roughly speaking, the characteristics of the changes in the Mössbauer parameters in the electron irradiation, have opposite tendencies to those in neutron irradiation. For instance, the total resonance area and the FWHM increased after the 260 K annealing in the former, but decreased in the latter, as are shown in Figs. 3.10 and 3.11 . The peak intensity ratios of I_2/I_1 and I_3/I_1 gradually decreased and increased during the annealings, respectively, which are also opposite.

The reason why the atomic spins were inclined to the direction of the specimen surface is thought that the magnetic field arising from the electric currents during the irradiation could incline the atomic spins to the direction of the surface, which is perpendicular to that of the electron beam, and that the magnetic domain structure during the irradiation was "frozen" in the low temperature. During the annealings, the frozen magnetic damain structure could be recoverd, leading to the decrease in the intensity ratio I_2/I_1 and the increase in that of I_3/I_1.

After the annealing at 260 K , the WHM of the spectrum remarkably increased, from 0.35 to 0.45 mm/sec. This is probably not due to the change in a spectrum-broadening due to abnormal mations of the driver system. Whether the change at 260 K is originated from the defect-recovery in the specimen or from the experimental error is not decided yet, but from the next measurement just after that at 260 K , the Mössbauer spectrum with a sharp six line profile was

obtained. In addition, taking into account of the remarkable change at 260 K in the neutron irradiation, the broadening seems to arise from a rearrangement by the stage III defects.

The magnitudes of the average hyperfine field obtained from the isochronal annealings are a little smaller than those from the results shown in Fig. 3.15 . These differences may be mainly due to the heating-up of the specimen temperature during the transfer as is mentioned before.

For the detailed discussions in the absorber experiment, further experiments must be done, including to the thermal scan measurement using a ^{57}Co doped Fe source and a irradiated Fe absorber specimen. Nevertheless, within the above results, a few discussions will be given later relating to the appearance and disappearance of a component with a different isomer shift during the Stage II.

3.2.3 Dynamical thermal scan measurement

As the last paragraph of the section of electron irradiation experiments, a preliminary result of the dynamical thermal scan measurement will be introduced in order to mention how useful information can be obtained by this technique and yet what sorts of experimental problems concerning this new technique still remain.

As was already mentioned the dynamical thermal scanning is a technique to measure the count rate at zero velocity of gamma-rays transmitted through an absorber during conrinuous heating the specimen. In the first place, in order to check the temperature bariation of the count rate of other undersirable origins than the changes of the Mössbauer resonance fraction and/or the defects annealing, the counts per 100 sec of the off resonance 6 keV X-

rays were measured by advancing in steps the channels of the multi-channel analyzer, during continuous heating, as shown in Fig. 3.18 . The source and the absorber were the ^{57}Co-doped-Fe and the Fe foil before irradiation, respectively. A remarkable increase in the count rate accured between the channels, about 240 and 400, which corresponded 77 and 130 K , respectively. This increase probably arose from the decrease in the thickness of gamma-ray path due to the excluded evaporation of a thin film of liquid nitrogen or oxygen condensed on the specimen surface during the transfer of the specimen from liquid nitrogen to the cryostat. Such a disturbence of extraneous origin must be excluded in the data analysis when the resonant 14.4 keV gamma-rays were used in the irraditaion experiment as will be mentioned later. It was considered that the gas condensation on the specimen surface might have occured in the static thermal scan measurement too. So that, the count rate of the 6 keV X-rays after all annealings was monitored during the static thermal scanning of the irradiated specimens which was already mentioned in the preceding paragraphs, and it was confirmed that the condensation effect had little influence to the count rate in that case. This means that the thickness of the condensed film of liquid nitrogen or oxygen was kipt relatively constant during the gamma-ray measurement at every step of the isochronal annealing experiment.

Figure 3.19(a), (b), and (c) shows the results of the dynamical thermal scan measurement of the 14.4 ke Mössbauer gamma-rays on the unirradiated ^{57}Co-doped-Fe source, the electron irradiated ^{57}Co-doped-Fe source, and the neutron irradiated Fe absorber specimen, respectively. In the two formers, the unirradiated Fe absorber placed together with the source specimen was used, and in the latter, the unirradiated ^{57}Co-soped-Fe source with the irradi-

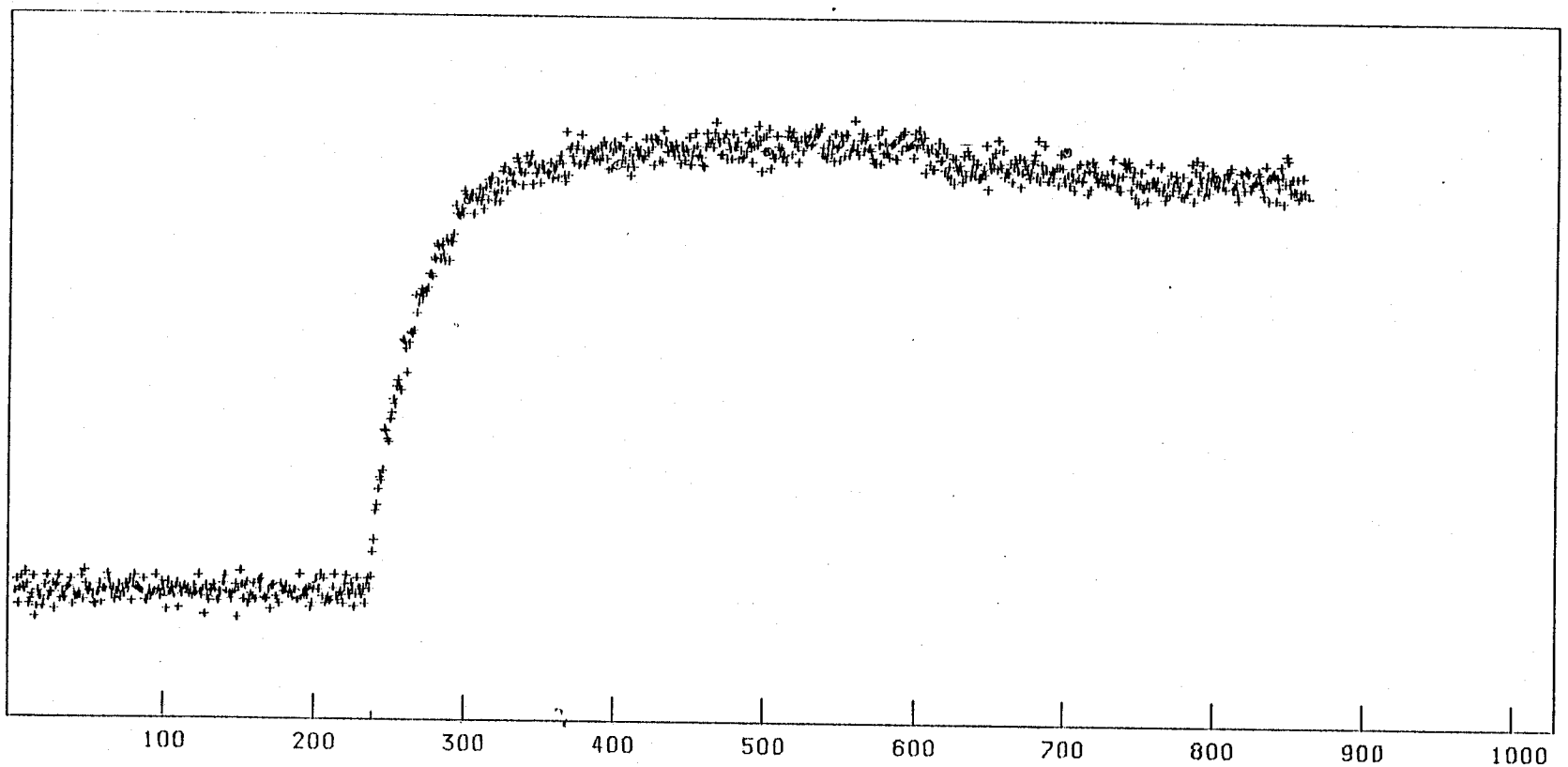

Fig. 3.18 Dynamical thermal scanning by 6 keV X-rays on the ^{57}Co doped Fe specimen.

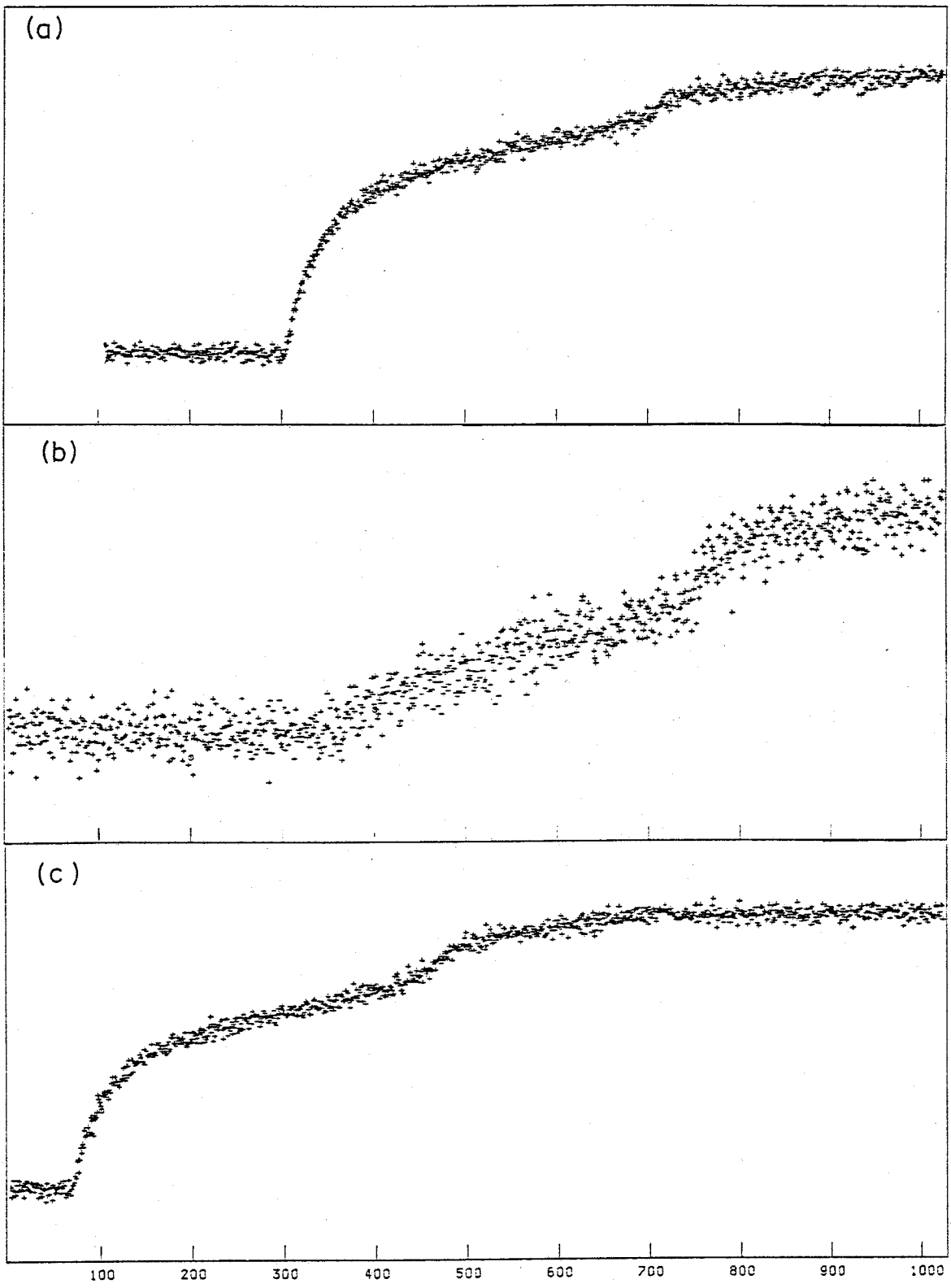

Fig. 3.19 Dynamical thermal scanning by 14.4 keV Mössbauer gamma rays on the unirradiated source specimen, (a), the electron irradiated source specimen, (b), and the neutron irradiated Fe absorber specimen, (c).

ated absorber specimen. These data are replotted as the functions of the specimen temperature by transfering the channel numbers to the corresponding temperatures, as in Fig. 3.20(a), (b), and (c), respectively. The counts in the ordinate were normalized by the starting value before heating in each run. All of them equally show a sudden increase at around 100 K, as before mentioned, and the second small increse of the counts in the middle of the curves, disappear. The latter apparent change most likely arose from the non-linear temperature rise due to the evaporation of the final amount of liquid nitrogen in the cryostat. After these corrections and considerations, however, characteristic of the curves are different after all. For the comparison between the results before and after the irradiation, the curve of (a) was subtracted from that of (b) and that of (c), respectively, as shown in Fig. 3.20(d) and (e). The curve (d) obtained from the irradiated ^{57}Co-doped-Fe cource shows a gradual decrease up to 150 K, and increase up to 290 K. The curve (e) in Fig. 3.20, obtained from the neutron irradiated Fe absorber specimen, has the same tendency in the count rate changes. The decrease of the relative difference curve like (d) must be associated with the increase in the number of the ^{57}Co atoms satisfying the resonant condition with the ^{57}Fe atoms in the absorber. At least, two origins can be considered for it, that is, the increase in the number of the ^{57}Co atoms released from the defects, or the increase in the Debye-Waller factor of the ^{57}Fe atoms enitting gamma-rays. Likewise, the increase of the relative difference must be due to the decrease in the number of the ^{57}Co atoms in the resonant condition with the unperturbed ^{57}Fe atoms, or the decrease in the Debye-Waller factor. The decrease in the Debye-Waller factor is directly connected increase in the mean square displacement of the prove atoms, $\langle x^2 \rangle$,

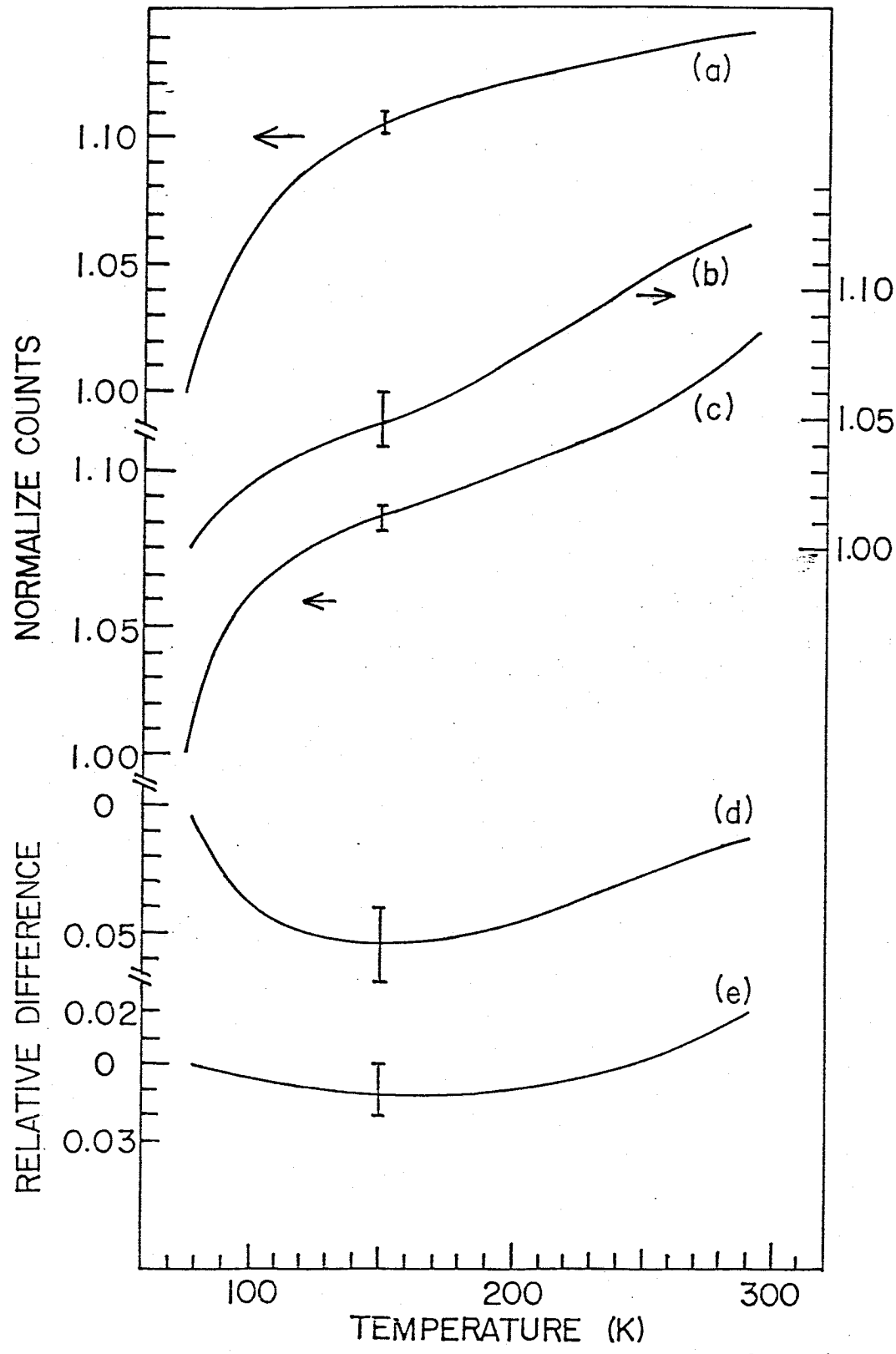

Fig. 3.20 Dynamical thermal scanning plotts as the functions of the specimen temperature; (a) the unirradiated source specimen, (b) the electron irradiated source specimen, and the neutron irradiated absorber specimen, (c), and their subtraction (d) = (a) - (b), (e) = (a) - (c).

or the increase of the jump frequency of either the prove atoms or the neighbor atoms of them coming comparable to the reciprocal of the life time of ^{57}Fe, ~ 10^7/sec , as are already discussed before.

From the results of the static thermal scan measurement, it is suggested that the trapping of the defects may occur below the stage II around 150 K , and the detrapping of another kind of defects above the stage III around 220 K . Nevertheless,comparison between Fig. 3.5 and Fig. 3.20(d) and (e) tells us that the tendencies of increase and decrease in these temperature regions are opposite, and, therefore, if only the idea of trapping and detrapping during the heating was introduced in the analysis of the dynamical thermal scan measurements, a failure conclusion that the detrapping process occured below the stage II and the trapping occured at the stage III would be drawn. A possible interpretation for the opposite result of the dynamical thermal scan measurement could be the effect of atomic jumps, but the corrections of the data of the dynamical measurement are not yet exact enough, as mentioned before, so that further discussions will not be given here.

3.3 Self-Ion Irradiation

As the final trial of the search for the "defect lines" in the Mössbauer spectrum, the specimens irradiated with two kinds of self-ions, $^{56}Fe^{+}$ and $^{57}Fe^{+}$, were investigated by both the transmission and the scattering method of Mössbauer spectroscopy. In addition, in order to know the distribution and the nature of the defect clusters introduced by irradiation, the transmission electron microscopic observation was done, too. In this investigation, the iron foils with the resistivity ratio, $RRR_H = 500$, were used. In the following, first, the result of the transmission electron microscopy, and in the second, that of the transmission Mössbauer measurement, and in the third, that of the scattering Mössbauer measurement will be given in this order. Ultimately, clear defect lines were not observed in the Mössbauer spectrum after the irradiation at room temperature as well as in the case of neutron and electron irradiation, but an asymmetrical spectrum different from the unperturbed pure iron spectrum was obtained as a remnant in the subtraction analysis, and it was decomposed into two components by computer analysis. Futher more, two kinds of the components with different hyperfine fields were detected at the different depths of the specimen, by using the scattering method, corresponding to the depth distribution of the small defect clusters obtained by the stereoscopic observation of the electron micrographs.

3.3.1 Transmission elctron microscopy

Figure 3.21(a) and (b) show the electrom micrographs* of the speci-

---

* The micrographs were taken by Mr. T. Ezawa.

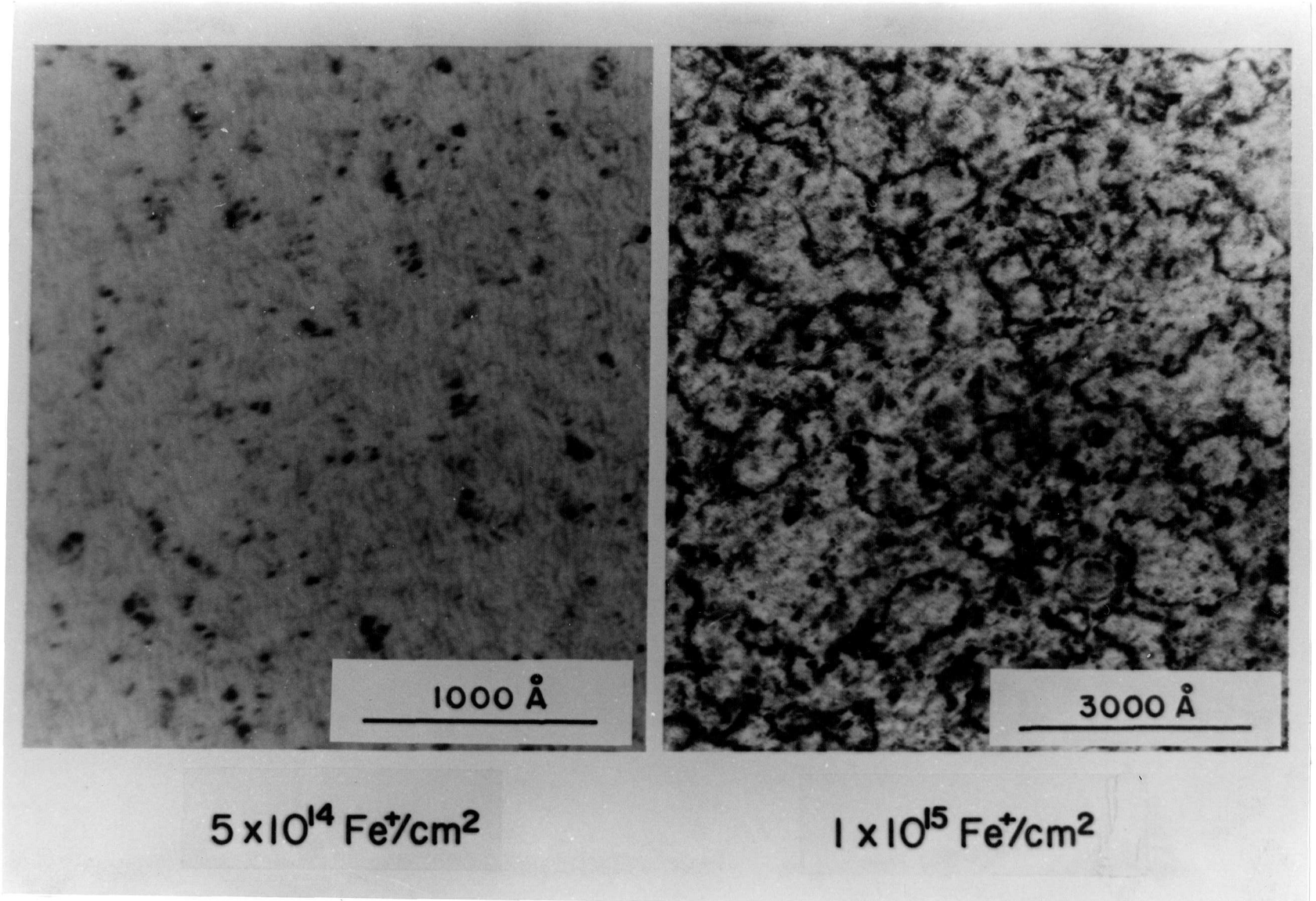

Fig. 3.21 Electron micrographs of the Fe^+ ion irradiated Fe; (a) 5 x 10^{14} ions/cm^2, and (b) 1 x 10^{15} ions/cm^2.

mens irradiated at room temperature by the 200 keV Fe^+ ions with the total doses of 5×10^{14} and 1×10^{15} Fe^+/cm^2, respectively. In the former specimen, the small defect clusters with a diameter between 1 and 5 nm randomly distribute. The areal number density of the small clusters was about 7×10^{16} clusters/cm^2, and did not depend on the thickness except for at a very thin part of the specimen, which is not included in the figure. On the other hand, in the latter specimen, both a large number of small defect clusters and tangled dislocations were observed. In order to identify the small defect clusters, that is to find whether they are the interstitial type or the vacancy type dislocation loops, the electron irradiation experiment at room temperature by the high voltage electron microscopy operated with 200 kV was done. As is well known [83], the size of the clusters will increase during the irradiation when they are the interstitial type dislocation loop, and decrease when they are the vacancy type dislocation loops. In the specimen irradiated at room temperature by the Fe^+ ions with a total dose of 5×10^{14} Fe^+/cm^2, it was found that the cluster sizes increased slightly by the electron irradiation, so that the small clusters are suggested to have the nature of the interstitial type dislocation loops.

In order to know the depth distribution of the interstitial type dislocation loops in the specimen, the stereoscopic electron micrographs were taken as shown in Fig. 3.22 [84]. The specimen surface could be identified with a dislocation as is seen in the left upper parts of the micrographs. The determined depth distribution is given in Fig. 3.23(a). It is clearly seen in the figure that the small interstitial loops distribute in a certain range of the depth from the incident surface of ions; the range

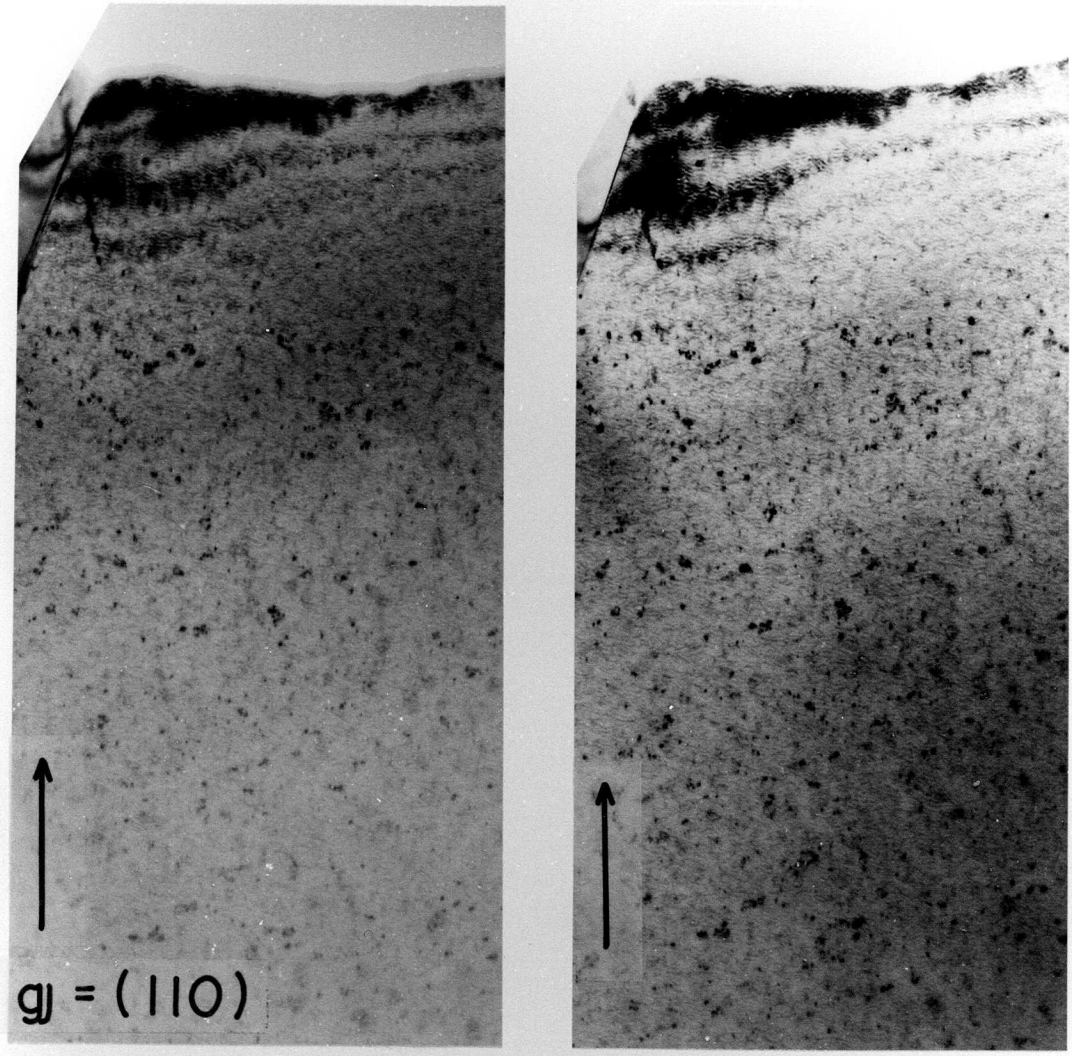

Fig. 3.22 Stereoscopic electron micrographs of Fe irradiated by Fe^+ ions at room temperature.

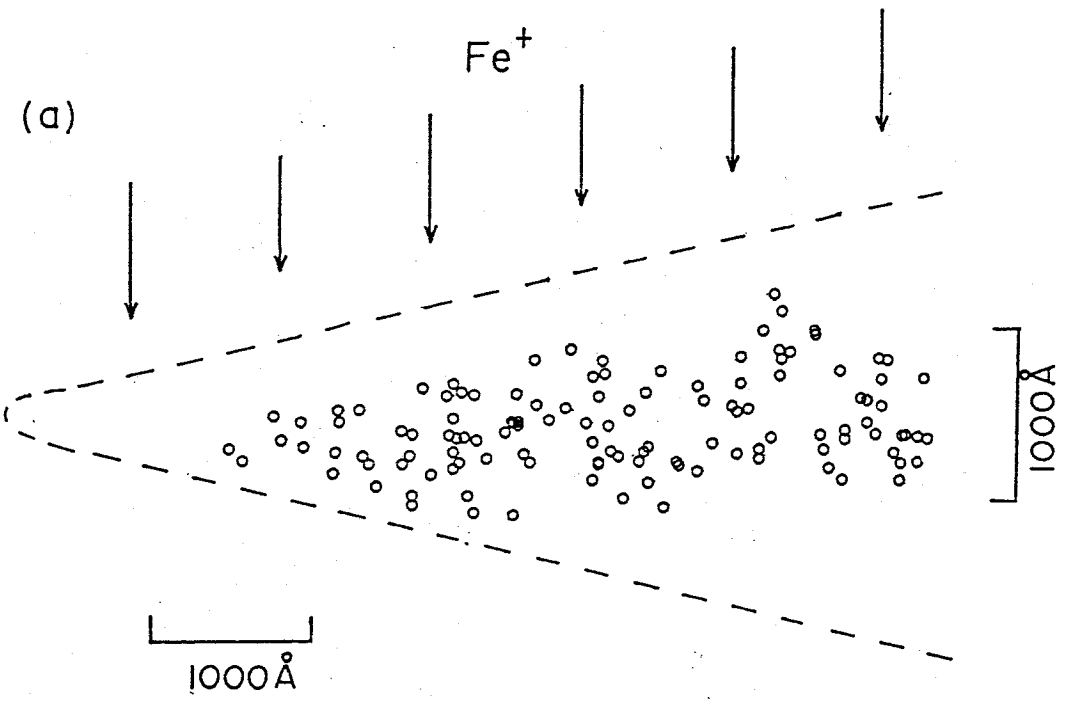

Depth Distribution of Defect Clusters

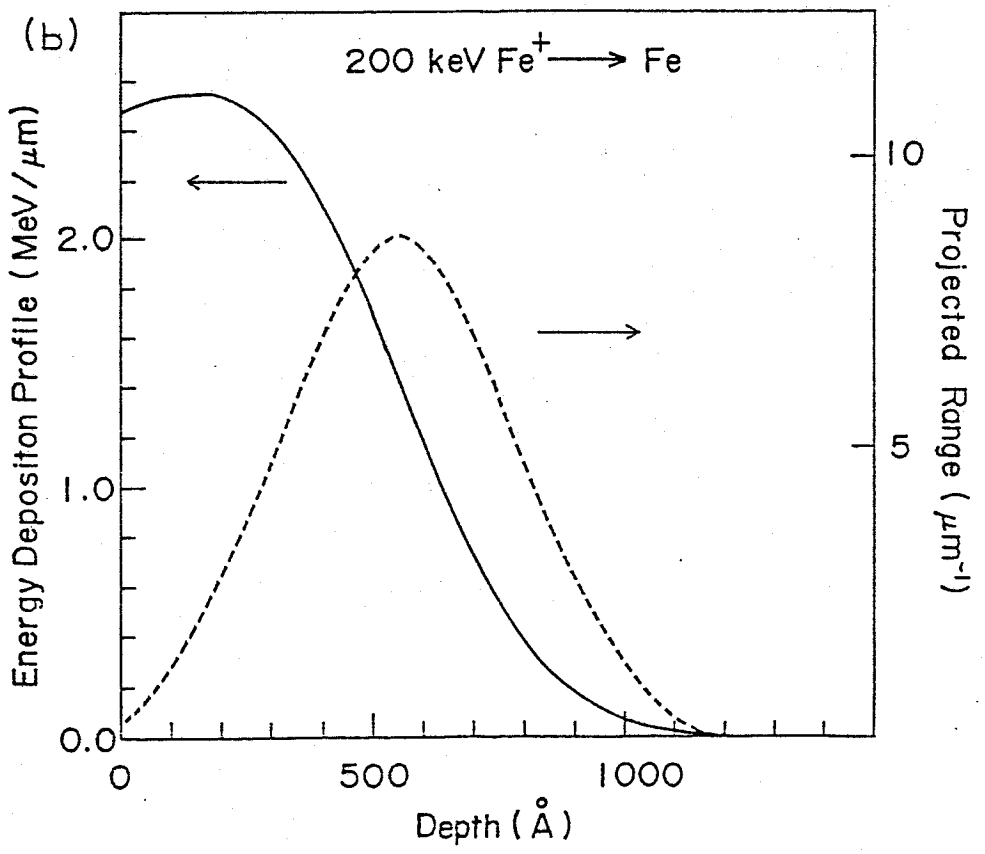

Fig. 3.23 Depth distribution of defect clusters, (a), and calculated energy deposition and projected range profiles, (b).

is between about 50 and 150 nm. In the part shallower than about 50 nm, no visible defect clusters existed. The center of the distribution of the defect clusters was around 100 nm from the incident surface, the value of which is larger than that of the projected range of ions calculated from the E-DEP-I program [69], as is shown in Fig. 3.23(b).

In general, the defect production is expected to occur as a cascade damage already mentioned before, in a region of the maximum energy deposition shown in Fig. 3.23(b). As was first suggested by Seeger [67], the cascade damage would introduce in the energy deposition region the vacancy rich volumes of some nanometers in diameter each surrounded by the intersitial rich zone. During the irradiation a large majority of such cluster regions would vanish out by the mutual annihilation between vacancies and interstitial atoms, but some of them could survive as they are, or collapse into the vacancy type dislocation loops. Any secondary defects, such as vacancy or interstitial loops or uncollapsed regions were not observed by the electron microscopy by Jenkins and others [85] in the Fe specimens, which irradiated by self-ions of the energy between 40 and 240 keV with a total dose of less than 5×10^{12} Fe^{+}/cm^{2}. In the present observation, however, small interstitial type dislocation loops were clearly observed in the region between 50 and 1500 nm in the depth, although no visible defect clusters existed in the maximum energy deposition range of 20 nm. The reason why the distribution of the interstitial loops shift to the region deeper than either the projected range and the maximum energy deposition range is thought whether the ranges were evaluated to be smaller than the real ones in the specimen or the interstitial atoms diffuse into the deeper regions during

the irradiation by the long range jumping process or the channeling processes of the interstitial atoms.

Detailed discussions, especially about the unvisible defects in the electron microscopy, will be given later, taking into account of the result of the Mössbauer measurement.

3.3.2 Transmission Mössbauer spectrum

As discussed before, in order to detect the defect perturbations in the mössbauer spectrum, the $^{57}Fe^{+}$ ion irradiation technique is expected to be more sensitive than the $^{56}Fe^{+}$ ion irradiation because the projected $^{57}Fe^{+}$ ions, which will act as both an initiator to produce the cascade damage during irradiation and an prove for the mössbauer measurement, are supposed to get into the defect rich regions. On the other hand, the $^{56}Fe^{+}$ irradiated specimen will show the Mössbauer spectrum accompanied with the perturbations depending on the concentrations of each kind of defects produced by the irradiation, the interstitial or vacancy type defects. The total doses of the $^{56}Fe^{+}$ and $^{57}Fe^{+}$ irradiation were equalized to 5×10^{16} Fe^{+}/cm^{2} each other for the Mössbauer measurements, but they were 15 times as large as the maximum dose of 1×10^{15} Fe^{+}/cm^{2} in the specimens for the electron microscopy.

The Mössbauer spectra of the Fe absorber taken at room temperature before and after the irradiation by the $^{56}Fe^{+}$ ions are shown in Fig. 3.24(a) and (b), respectively. All Mössbauer fitting parameters are given in Table 3.3 , together with the parameters obtained from the other spectra in the self-ion irradiation experiment. The spectrum before irradiation was subtracted from that after irradiation, and the subtraction spectrum is in Fig. 3.24(c).

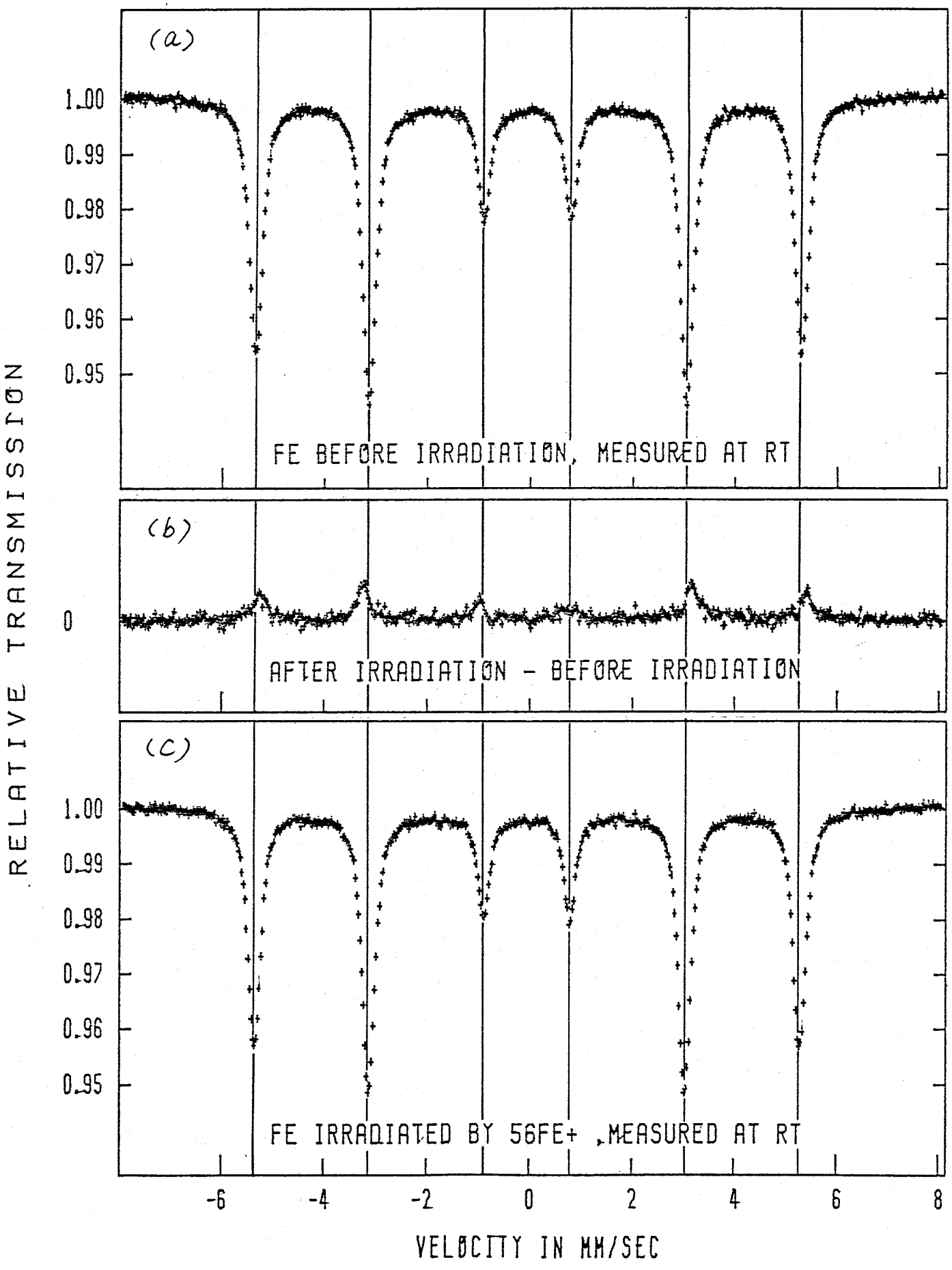

Fig. 3.24 Transmission Mössbauer spectra before, (a), and after the $^{56}Fe^{+}$ irradiation (b), and their subtraction (c).

It is clearly seen in the figure (c) that the tatal resonance area are decreased remarkably ofter irradiation. The profile of the subtraction tells us both the disappearance of a unperturbed component and teh appearance of a new component corresponding to a defect perturbation. The decrease of the total resonance area after irradiation, which was already seen in the case of the neutron and electron irradiation as mentioned before, suggests the formation of a vacancy rich region arising from the cascade damage. In that region, the Debye-Waller factor may be too small to be detected by the Mössbauer effect at room temperature, corresponding to the above mentioned decrease. In order to separate the defect perturbation in teh Mössbauer spectrum as in the figure (b), more sophisticated technique in the subtraction analysis was performed as shown in Fig. 3.25 . The new subtractions were obtained by subtractions the spectrum before irradiation by reducing the absoption scale by a variable factor, V0, from teh spectrum after the irradiation so that the contribution of the unperturbed component in the spectrum after irradiation vanish completely after the subtraction treatment. Whether the contribution remains or not was determined by the disappearance of the positive components, which, for instance, remains appreciably in Fig. 3.24(c) . According to this criterion the subtraction spectrum in the lowest part of Fig. 3.25 to find the defect-perturbed components. The lowest subtraction curve thus obtained is very similar to that from the transmission Mössbauer spectrum after the $^{57}Fe^{+}$ ion irradiation, which will be mentioned in the following paragraphs. More details will be discussed in the last section, taking into account of all "defect lines" obtained from all measurements of the self-ion irradiation.

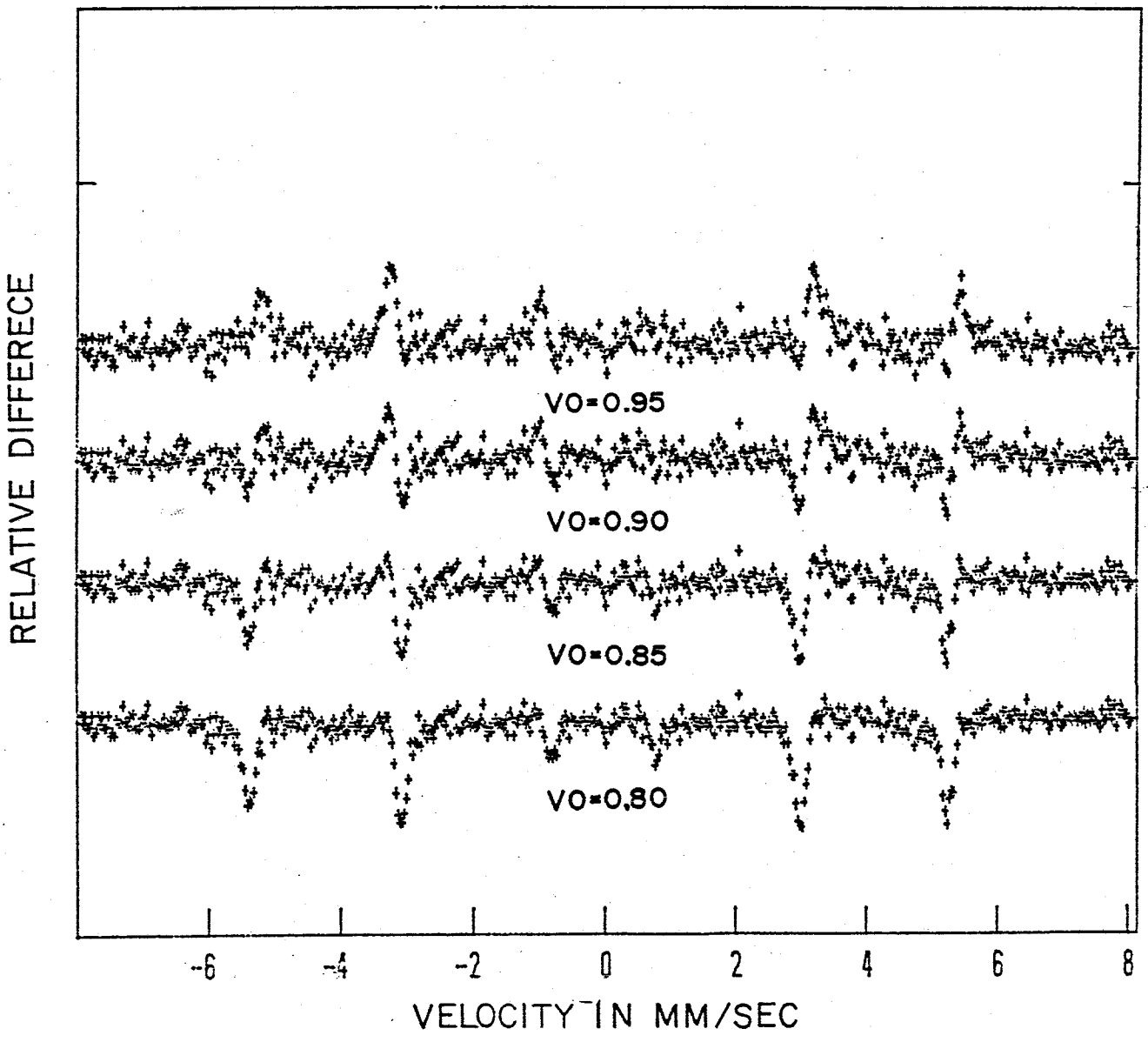

Fig. 3.25 Subtraction analysis on the $^{56}Fe^{+}$ irradiation spectra.

In the second, the results of the $^{57}Fe^{+}$ irradiation will be mentioned below. Figure 3.26 shows the Mössbauer spectra before irradiation, (a) and after irradiation, (b), and their subtraction spectrum, (c). The peak absorption before irradiation is deeper than that in the $^{56}Fe^{+}$ irradiation as in Fig. 3.24(a), which mainly arose from the different efficiencies of the counting systems for the Mössbauer measurement between them. After the irradiation of the $^{57}Fe^{+}$ ions, the total resonance area increased remarkably because addition of the ^{57}Fe atoms projected in the specimen naturally increased the total number of the resonant Mössbauer atoms. Since the projected ^{57}Fe atoms were additional ones in the resonance absorption, their contricution can be obtained by subtracting the spectrum before iffadiation from that after irraditaion, which is shown in Fig. 3.25(c) . It shows a broad six line profile different from that of pure iron, suggesting that the projected ^{57}Fe atoms stopped at various sites with different environments. Roughly speaking, therefore, the subtraction spectrum of the figure (c) is expected to consist of three components, which are originated from the ions on the normal lattice sites, the vacancy rich sites, and the interstitial rich sites. If the three components were separated into three sets of six lines, where the projected ions stopped could be identified from the fitting parameters, such as the magnetic hyperfine field, the isomer shift, the electric quadrupole effect and how many atoms stayed at each region could be found from the area ratios of each component. For the separation, first spectrum before irradiation was subtracted from that after irradiation by changing the saling parameter, V0, of the former, as shown in Fig. 3.27 . As mentioned before, the unperturved component rising from the prove atoms on the normal lattice sites was successfully dropped by chosing an appropriate value of Vo of about 1.2

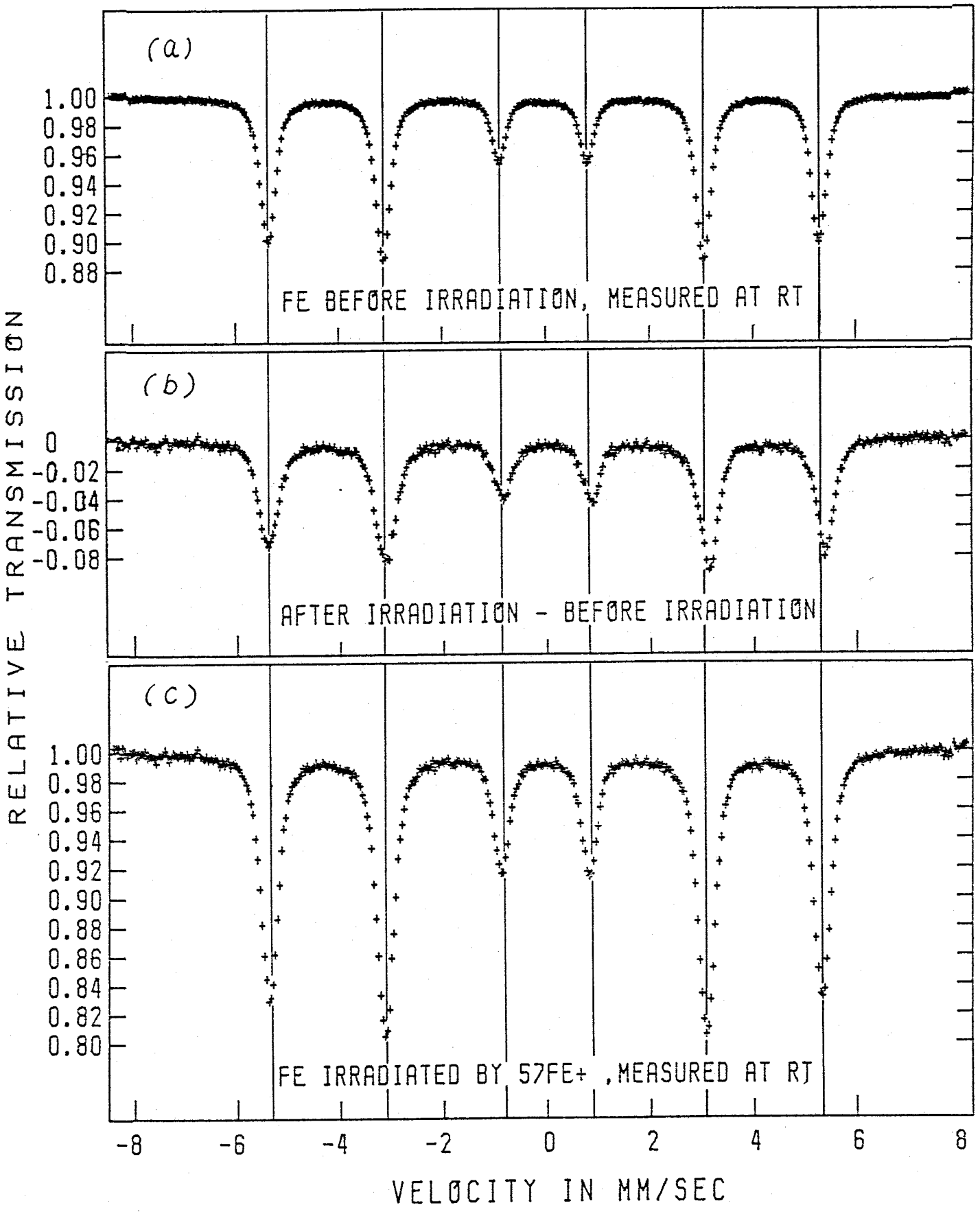

Fig. 3.26 Transmission Mössbauer spectra before, (a), and after the $^{57}Fe^{+}$ irradiation, (b), and their subtraction, (c).

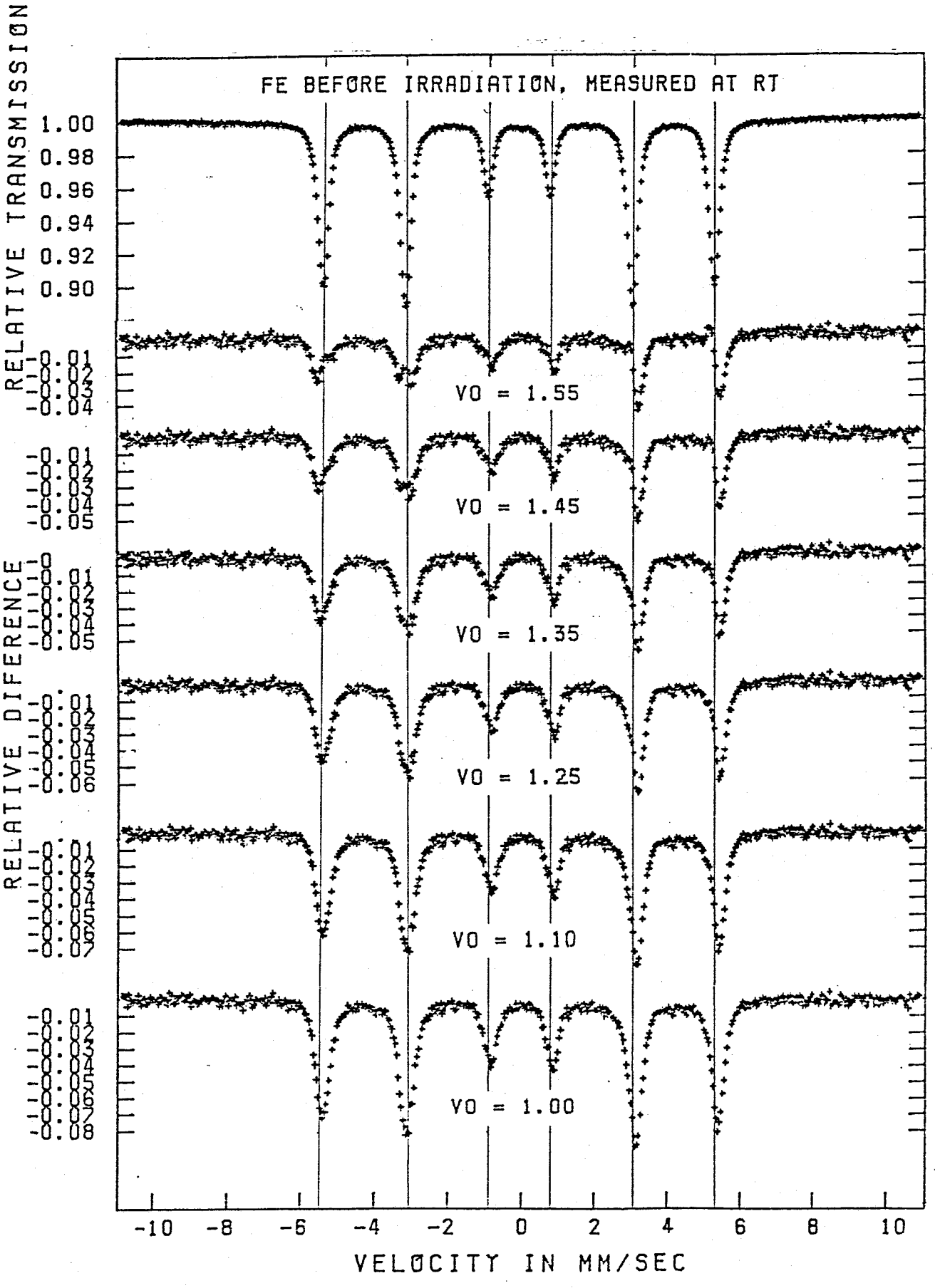

Fig. 3.27 Subtraction analysis on the $^{57}Fe^{+}$ irradiation spectra.

and the remnant spectrum was fitted by the two six line components. After further fitting analysis, the obtained "defect lines" are shown in Fig. 3.28 , and the fitting parameters are given in Table 3.4 . Although the fitting analysis using more than two components is still possible, the two component analysis is satisfactory enough. One component is characterized by a large hyperfine field of 334 kOe and the other by a large isomer shift of -0.16 mm/sec and the electric field of 0.32 mm/sec. It is worthy of note that the former defect line is similar to the "defect line" with larger hyperfine field obtained from the scattering measurement. Further comparison of the defect lines will be done later.

3.3.3 Scattering Mössbauer spectrum

For the search of the defect perturbations, the scattering method in the Mössbauer measurement must be more powerful than the transmission method, because the projected Fe ions are thought to stay near the surfac3 of the specimen, in the range less than 100 nm from the surface, while it is known that the scattering method detects the range of nearly the same depth [86]. The scattering Mössbauer spectra measured at room temperature before irradiation, (a), after the $^{56}Fe^{+}$ irradiation, (b), and after the $^{57}Fe^{+}$irradiation, (c), are shown in Fig. 3.29 . Clear defect lines were not observed as they are. In the scattering measurement, the cubtraction analysis is supposed to be more difficult, especially for the comparison of the area, than in the transmission measurement because the counting characteristics of the gas flow type electron counter will change with time during the measurement and, accordingly, the constant signal-to-noise-ratio can not be maintained. Futhermore, the cosθ effect due to the geometrical variation associated with the to-and-fro motion of the driven system during the

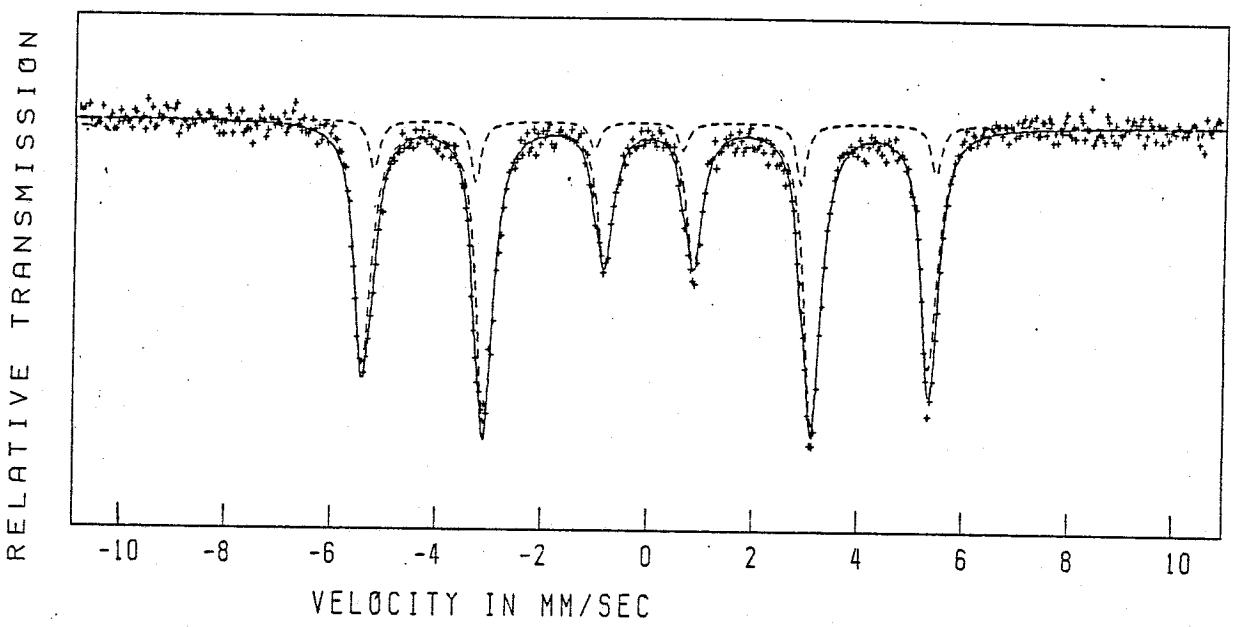

Fig. 3.28 "Defect Lines" obtained by subtraction analysis

AREA	H_{int}(kOe)	FWHM(mm/sec)	I.S.(mm/sec)	eqQ(mm/sec)
0.8893	334.3 ± 0.14	0.394 ± 0.010	0.069 ± 0.016	-0.058 ± 0.008
0.1107	331.9 ± 0.55	0.238 ± 0.036	-0.155 ± 0.047	0.316 ± 0.021

Table 3.3 Mössbauer parameters of "Defect Lines"

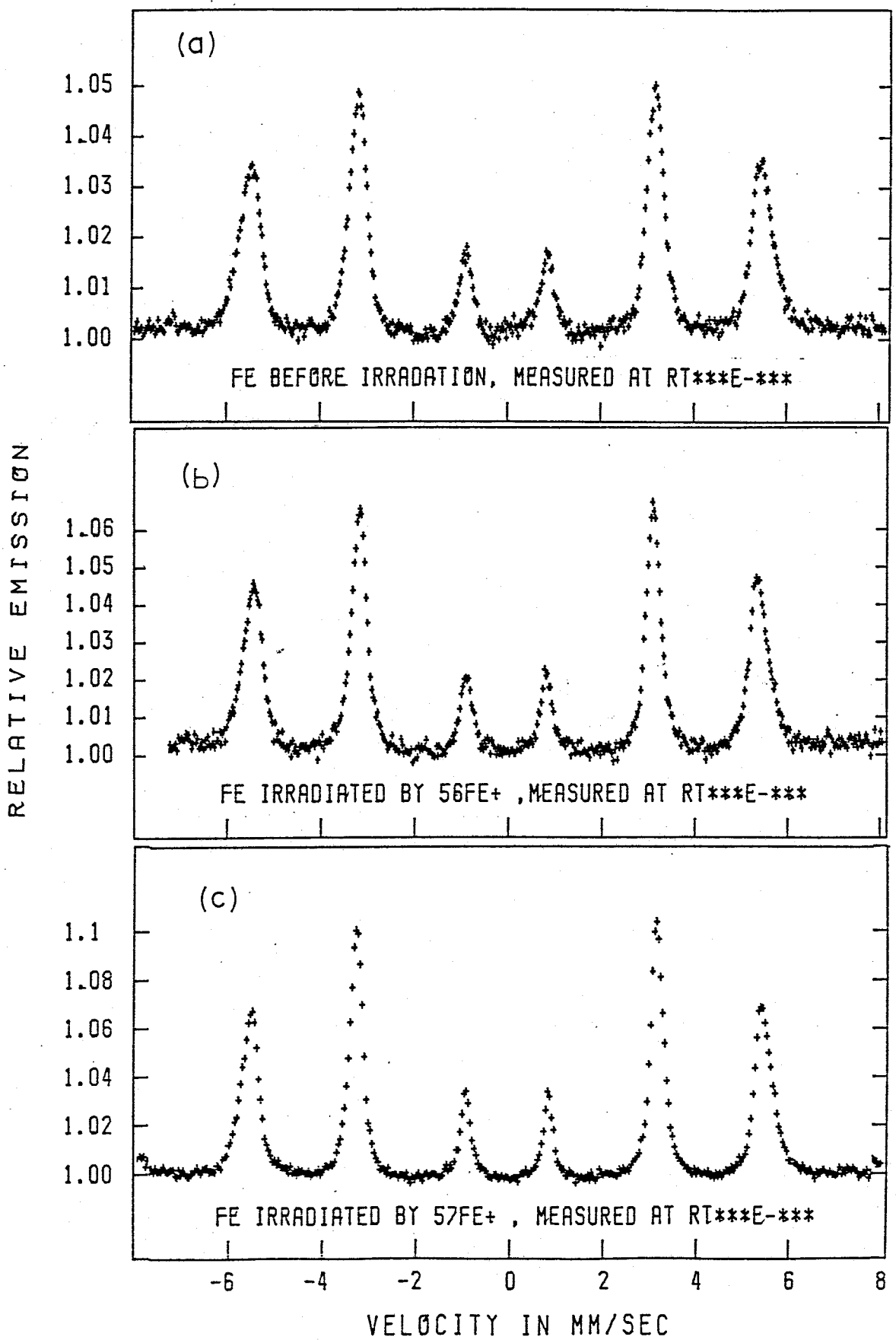

Fig. 3.29 Scattering Mössbauer spectra before, (a), and after the $^{56}Fe^{+}$ irradiation, (b), and after the $^{57}Fe^{+}$ irradiation.

spectrum measurement affects the profile of the scattering spectrum, so that the comparison of the Mössbauer fitting parameters, i.e. the average hyperfine field, to those of the transmission spectra is very difficult. The fitting parameters were already given in Table 3.4 , together with the others from the transmission spectra.

The parameters of the scattering case would include the information about the defects in the whole range of about 100 nm deep near the specimen surface, as mentioned in the above. However taking into account of the result of the electron microscopy introduced in 3.3.1 , which tells us that no visible defect clusters existed in the shallower part, less than 50 nm, and interstitial type dislocation loopes in the region between the depth of 50 and 150 nm, it is necessary to decompose the depth of 100 nm detected by the scattering Mössbauer measurements into at least two parts, shallower one and deeper one. In order to know what kind of perturbations occured in the shallwer region, only the higher energy part (A) of the energy spectrum in Fig. 2.16 , which was estimated to arise from the region less than 50 nm in depth, was selected by the single channel analyser and the scattering spectrum was measured. Then, the subtraction of the spectrum, (d), which corresponds to the energy range (A) from the whole range spectrum (c) , which corresponds to the energy range (B) in Fig. 2.16 , will give the difference between the shallower and deeper part. The result is in Fig. 3.30 which shows that a component with a smaller hyperfine field exists in the part shallower than 50 nm and a component with a larger hyperfine field in the deeper part in the specimen. Comparing with the result of electron microscopy, it is suggested that the invisible defects, possibly vacancies or their clusters, in the shallower region give rise to tha smaller hyperfine field

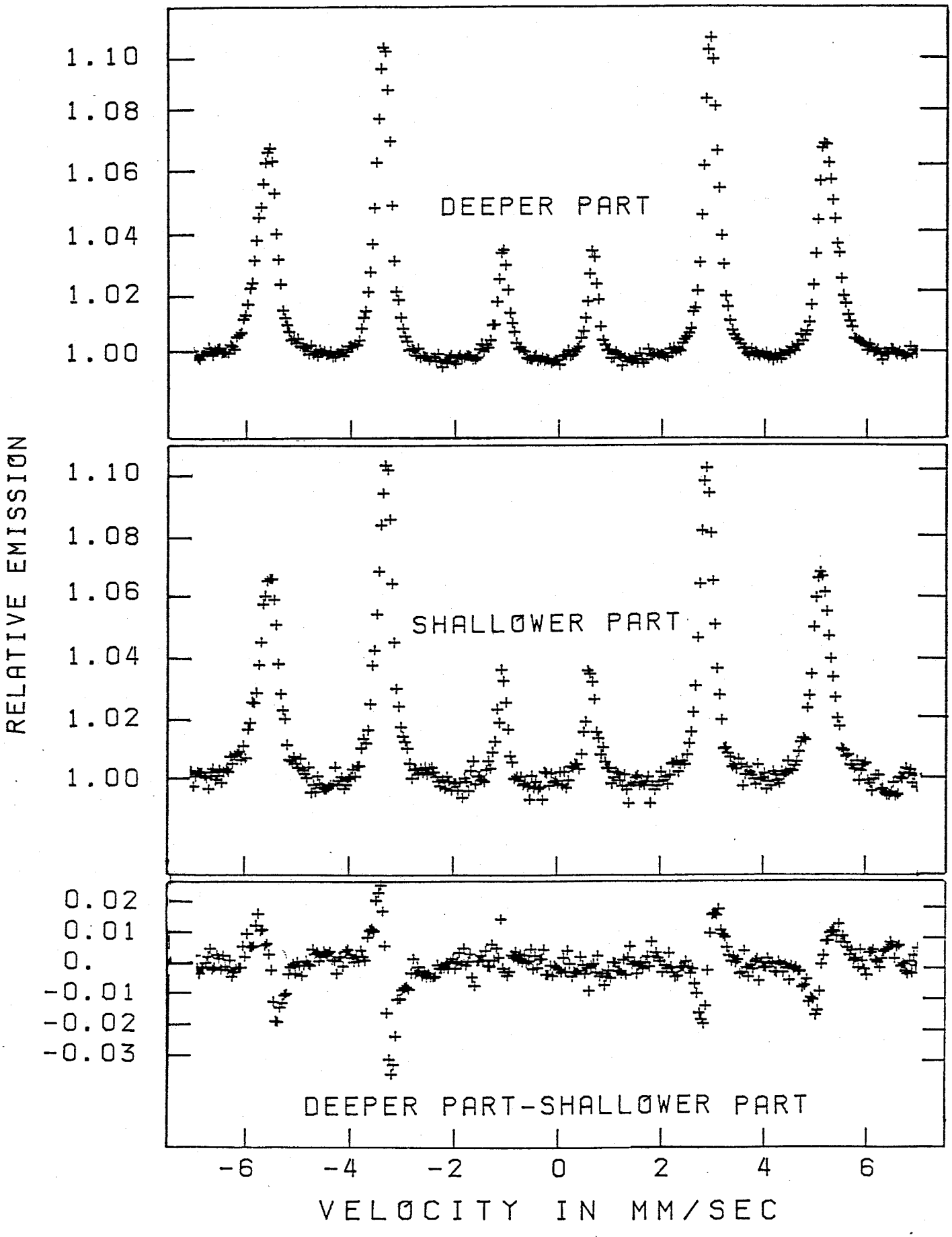

Fig. 3.30 Subtraction analysis on the $^{57}Fe^{+}$ irradiation scattering spectra.

and the interstitial loops in the deeper region give the larger hyperfine field. The defect vomponents obtained from the transmission spectra in the $^{57}Fe^{+}$ ion irradiateion are in good agreement with the components with the smaller and larger hyperfine field obtained from the scattering measurements. Therefore, the above identification of the defect lines seems to be most probable.

Further experiments are necessary to get the final decisive assignments for the defect lines; for instance, the annealing experiment and the low temperature irradiation experiment like in the case of the before mentioned neutron and electron irradiation.

4. DISCUSSION AND CONCLUSIONS

4.1 General Discussion on the Low Temperature Irradiation Experiment

In the present ^{57}Fe Mössbauer study on point defects in pure iron irradiated by fast neutrons and electrons at low temperatures, the effects of defects were successfully observed in the source experiments immediately after irradiation, and during isochronal annealings. Especially, it was remarkable that the three recovery stages were clearly found at around 110 K , 160 K , and 220 K , in the measurement of the count-rate at zero velocity, the total resonance area, and the full width at half maximum. These stages are in good agreement with those obtained by other investigators, and may be attiributed to the recovery of self-intersittials, small interstitial clusters, and vacancies, respectively. The above identification of recovery stages and behavior of point defects in them, so called the one interstitial model, has been widely accepted by a majority of the investigators in this field. However, Seeger [20] and others [87] have proposed a fairly different idea on the recovery stages identification, i.e., the two interstitial model. According to them, the stage I is attributed to the movement and conversion of the crowdion type self interstitials into the ordinary unextended type ones, the stage II to the similar changes of the crowdion clusters, and the stage III to the free migration of the converted interstitials and their disappearance at the sinks, which were supposed to be mostly vacancies and partly dislocations, surfaces and other lattice defects. The stage of free migration and disappearance of vacancies, which survive after the annihilation with the interstitials, is identified by them to be the stage V at around 200 °C in the case of bcc iron. Although the controversies are not yet fully settled, the latter idea seems to be faced by some difficulties

rising from the experimental facts. For an example, let us consider the changes of the count rate at zero velocity from a superpure iron specimen doped by ^{57}Co, irradiated by neutrons, and annealed isochronally, which are shown in Fig. 3.5 . The changes take place in completely different ways below and above 180 K , which may lead us to a conclustion that the recoveries below and above 180 K are originated by the completely different kinds of defects. That is, the present result is clearly in favor of the identification based on the one interstitial model employed by other investigators than Seeger and his grounp. The changes in the count rate rise from the appearance and disappearance of the components with different Mössbauer parameters, so that the above conclusion could be confirmed rigidly by the more precise analysis of the Mössbauer parameters are considered to be largely influenced by the effects of impurities and distribution of the defects, and one must be careful in the parameter analysis and interpretation, as will be discussed in the following sections. For the precise discussion developed hereafter on the nature and behabior of the point defects concerned with the recovery stages, the changes of the Mössbauer parameters at the above three stage and, in addition, other stages related with carbon movements will be briefly summarized below.

After the irradiation, the total resonance area in the Mössbauer spectrum decreased due to the reduction of the Debye-Waller factor, which suggested the formation of complexes between the ^{57}Co atoms and the vacancies during irradiation because the mean square displacement of atoms $< x^2 >_T$ is expected to be larger especially near vacancies than that of normal sites. The role of interstitials would be smaller in the change of the total resonance area. On

the other hand, the average hyperfine field increased in the neutron-irradiated specimen and decreased in the electron-irradiated specimen after irraditaiton. These defference must be originated from the different defect distributions, and futher discussions will be later.

After the annealing at around 110 K , the stage I, the total resonance area increased, as shown in the section 3.1 and 3.2, which could be interpreted as a result of mutual annihilation between the mobile interstitials and the immobile vacancies trapped by the ^{57}Co atoms, leading to the decrease in the number of the ^{57}Co atoms associated with vacancies. The average hyperfine field decreased remarkably in the neutron irradiated specimen and increased in the electron irradiated specimen. This is probably due to the difference in the distribution of defects before the annealing, as will be discussed in the next section. At the stage II, most remarkable is the changes of the count rate in the thermal scan measurement. In the purest specimen irradiated by neutrons, the count rate sharply dropped by about 4 % at stage II between 130 K and 170 K . This change can be interpreted by the process of clustering of interstitials,presumably at the ^{57}Co atom sites, in accordance with the electron microscopical observation. A precise interpretation will be given in the section 4.3 . The changes of the isomer shift, the hyperfine field and the half width appeared at the stage II will also be discussed there. The stage III is a complicated one. The count rate changes up and down, the total resonance area largely depend on the irradiation paricles and the specimen purity, and the assignment of the spectral components obtained from the curve fitting analysis is difficult. The increase of the total resonance area at the stage III in the specimen irradi-

ated by neutrons shown in Fig. 3.4., is in accordance with its interpretation by the vacancy recovery. However, when the purity of the specimen was increased, the total area change became complicated and rather unidendified. It will be further examined in the section 4.4 .

4.2 The as irradiated state

Comparisons between the Mössbauer spectra obtained from the neutron and electron irradiated purest iron are as follows. As is shown in Fig. 3.13 , the total resonance of area of the Mössbauer spectrum measured at 77 K decreases in the both cases after irradiation, but the average hyperfine field decreases in the electron irradiated specimen contrary to the increase of it in the neutron irradiated specimen. In the case of the measurements of the same specimens at 4.2 K , the increment of the total resonance area is larger in the former than that in the latter, and in addition, the average hyperfine field largely increases from 335 kOe to 339 kOe in the former and increases in the latter from 339 kOe to 340 kOe. These differences must be originated from the difference in the distribution of defects, which are supposed to be homogeneous in the distribution of Frenkel pairs after electron irradiation, and heterogeneous due to cascade damages after neutron irradiation. From the measurement of electrical resistivity the total Frenkel-pair concentration is evaluated to be about 200 at.ppm in the electron irradiated specimen, while about 500 at.ppm is given in the specimen irradiated by 5×10^{16} neutron/cm^2 by the Kinchin-Pease model calculation.

The decrease of the total resonance area arises from the reduction of Debye-Waller factor, which is closely related to the dynamical motions of atoms, as was mentioned in the paragraph 1.3.1(b). Three kinds of atom motions concerning with the Mössbauer measurement can be considered; the lattice vibration of the prove nuclei emitting gamma-rays, on which the Debye-Waller factor, as shown in the expression (1.10), depends through the mean square displacement

of atoms, and in the second place, the local motions of the prove atoms or their neighbor atoms, like a cage motion [70,71], and, as the third one, the long range migration by jump motions, the two latters of which reduce the Debye-Waller factor due to the gamma-ray coherency break down by the jumps of the atoms. The measurement temperatures are 77 K and 4.2 K, at which the long range migration of vacancies, or interstitials can not occur, so theat the third kind of motion to reduce the Debye-Waller factor can be excluded from the consideration. The first kind of motion may ofter the most possible explanation for the decrease of the resonance area because the large mean square displacement, $<x^2>$, is expected near the vacancies. Considering the decrease of the resonance area after irradiation and the changes of the area between 4.2 K and 77 K, in the neutron irradiated specimen, it is strongly suggested that the regions, are formed after irradiation, arising from the associations of the ^{57}Co atoms with vacancies during irradiation. In the electron irradiation, the resultant Debye-Waller factor irradiation is supposed to be not so small as that in the neutron irradiation, because the increment of the resonance area from 77 K to 4.2 K is considerably large and is nearly equal to that of the decrease of the area after irradiation. This result may be explained by the fact that in electron irradiation, a large part of the ^{57}Co atoms is expected to associate with single vacancies, so that the Debye-Waller factor of the ^{57}Co atom-vacancy complex seems to be large enough to detect the Mössbauer resonance effect at 4.2 K but too small to detect that at 77 K. Accordingly, in the neutron irradiation, the ^{57}Co atoms could be associated with more than two vacancies in the depleted zone. A similar result of the reduction of the Debye-Waller factor was already reported by de Waard et al. [52,53].

Another possible explanation for the reduction of the resonance area is that the local motion of the ^{57}Fe atom emitting gamma-rays reduce the Debye-Waller factor. During irradiation, the ^{57}Co atoms could be associated with vacancies and form the complexes, the recoil energy in decay process of the ^{57}Co Mössbauer-parent atoms by the electron caprure, which are about 6 eV larger than that of the vacancy free migration energy, would indece the local jumping motions of the ^{57}Fe atom emitting Mössbauer gamma-rays, leading to the decrease in the Debye-Waller factor. In addition, as was reported by Lynch et al. [59], the decay process might cause an internal cascade damage, which is accompanied with the excitation of local phonons with the life-time a little shorter than that of the ^{57}Fe 14.4 keV excited state, 97.7 nsec. In the present case, these internal damage process and excitation of local phonon modes would enhance the decrease of the Debye-Waller factor.

The changes in the average hyperfine field in the neutron and electron case are opposite. In the neutron irradiated specimen, it increases after irradiation and then decreases after the annealing at 110 K , and in the electron irradiated specimen, it decreases after irradiation and later increases after the annealing at 110 K . In the neutron irradiation, the interstitials are expected to be localized around the depleted zone just after irradiation due to the production of the cascade damage [67] and in addition, the interstitial migration may cause the diappearance of the interstitial rich zones, so that the large hyperfine field seems to arise from that zones. On the other hand, a possible reason for the hyperfine field decrease in the electron irradiated specimen is the decrease in the Curie temperautre due to the magnetic exchange interaction disturbed by vacancies, which will be suggested from a comparison between the spectra of the neutron and electron irradiated specimen at both 72 K and 4.2 K later.

4.3 Stage I Recovery

In the neutron irradiated source specimen of super pure Fe which had the resistivity ratio, $RRR_H = 5000$, and doped with ^{57}Co, the count rate through the iron absorber kept at 77 K increased by annealing at around 110 K and that through the absorber at room temperature decreased there, as are shown in Fig. 3.5 . This suggested that a reaction between ^{57}Co atoms and defects of some kind occured and new complexes were formed during the annealing. Since the number of the ^{57}Co atoms on the normal sites can be monitored by the count rate through the absorber at 77 K , and that of ^{57}Co atoms on the sites associated with defects by the count rate through the absorber at room temperature as before mentioned, the increase in the former count rate must show the decrease in the normal ^{57}Co atoms and the decrease in the latter count rate must show the increase in the defect sited ^{57}Co atoms. The stage I defect are widely accepted to be self-interstitials, and if it is true, the resultant complexes after the 110 K annealing are thought to be the ^{57}Co-interstitials complexes.

The results of Fig. 3.7 tell us some more details on the behavior of interstitials and impurities interacting with them. The total resonance area increased more remarkably in the stage I than in the stage III around 220 K , while the increase of the resonance in the stage I in the low purity iron was only a half of that in the stage III. The origin of this difference is not clear, but the differences in the specimen purity and/or the total dose of the fast neutrons seem to strongly affect the recovery behavior. For instance, the radiation produced interstitials in the super pure Fe specimen would easily move and mostly disappear in the stage I, while they would survive by forming complexes of certain type with

impurities until the stage III, The average hyperfine field decreases after the annealing at 110 K probably due to the changes in the configurations of defect by the interstitial migrations. The hyperfine field of the ^{57}Fe in the defect and/or impurity complexes may depend on the number of the associated defects, possibly interstitials, or their configuration of association, but the actual structures of the complexes between the ^{57}Co atoms, defects, and/or impurities are not yet identified at the present stage of investigation. What kinds of complexes between the ^{57}Co atoms and defect correspond to the various hyperfine fields is yet an open question.

In the electron irradiated specimen, as is shown in Fig. 3.14 , the stage I recovery is more complex than that in the neutron irradiated specimen. The count rate through the absorber at room temperature shows the up-and-down changes up to 140 K in the stage I, and that through the absorber at 77 K shows the increase with small up-and-down changes. These differences are supposed to arise from the different distribution of defects in the neutron and electron irradiated specimen. This is another important problem to be solved by future investigations.

4.4 Stage II Recovery

In the stage II recovery, which took place at around 160 K , remarkable differences were observed in the count rate at zero velocity in the neutron irradiated specimens with different purities. In the purest iron with the resistivity ratio, $RRR_H = 5000$, the count rate decreased prominently ty the annealing at around 150 K , as is shown in Fig. 3.5 , while in the low purity iron with $RRR_H = 500$, it showed the up-and-down change up to 180 K , as in Fig. 3.4 . On the other hand, the average hyperfine field increased linearly up to 180 K in the former as in Fig. 3.7 , and kept a constant value in the same temperature region in the latter as in Fig. 3.3 . These differences can be also found in the subtraction spectra in Fig. 3.2 and 3.6 . The changes in the count rate and the average hyperfine field tell us that the association between the ^{57}Co atoms and interstitials are strongly affected by the impurity concentration in the iron matrix, and the resultant complexes after the stage II annealing must have different iron matrix, and the resultant complexes after the stage II annealing must have different structures with different hyperfine fields of ^{57}Fe. Accordingly, the species of the mobile defects in the stage II are expected to be different in the pure iron and impure iron, depending on the interactions of the stage II defects with the impurity atoms.

In the electron irradiated specimen with $RRR_H = 5000$, the recovery behavior was rather different from that of the neutron irradiated specimen, as is shown in Fig. 3.14 . As was mentioned before, in electron irradiation, the simple Frenkel pairs are expected to be distributed homogeneously in the specimen in contrast with the heterogeneous distribution of cascade damages in neutron irradi-

ation, so that the different defect distributions may induce the different reactions between the ^{57}Co atoms and defects, leading to the formations of different complexes. It is noteworthy that in the electron irradiated specimen, the magnitudes of the isomer shift in the Mössbauer spectra were changed considerably in the stage II , as is easily seen in the subtraction spectra in Fig. 3.12 , indicating that the appearance and disappearance of the complexes with the different isomer shifts occured.

4.5 Stage III Recovery

The stage III in the recovery process has been identified by many investigators, who employed other experimental techniques and various defect theories, to be the stage where vacancies became mobile freely, as mentioned already. When carbon impurity exists, the vacancies would most likely be trapped by them, and, when the specimen is pure enough, the vacancies would move to other sinks and disappear. The result of the present Mössbauer measurements seem to support the above idea, since the total resonance area increased, the count rate through the 77 K absorber decreased, and the annealing behavior in the stage III was fairly different from that in the stage I and II, all of which could only be interpreted by the idea of release of vacancies from ^{57}Co atoms. Nevertheless, the annealing behavior at the stage III strongly depends on the purity of the specimens, again indicating strong and complicated interactions between the migrating vacancies and impurities, and, consequently, definite and precise pictures of the vacancies-^{57}Co atom-carbon aroms interaction and complec formation at the stage III are not yet understood. Futher Mössbauer experiments, desirably combined with other thchniques, are awaited. The stages in higher temperature ranges stage IV around 320 K and stage V around 470 K, were also found in this study. The former presumably corresponds to the free carbon migration to the free ^{57}Co atoms resulting in the small carbon clusters including the ^{57}Co, and the latter may be related to the dissociation of the vacancy carbon complexes. The ε carbide formation, which takes place at 370 $\sim$ 420 K might also be included in the changes in the present Mössbauer measurements.

4.6 Self Ion Irradiation

Two noticable results has been obtained by the self ion irradiation experiment, especially using the ^{57}Fe ions. One was that a defect influenced component, which had a hyperfine field about 5 kOe larger than that of normal Fe, was found in the refion 500 Å or deeper from the irradiated surface. Since the electron microscopy revealed that a large number of small interstitial type dislocation loops existed in this region, it was concluded that the ^{57}Fe atoms associated with interstitial clusters have the larger hyperfine field. At a glance, this result seems to contradict to the high pressure experiment, where the hyperfine field decreased by static compression, since the ^{57}Fe atoms were supposed to be ingluenced by the compression field induced by nearby interstitials. In the present case, however, the lattice must have been extensively perturbed by the interstitial defects and the electronic configuration of 3d shell of the ^{57}Fe atoms concerned would be so largely changed that the comparison with the high pressure experiment would no longer be possible. The second remarkable result was that the Mössbauer signals from the region shallower than 500 Å gave another new component with the hyperfine field 2 or 3 kOe smaller than the normal value. This showed that the defects of vacancy type did exist in that region, although they were invisible by the electron microscopy, and vacancies in the iron lattice decreased the hyperfine field of neighboring Fe atoms. This is also an important and suggestive consequence from the Mössbauer analysis in the present study, which requires theoretical considerations on the electronic structures associated with the lattice defects.

4.7 Conclusions

(1) In order to detect the defect perturbations and the recovery behavior in irradiated pure iron, the Mössbauer effect studies were performed by using the various new methods; the defect trapping method, the thermal scan method, and the self-ion irradiation method.

(2) ^{57}Fe Mössbauer spectra of PUre Fe foils were measured and compared before and after irradiations with neutrons and electrons at low temperatures. Clear satellite lines due to Fe perturbed by the defects were not observed in the Mössbauer spectra at 77 K and 4.2 K after irradiation and after the annealings both in the source and absorber experiment. But, instead, remarkable changes were observed in the total resonance area, the hyperfine field, the full width at half maximum, the count rate at zero Doppler velocity, etc.

(3) The thermal scan method was successfully applied to the investigation of the annealing behavior of point defects in pure iron by using the iron absorvers kept at room temperature and at 77 K .

(4) Clear annealing stages were observed in the isochronal curve of the count rate at zero velocity both in the neutron and electron irradiated source specimen. These stages are in good agreement with the results obtained by the other investigatiors; the stage I appeared at around 110 K , the stage II aroung 160 K and the stage III at around 220 K .

(5) Considering the changes in the count rate during the isochronal

annealings, the defect trapping method is useful to study on the nucleation process of defect clusters.

(6) The total resonance areas after neutron and electron irradiation in the source experiments were smaller than those before irradiation, and increased by the subsequent annealings at around 110 K and 220 K probably due to the mutual annihilation between vacancies and interstitials. The smaller total resonance areas are originated from the reduction of the Debye-Waller factor, which may arise from the association of the ^{57}Co atoms with vacancies and/or their complexes.

(7) The total resonance areas of Mössbauer spectra at 4.2 K and 77 K were obtained and compared for the neutron and electron irradiated specimen. In the electron irradiated specimen, the magnitude of area measured at 4.2 K was roughly equal to that before irradiation, while in the neutron irradiated specimen it was nearly equal to that of the area at 77 K after irradiation, which was 8 ∿ 20 % smaller than that before irradiation. This mean theat the decrease in the Debye temperature is larger in the neutron irradiated specimen that in the electron irradiated specimen and, therefore, suggests that the association of the ^{57}Co atoms with vacancies are stronger and perhaps more frequent in the latter than in the former.

(8) The magnitude of the average hyperfine field obtained just after neutron irradiation was larger than that obtained before irradiation, and decreased by the subsequent annealings at around 110 K , the stage I, which is supposed to be the recovery stage of the interstitials. Accordingly, it is concluded that the existence of interstitials causes the larger hyperfine field.

(9) The magnitude of the average hyperfine field obtained after electron irradiation was smaller than that before irradiation, and increased after the 110 K annealing, which are opposite to the changes in the neutron irradiated specimen. So that, the hyperfine field of the ^{57}Fe in the defect complexes seems to be strongly affected by the number of the associated defects or their configurations.

(10) The difference of the average hyperfine fields between the 4.2 K and 77 K spectrum was larger in the electron irradiated specimen. This shows that the magnetic perturbations is larger in the former than that in the latter.

(11) The recovery bahavior in the total resonance area, the average hyperfine field, the FWHM and the count rate at zero velocity strongly depend on the specimen purity, the kinds of irradiation particles and the total doses.

(12) In the irradiated absorber experiments, appereciable effects of defects were also found, but for the detailed discussion, further precise experiments are necessary.

(13) The dynamical thermal scanning was expected to yield another interesting result in this investigation, since it could give us new information on the dynamical migration behavior of point defects. Some result was actually obtained, but before leading to a clear conclusion it seemed that some experimental difficulties were required to be overcome.

(14) The subtraction analysis was formed to be very powerful tool to investigate the small changes in the Mössbauer spectra before and after irradiation and after the annealings.

(15) The transmission and scattering Mössbauer measurements were performed on the self-ion irradiated Fe foils, and compared with the observations by the electron microscope. In the deeper parts of the specimen, which are in the range between 500 Å and 1500 Å, the small interstitial type-dislocation loops were observed by the electron microscope, but in the shallower parts, visible defect clusters were not observed. The Mössbauer subtraction analysis showed the defect perturbations consisting of two components, one of which is probably originated from the vacancy clusters with a lower hyperfine field in the shallower parts, and the other is due to the interstitial loops with a higher hyperfine field in the deeper parts.

ACKNOWLEDGEMENTS

The author wishes to express his hearty gratitudes to Profs. F. E. Fujita and S. Nasu for their continuous guidance and encouragement through this doctor thesis work. Hearty thanks are also due to Profs. M. Kiritani and R. Oshima in the same laboratory for their valuable discussions and comments. A large part of the present study has been done at the Research Reactor Institute of Kyoto University by using the Mössbauer spectrometer, neutron irradiation facility, and LINAC, for which the author largely ows kind permission, instruction, machine operations and helps in the experiments to Profs. Y. Maeda, H. Yoshida, and M. Nakagawa, Dr. Sakai, Messrs. S. Uehara, . Mizota and .Warashina. The LINAC irradiation was performed in cooperation with Prof. K. Kitajima and his group in Kyushu University, to whom the author is largely indebted too. Self-ion irradiation by an ion implanter was done at the Electrotechnical Laboratory, Tsukuba, by the kind helpful cooperation by Drs. N. Hayashi, I. Sakamoto, T. Kanayama, and H. Tanoue.

The iron specimen of the highest purity were made by Profs. K. Igaki, Drs. M. Isshiki, and M. Nagano and kindly offered to the author for this study. The electron micrographs of self-ion irradiated iron specimens were taken with a great heop by Mr. T. Ezawa, and the helps in typing the manuscript and drawing the figures were by Messers. M. Arita and others in the laboratory.

REFERANCES

[1] M. Kiritani, in Progress in the Study of Point Defects, edited by M. Doyama and S. Yoshida (University of Tokyo Press, Tokyo, 1977), p247.

[2] M. Kiritani and H. Takata, Proceedings of International Conference on properties Atomic Defects in Metals (Argonne, 1976), J. Nuclear Materials 69&70, 227(1978).

[3] M. Kiritani, Proceedings of Yamada Conference V on Point Defects and Defect Interactions in Metals,(Kyoto,1981), p59.

[4] J. Nihoul, in Vacancies and Interstitials in Metals, edited by A. Seeger, D. Schumacher, W. Schilling, and J. Diehl (North-Holland, Amsterdam, 1970), p389.

[5] M. Weller and J. Diel, in Internal Friction and Ultrasonic Attenuation in Solids, edited by R. R. Hasiguti and N. Mikoshiba (University of Tokyo Press, Tokyo, 1977), p425.

[6] P. Moser, see in ref.[5], p63.

[7] H. Kimura, see in ref.[1], p119.

[8] L. J. Cuddy and J. C. Raley, Acta metall., 14, 441(1966)

[9] L. J. Cuddy, Acta metall., 16, 23(1968)

[10] H. Kugler, I. A. Schwirtlich, S. Takaki, U. Ziebart and H. Schultz, see in ref.[3], p191.

[11] W. Glaeser and H. Wever, Phys. Stat. Sol., 35, 367(1970).

[12] Y. Ikeda, T. Gotoh, K. Abiko and H. Kimura, Crystal Lattice Deffects, 5, 163(1974).

[13] M. Weller, J. Diehl and W. Triftshäuser, Solid St. Commun, 17, 1223(1975).

[14] N. Yoshida, M. Kiritani and F. E. Fujita, J. Phys. Soc. Japan, 39, 170(1975).

[15] J. Diehl, U. Merbold and M. Weller, Scr. Metall., 11, 811(1977).

[16] M. Kiritani, H. Takata, K. Moriyama and F. E. Fujita, Philos. Mag. A40, 779(1979).

[17] F. E. Fujita and A. C. Damask, Acta metall., 12, 331(1964).

[18] F. Maury, M. Biget, P. Vajda, A. Lucasson and P. Lucasson, Phys. Rev. B14, 5303(1976).

[19] W. Schilling, P. Erhart and K. Sonnenberg: Interpretation of Defect Reactions in Irradiated Metals by One Interstitial Model in Fundamental Aspects of Radiation Damage in Metals, edited by M. T. Robinson and F. W. Young, jr., U.S.E.R.D.A.Conf. 751006, 1976. p470.

[20] A. Seeger: The Interpretation of Radiation Damage in Metals. see om ref.[19], p493.

[21] J. L. Leveque, T. Anagnostopoulos, H. Bilger and P. Moser, Phys. Status Solidi, 31, K47(1969).

[22] H. Wagenblast and A. C. Damask, J. Phys. Chem. Solids, 23, 221(1962); R. A. Arndt and A. C. Damask, Acta Metall., 12, 341(1964); H. Wagenblast, F. E. Fujita and A. C. Damask, ibid. 12,347(1964).

[23] T. Takeyama and H. Takahashi, see in ref.[19], p1100.

[24] P. Hautojärvi, T. Judin, A. Vehanen, J. Yli-Kauppila, J. Johansson, J. Verdone and P. Moser, Solid State Commun., 29, 855(1979).

[25] P. Hautojärve, J. Johansson, P. Moser, L. Pöllänen, V. Vehanen and J. Yli-Kauppila, see in ref.[10], p504.

[26] P. Hautojärve, J. Johansson, A. Vehanen, J. Yli-Kauppila and P. Moser, Phys. Rev. Lett., 44, 1326(1980).

[27] A. Vehanen, P. Hautojärve, J. Johansson and J. Yli-Kauppila and P. Moser, Phys. Rev. B25, 762(1982).

[28] A. Möslang, H. Graf, E. Recknagel, A. Weidinger, Th. Wichert and R. I. Grynszpan, see in ref[10], p11.

[29] S. Nasu, Y. Yoshida and F. E. Fujita: in Proc. of Int. Conf. on Applications of the Mössbauer Effect, Jaipur, 1981.

[30] R. L. Mössbauer, Z. Physik 151, 124(1958); R. L. Mössbauer, Naturwissenschaften 45, 538(1958).

[31] H. Franufelder: The Mössbauer Effect, New York: Benjamin 1962.

[32] G. K. Wertheim: Mössbauer Effect: Principle and Applications, New York: Academic Press 1964.

[33] L. May (ed.): An Introduction to Mössbauer Spectroscopy. New York: Plenum Press 1971.

[34] U. Gonser (ed.): Mössbauer Spectroscopy, in Topics in Applied Physics, vol.5.Berlin-Heidelberg-New York: Springer 1975; U. Gonser (ed.): Mössbauer Spectroscopy II: The Exotic Side of the Method: Berlin-Heidelberg-New york: Springer 1981.

[35] P. Gütlich, R. Link and A. Trautwein: Mössbauer Spectroscopy and Transition Metal Chemistry, Berlin-Heidelberg-New york: Springer 1978.

[36] U. Gonser, see in ref[4], p649.

[37] G. K. Wertheim, A. Hausman and W. Sander: The Electronic Structure of Point Defects, North Holland 1971.

[38] H. de Waard: Mössbauer Spectroscopy and its Applications, IAEA (Vienna 1973), p123.

[39] G. Vogl, J. Physique Colloq.,35, c6-165(1974).

[40] G. Vogl, Hyperfine Interactions, 2, 151(1976).

[41] C. Minier and M. Miner, see in ref[3], p27/

[42] Th. Wichert, see in ref[3], p19.

[43] J. Christiansen, E. Recknagel and G. Weyer, Phys. Lett., 20, 46(1966).

[44] J. Christiansen, P. Hindenach, V. Morfeld, E. Recknagel, D. Riegel and G. Weyer, Nucl. Phys. A99, 345(1967).

[45] G. Czjzek, J. L. C. Ford Jr., F. E. Obenshain and H. Wegener, Phys. Rev. 174, 331(1968).

[46] G. D. Sprouse, G. M. Kalvius and S. S. Hanna, Phys. Rev. Lett., 18, 1041(1967).

[47] G. D. Sprouse and G. M. Kalvius: Mössbauer Effect Methodology, vol.4,(edited by I. J. Gruverman, New York: Plenum Press), 1968, p37.

[48] H. de Waard and S. A. Drentje, Phys. Lett. 20, 38(1966).

[49] R. L. Cohen, G. Beyer and B. I. Deutch, Application of Ion Beams to Metals, (edited by S. T. Picranx, E. P. Eer Nisse and F. L. Vook, New York: Plenum Press), 1974, p361.

[51] H. de Waard, S. A. Prentje, Proc. Roy. Soc. A311, 139(1969).

[52] S. R. Reintsema, S. A. Drentje, P. Schurer and H. de Waard, Rad. Eff., 24, 145(1975).

[53] S. R. Reinstsema, S. A. Drentje and H. de Waard, Hyperfine Interaciton, 5, 167(1978).

[54] R. L. Cohen, H. de Waard, S. R. Reinstema and S. A. Prentje, J. Physique Colloq. 35, C6(1974).

[55] G. Czjzek and W. G. Berger, Phys. Rev., B1, 957(1970).

[56] M. Van Rossum, G. Langouche, H. Pattyn, G. Dumont, J. Odeurs, A. Meykeus, P. Boolchand and R. Coussement, J. Physique Colloq., 35, C6(1974).

[57] B. D. Sawicka: Hyperfine Interactions of ^{57}Fe Implanted in Solids Studied by Conversion Electron Mössbauer Spectroscopy, Rpt NO. 1030/PL, Institute of Nuclear Physics, Cracow (1978).

[58] B. D. Sawicka and J. A. Sawicki, see in ref[34]. (1981), p139.

[59] F. J. Lynch, R. E. Holland and M. Hamermesh, Phys. Rev., 120, 513(1960).

[60] H. J. Wollenberger, see in ref[4], p215.

[61] P. Lucasson, see in ref[19], p42.

[62] M. T. Robinson, see in ref.[19], p1.

[63] Chr. Lehmann: Interaction of Radiation with Solids and Elementary Defect Production: North-Holland-Amsterdum, 1977.

[64] G. H. Kinchin and R. S. Pease, Rep. Progr. Phys., 18, 1(1955).

[65] P. Sigmund, Rad. Effects 1, 15(1969).

[66] M. T. Robinson and I. M. Torrens, Phys. Rev. B9, 5008(1974).

[67] A. Seeger: Radiation Damage in Solids, (IAEA,Vienna 1962), p101.

[68] J. W. Corbett: Solid State Physics, Supple. 7, ed. F. Seitz and D. Turnbull, Academic Press, New york and London (1966). p1.

[69] I. Manning and G. P. Mueller, Comput. Phys. Commeun. 7, 85 (1974).

[70] W. Mansel, H. Mayer and G. Vogl, Rad. Eff. 35, 69(1978).

[71] G. Vogl and W. Mansel, see in ref[19], p349.

[72] W. Mansel, J. Marangos and G. Vogl, Hyperfine Interactions 10, 687(1981).

[73] S. Takaki and H. Kimura, Scripta Met. 10, 701(1976).

[74] S. Takaki and H. Kimura, Scripta Met. 10, 1095(1976).

[75] K. Kitajima, K. Futagami, E. Kuramoto, H. Abe, N. Tsukuda, Y. Akashi, H. Yoshida and Y. Fujita, Annu. Rep. Res. Reactor Inst. Kyoto Univ. 10, 91(1977).

[76] F. E. Wagner, J. Physique Colloq. 37, C6-673(1976).

[77] S. Uehara, T. Seo, Y. Nakano and T. Hayashi, Annu. Rep. Res. Reactor Inst. Kyoto Univ. 7,10(1974).

[78] W. Kündig, Nucl. Inst. Meth. 48,219(1967).

[79] S. Nasu, Y. Murakami, Y. Nakamura and T. Shijo, Scripta Met. 2, 647(1968).

[80] R. S. Preston, S. S. Hanna and J. Heberle, Phys. Rev. 128, 2207(1962).

[81] S. Chikazumi: Physics of Magnetism, p73, Fig. 4.9: John Willey &Sons, Inc., New York, 1964.

[82] K. Atobe, M. Okada, H. Yoshida, H. Kodaka, K. Miyata, T. Matsuyama, H. Chatani, M. Nakagawa and T. Shibata, Ann. Rep. Res. Reactor Inst. Kyoto Univ. 9, 139(1976).

[83] M. Kiritani and N. Yoshida, Crystal Latt. Defects 3, 83(1973).

[84] Z. S. Basinski: Proc. 5th Int. Congr. for Electron Micorsc. vol.1, B.13(1962): New York, Academic Press.

[85] M. L. Jenkins, C. A. English and B. L. Eyre, Phil. Mag. 38, 97(1978).

[86] K. R. Swanson and J. J. Spijkerman, J. Appl. Phys. 41, 3155 (1970).

[87] W. Frank, see in Ref.[3], p203.